



TECHNISCHE
UNIVERSITÄT
WIEN
Vienna University of Technology

DIPLOMARBEIT

Development of a peak deconvolution software for X-ray fluorescence spectra

zur Erlangung des akademischen Grades
Diplom-Ingenieur

im Rahmen des Studiums
Technische Physik

eingereicht von
Johannes Zlabinger
Matrikelnummer 1025228

ausgeführt am Atominstitut
der Fakultät für Physik der Technischen Universität Wien

Betreuung
Betreuerin: Ao.Univ.Prof. Dipl.-Ing. Dr.techn. Christina Strelt
Mitwirkung: Univ.Ass. Dipl.-Ing. Dr.techn. Dieter Ingerle

Wien, 16.10.2022

(Unterschrift Verfasser)

(Unterschrift Betreuerin)

Abstract

X-ray fluorescence (XRF) analysis is a well established non-destructive analytical method for determining the chemical composition of a sample. After recording a spectrum with an XRF spectrometer it has to be processed with deconvolution software to retrieve the net intensities of the peak representing the respective element.

In this master thesis I present JPeakFit, a new Java-based deconvolution tool that comes with a graphical user interface (GUI). JPeakFit was developed with ease of use and functionality in mind. A comparison of JPeakFit with established deconvolution software packages AXIL and PyMCA illustrates the respective strengths of each tool. JPeakFit combines functionality from AXIL not available in PyMCA with a GUI of comparable ease of use as PyMCA. The state-of-the-art design pattern Model-View-Presenter was used to achieve a well structured program.

This thesis explains every part of the developed software, both how it can be used as well as how it is structured programmatically. An example fit is given, where every step to fit a spectrum is explained. Finally the results of five different spectra are evaluated and compared with AXIL and PyMCA, whereby good agreement was found.

Kurzfassung

Röntgen Fluoreszenz (XRF) Analyse ist eine etablierte, zerstörungsfreie Analysemethode für die Bestimmung der chemischen Zusammensetzung einer Probe. Nachdem ein Spektrum mit einem XRF Spektrometer aufgenommen wurde, muss es mit einer Dekonvolutions-Software verarbeitet werden, um die Peak Intensitäten der entsprechenden Elemente zu bestimmen.

In dieser Masterarbeit präsentiere ich JPeakFit, eine neue Dekonvolutions-Software entwickelt in Java mit graphischer Benutzeroberfläche (GUI). Einfache Handhabung und Funktionalität waren die Entwicklungsziele. Ein Vergleich von JPeakFit mit den etablierten Deconvolutions-Softwarepaketen AXIL und PyMCA zeigt die jeweiligen Stärken jeder Software. JPeakFit vereint Funktionalität von AXIL die nicht in PyMCA enthalten ist mit einer GUI mit ähnlicher Bedienungs-freundlichkeit wie PyMCA. Das State of the Art Entwurfsmuster Model-View-Presenter wurde eingesetzt um ein gut strukturiertes Programm zu erzeugen.

Diese Arbeit erklärt alle Teile der entwickelten Software, sowohl wie sie verwendet werden kann als auch wie sie programmatisch strukturiert ist. Ein Beispielfit wird präsentiert, in dem jeder Schritt für das Fitten eines Spektrum erklärt wird. Abschließend werden die Resultate fünf verschiedener Spektren evaluiert und verglichen mit AXIL und PyMCA, wobei eine gute Übereinstimmung gefunden wurde.

Contents

1. Physical principles	1
1.1. The atomic spectrum	1
1.2. Bohr's atomic model	1
1.3. The electromagnetic spectrum	2
1.4. X-radiation	2
1.4.1. X-ray tube	3
1.4.2. Bremsstrahlung	4
1.4.3. Characteristic radiation	4
1.5. X-ray fluorescence analysis	6
1.5.1. EDXRF	7
1.5.2. WDXRF	8
1.5.3. Detection of X-rays	8
2. Spectrum evaluation	11
2.1. Components of an X-ray spectrum	11
2.1.1. Characteristic lines	11
2.1.2. Continuum	12
2.1.3. Scatter peaks	12
2.1.4. Escape peaks	12
2.1.5. Sum peaks	14
2.1.6. Sample self absorption	14
2.2. Spectrum processing	15
2.2.1. Smoothing	15
2.2.2. Savitzky-Golay filter	15
2.2.3. Low statistics digital filter	18
2.2.4. Peak search	19
2.3. Continuum Estimation	22
2.3.1. Peak stripping	22
2.4. Net peak area determination	23
2.4.1. Least-squares fitting using analytical functions	23
3. GUI	27
3.1. File Tab	27

3.2.	Calibration Tab	29
3.2.1.	ROI	30
3.2.2.	Energy Calibration	30
3.2.3.	KLM-Marker	32
3.3.	Fitting Tab	33
3.3.1.	Element Chooser	33
3.3.2.	Escape Peaks	35
3.3.3.	Sum Peaks	36
3.3.4.	Background Settings	36
3.3.5.	Detector	39
3.4.	Plot Settings Tab	39
3.5.	Results Tab	40
3.5.1.	Export Results	42
3.6.	Plot	42
4.	Description of classes	45
4.1.	Model-view-presenter	45
4.2.	Model	45
4.3.	View	45
4.3.1.	Spectrum Chart	46
4.4.	Presenter	46
4.5.	JPeakFit CLI	46
4.5.1.	Description of the fit routine	46
4.5.2.	Fit function	47
4.5.3.	EC - EnergyCalibration	47
4.5.4.	BG - Background	47
4.5.5.	Fit algorithm	47
4.5.6.	Data bank	49
4.6.	SNIP filter	49
5.	Example fit	51
5.1.	Example fit of NIST SRM 1412	51
6.	Results and Discussion	59
6.1.	Results NIST 1412	60
6.2.	Discussion NIST 1412	62
6.3.	Results NIST 621	63
6.4.	Discussion NIST 621	65
6.5.	Results NIST 1640A	66
6.6.	Discussion NIST 1640A	68
6.7.	Results NIST 1643F	69

6.8. Discussion NIST 1643F	71
6.9. Results NaMgAlCa25	72
6.10. Discussion NaMgAlCa25	74
7. Conclusion and perspective	75
Bibliography	i
A. Data sheets	v
A.1. NIST 621 data sheet	v
A.2. NIST 1412 data sheet	viii
A.3. NIST 1640A data sheet	xi
A.4. NIST 1643F data sheet	xviii

1. Physical principles

1.1. The atomic spectrum

As early as 1859, Gustav Kirchhoff and Robert Bunsen discovered that atoms can absorb and emit light at very specific wavelengths. These wavelengths are called absorption and emission spectrum. Through a number of experiments it was determined that every wavelength that can be absorbed can also be emitted if an atom gets excited with enough energy beforehand. The emission spectrum is also characteristic and distinct for each atom. This means that the emission spectrum of some sample can be used to determine its chemical composition. [1]

In 1885 Johann Balmer recognized, that the emission spectrum for hydrogen follows the simple correlation:

$$\lambda = (364,6nm) \cdot \frac{n_1^2}{n_1^2 - 4}, \quad n_1 = 3, 4, 5, \dots \quad (1.1)$$

Balmer already suspected that there existed an underlying general law, which the former expression was a special case of. This Rydberg formula was discovered by Johannes R. Rydberg and Walter Ritz:

$$\frac{1}{\lambda} = R \left(\frac{1}{n_2^2} - \frac{1}{n_1^2} \right) \quad (1.2)$$

where n_1 and n_2 are integers, with $n_1 > n_2$, and R is the Rydberg constant. In the following years many models for the atom were proposed to explain this observed behaviour until finally Niels Bohr's model from 1913 proved to be successful. [2]

1.2. Bohr's atomic model

Niels Bohr proposed his famous planet model of the atom as a theory for the observations of the emission spectrum of a hydrogen atom. In this model, the electron orbits the nucleus a certain distance of radius r . The electron can be considered as a matter wave, which has to form a standing wave around the circumference to be in a stationary state. This leads to restricted radii:

$$r = n^2 \frac{a_0}{Z}, \quad n = 1, 2, 3, \dots \quad (1.3)$$

where Z is the atomic number and a_0 is the Bohr radius which is roughly equal to 0.05 nm. The different radii correspond to different energy states of the atom, explaining the unique lines in the atomic spectrum. We can use the Planck relation $E = h\nu$ (where h is the Planck constant) to derive the frequency of the radiation emitted during a transition from energy state E_i to E_f . [2]

1.3. The electromagnetic spectrum

Electromagnetic waves are split into different parts by their wavelength and frequency. Since the speed of light in vacuum is constant for all electromagnetic waves, the product of wavelength and frequency is always equal to the speed of light:

$$\lambda\nu = c. \tag{1.4}$$

The borders between the areas are not strictly defined. Commonly used denotations are shown in figure 1.1. [2]

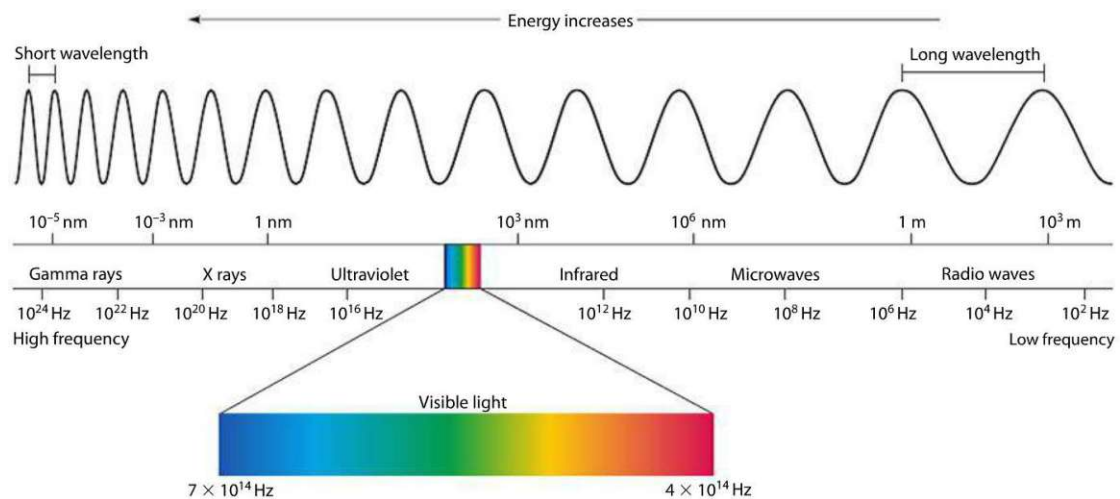


Figure 1.1.: The electromagnetic spectrum [3].

1.4. X-radiation

In 1895 Wilhelm Conrad Röntgen discovered a new kind of radiation, that could penetrate materials like glass, human tissue and wood. Since he didn't know a lot about the nature of this radiation, he called them X-rays. In the electromagnetic spectrum X-rays are located between ultraviolet and gamma rays.

1.4.1. X-ray tube

There are two processes that are used in an X-ray tube to create X-rays:

- The deceleration of electrons in matter, leading to a continuous intensity distribution, which is dependent on the energy of the electrons. The produced radiation is called bremsstrahlung.
- Electron transitions inside atoms, which lead to the already discussed characteristic radiation, where the frequency of the emitted photons is dependent on the difference in energy of the initial and final state.

An X-ray tube (figure 1.2) makes use of both these effects. Electrons are emitted

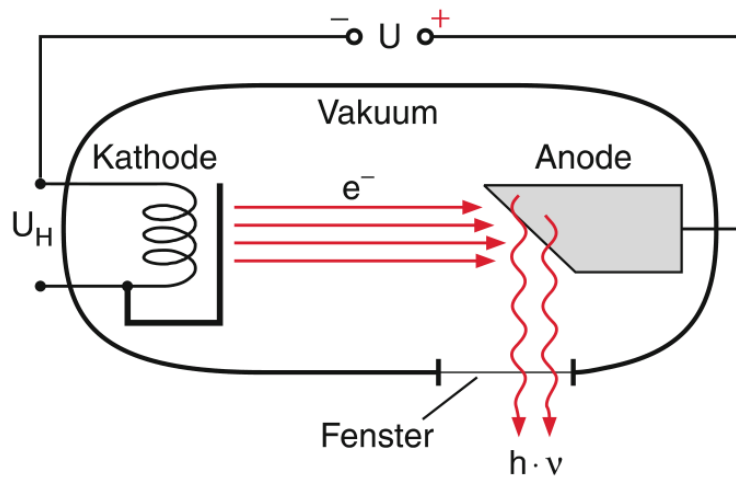


Figure 1.2.: Schematic setup of an X-ray tube [1].

from a heated cathode, usually a tungsten filament. These electrons are then accelerated in an electric field towards an anode, where the X-rays are created with the above described processes. Common elements for the anode are tungsten, molybdenum and rhodium. The created radiation then leaves through a window, which minimizes X-ray absorption. A common material for this is beryllium. This all happens inside a vacuum, to avoid the scattering of the electrons with air-molecules. Figure 1.3 shows what a typical spectrum emitted from an X-ray tube looks like, with both the continuous bremspectrum and the characteristic lines of the anode material. [4, 5]

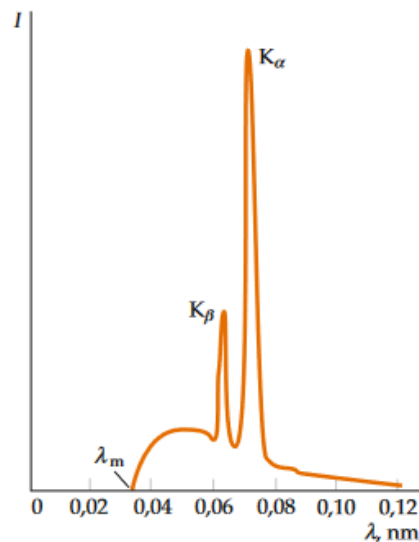


Figure 1.3.: X-ray spectrum emitted by a tube [2].

1.4.2. Bremsstrahlung

Bremsstrahlung in an X-ray tube is created when electrons are deflected in the coulomb field of the nuclei of the anode material. During this process part of the kinetic energy the electrons received in the electric field is transformed into radiation. The total kinetic energy one electron can receive is $E_{max} = e \cdot U$, where e is the elementary charge and U is the voltage between anode and cathode. Using this in combination with the Planck relation and equation 1.4 leads to the minimum wavelength a photon from the bremspectrum can have:

$$\lambda_{min} = \frac{h \cdot c}{e \cdot U}. \quad (1.5)$$

Since an electron doesn't have to deposit all its energy at once, bremsstrahlung also consists of photons with longer wavelength, which leads to a continuous spectrum. Figure 1.4 shows what this spectrum looks like for a tungsten anode for different voltages. [1]

1.4.3. Characteristic radiation

There is also another interaction of the electrons with the anode. If the energy of an electron is high enough, it can eject an electron from the inner shells of an atom of the anode material. This ionization of the atom leaves it in an higher energy state. The excess energy equals the binding energy of the electron that was

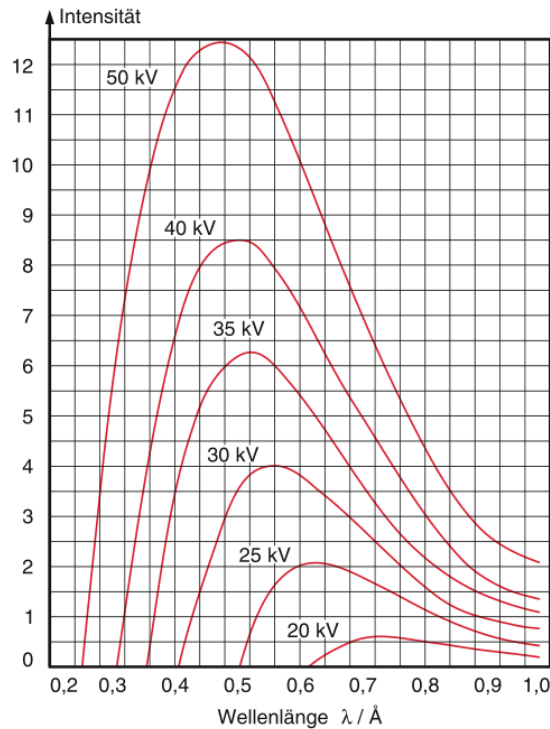


Figure 1.4.: Bremspectrum of a tungsten anode for different voltages [1].

removed. To minimize the energy of the ion, the hole is filled with an electron of an outer shell. During the transition a photon with the energy of the difference between the energy of the final and initial shell of the transition electron is emitted. Depending on the different combinations of initial and final shells, photons with different energies and therefore different wavelengths can be emitted. Transitions between two shells are restricted however, which leads to certain selection rules which can be derived in quantum mechanics. There is also a fixed intensity ratio between lines with the same final shell. Figure 1.5 shows the allowed transitions for the inner most shells of an atom, which are the most important for X-ray fluorescence analysis. [6]

To denote the different transitions there are two notations in use:

- **Siegbahn notation:** This notation was invented by Karl M. G. Siegbahn and is widely used in X-ray physics. It consists of an uppercase Latin alphabet letter, a lowercase Greek letter and if necessary a subscript number and sometimes even an apostrophe (e.g. $K\alpha_1$). The Latin letter thereby denotes the final shell of the transition, while the Greek letter indicates the line intensity (α more intense than β etc.). It grew historically and is therefore not

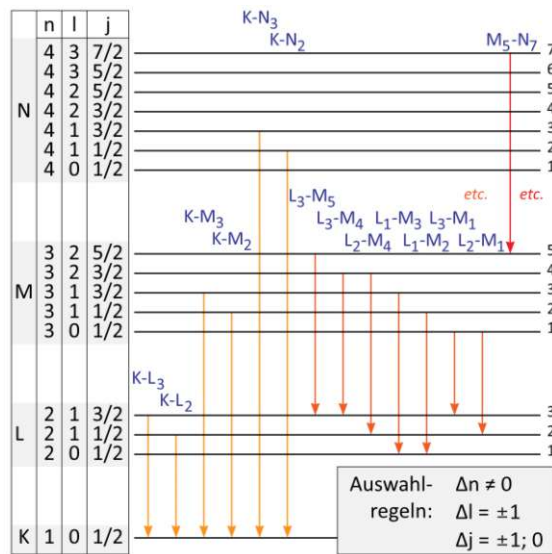


Figure 1.5.: Allowed transitions and selection rules [7].

completely systematic.

- IUPAC notation:** The International Union of Pure and Applied Chemistry (IUPAC) recommends another notation, which is commonly known as the IUPAC notation. It uses an uppercase Latin letter to denote the shell and a subscript number to differentiation between different energy levels within a shell, going from the lower energy to the higher. Both the final and initial shell of a transition are written in this way and are separated by a minus (e.g. $L_1 - M_3$).

Table 1.1 shows both notation for the transitions in figure 1.5. [8]

1.5. X-ray fluorescence analysis

With X-ray fluorescence (XRF) analysis it is possible to non-destructively determine qualitatively and quantitatively the chemical composition of a sample. It makes use of the above explained fact that different elements emit specific spectra. The atoms in a sample are excited with X-rays, which in turn emit characteristic radiation. By measuring the energies of the created photons, the chemical elements in the sample can be inferred. There are two principle ways of measuring those energies, Energy-dispersive XRF (EDXRF) and Wavelength-dispersive XRF (WDXRF).

Final shell	Initial Shell	IUPAC	Siegbahn
K	L_3	$K - L_3$	$K\alpha_1$
K	L_2	$K - L_2$	$K\alpha_2$
K	M_3	$K - M_3$	$K\beta_1$
K	M_2	$K - M_2$	$K\beta_3$
K	N_3	$K - N_3$	$K\beta'_2$
K	N_2	$K - N_2$	$K\beta''_2$
L_3	M_5	$L_3 - M_5$	$L\alpha_1$
L_3	M_4	$L_3 - M_4$	$L\alpha_2$
L_3	M_1	$L_3 - M_1$	$L\ell$
L_2	M_4	$L_2 - M_4$	$L\beta_1$
L_2	M_1	$L_2 - M_1$	$L\eta$
L_1	M_3	$L_1 - M_3$	$L\beta_4$
L_1	M_2	$L_1 - M_2$	$L\beta_5$
M_5	N_7	$M_5 - N_7$	$M\alpha_1$

Table 1.1.: IUPAC and Siegbahn notation.

1.5.1. EDXRF

In EDXRF there is no physical discrimination of the secondary radiation that leaves the sample, which means the energies of the characteristic photons have to be measured directly in the detector. Since the energies of the incoming photons have to be distinguished in the detector, the count rate of such detectors is lower than detectors without the need for energy selection. To counter this drawback the content of the incident spectrum has to be optimized for its useful information, which may require more than one acquisition to be made under different excitation conditions. High power X-ray tubes are needed to allow for selectivity to the excitation method. The most important modes for selective excitation in EDXRF are: [6]

- Selection of tube anode material
- Variation of tube voltage
- Use of primary beam filters
- Use of secondary targets

Another way to increase the peak-to-background ratio is the use of alternative geometries like Total-Reflection X-ray Fluorescence (TXRF). TXRF uses a very small incident angle of the primary beam on the sample, which then gets totally reflected. This offers a few advantages: [6]

- The background contribution from scattering of the primary beam is drastically reduced, since nearly 100% of the incident radiation is totally reflected.
- The sample is excited twice, both from the direct and the reflected beam.
- The detector can be located very close to the sample, which results in a large angle for detection.

1.5.2. WDXRF

While EDXRF is using selective excitation and broad-band detection, in WDXRF broad-band excitation and selective detection is used. To achieve this a crystal monochromator is used after the sample, which filters the exiting radiation to a small bandwidth. Since the energy of the photons that reach the detector is known beforehand, it only has to count the amount of entering photons and not their energies, which allows for higher count rates. On the other hand to get the entire spectrum, all the wavelength have to be selected with the monochromator one after another, which results in a longer overall measure time compared to EDXRF. The advantage however is better energy resolution. [6]

1.5.3. Detection of X-rays

As already discussed, for EDXRF a detector is needed that can distinguish the energy of the incoming photons. Such detectors are made of semiconductor materials like silicon or germanium. Figure 1.6 shows the cross section of Si(Li) detector. It

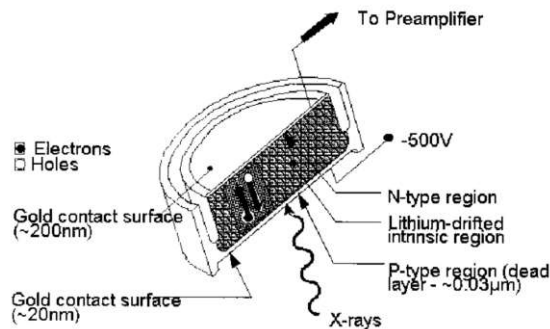


Figure 1.6.: Cross section of a Si(Li) detector. [6]

makes use of the photoelectric effect to determine the incoming photons energy. A photon hitting the active region of the detector creates a photo-electron and an inner-shell vacancy. Before coming to rest multiple low energy ionization events are

produced by the photo-electron. It is important to note that the total length this electron travels is much shorter than the dimension of the detectors active region. The inner-shell vacancy can either lead to an Auger electron or to multiple X-rays being emitted, which are then absorbed again by other atoms. An electric field gradient separates the electron-hole pairs that are essentially instantaneously created with these processes. Once they reach the contact surfaces the voltage pulse is recorded, which is directly proportional to the energy of the incident X-ray. [6]

Today silicon drift detectors (SDD) are also commonly used besides the classical Si(Li) detectors. They function on the same principle of electron-hole pairs being created. Figure 1.7 shows the design of a SDD. X-rays enter through the negatively

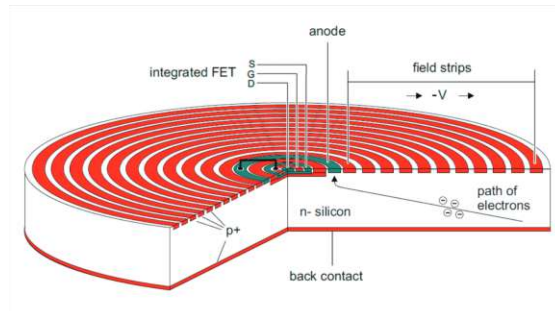


Figure 1.7.: Schematic of a silicon drift detector. [9]

charged back contact. A series of also negatively charged concentric circles, which decrease in voltage going inwards, push the electrons to the collection anode in the center. SDDs require less cooling, have a better energy resolution and experience less noise than Si(Li) detectors. [10]

2. Spectrum evaluation

The goal of spectrum evaluation is to extract the relevant information from an acquired X-ray spectrum. If a spectrum was noise free and only contained the characteristic lines this would be a lot easier. Unfortunately not all noise can be eliminated. Since the arrivals of photons to the detector are random events and the measurement lasts a finite time interval, there is always some channel to channel fluctuation. This is called amplitude noise and it obeys a Poisson distribution. Another distortion of the characteristic line peaks appears as energy noise. The natural bandwidth of a peak is 5-10 eV. The photon to charge conversion that happens inside the detector and the electronic noise in the pulse amplification and processing unit causes the peak to appear much wider in EDXRF spectra, about 140-250 eV. In WDXRF spectra the peaks are also widened because of imperfections in the diffraction crystal and collimation. [6]

2.1. Components of an X-ray spectrum

Aside from the characteristic lines a spectrum also consists of other components and artifacts. The most important ones will be listed here:

2.1.1. Characteristic lines

The characteristic radiation of atoms has a Lorentz distribution. When measured with a semiconductor detector this distribution gets convoluted with the nearly Gaussian detector response function, which is known as Voigt profile. The Lorentz width for elements with atomic number below 50 is on the order of 10 eV, while the width of the detector response function is on the order of 160 eV. Therefore a Gauss function is an adequate approximation of the line profile. The Lorentz contribution becomes significant only for the K lines of elements such as uranium. Figure 2.1 shows the difference between a Gaussian and a Lorentzian peak. Incomplete charge collection leads to the Gauss peak being shifted towards the low energy side of a peak, which is most pronounced for low energy X-rays. The shape of the peak can be further distorted by the Compton scatter inside the detector, which happens for photons above 15 keV. [6]

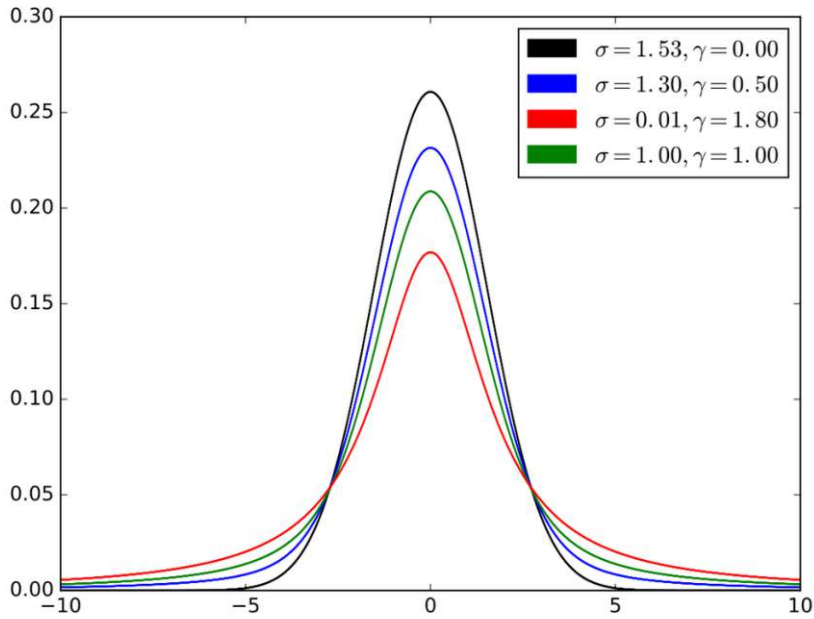


Figure 2.1.: Plot showing the Voigt profile for four cases. The black and the red line are the limiting cases for Gaussian ($\gamma = 0$) and Lorentzian ($\sigma = 0$) profiles respectively. [11]

2.1.2. Continuum

The main source for the continuum of an X-ray fluorescence spectrum stems from the excitation radiation being scattered coherently and incoherently by the sample. It depends both on the initial shape of the excitation spectrum and the sample composition, which can lead to a very complex shape. The continuum can be further complicated by incomplete charge collection of intense fluorescence lines. [6]

2.1.3. Scatter peaks

Scatter peaks of intense lines from the exciting radiation can also appear on the spectrum. Figure 2.2 shows the coherent and incoherent scatter peak of the KL line from the molybdenum anode. [6]

2.1.4. Escape peaks

Escape peaks are an artifact that appear in energy discriminating semiconductor detectors. If an impinging X-ray photon is absorbed near the edge of a detector,

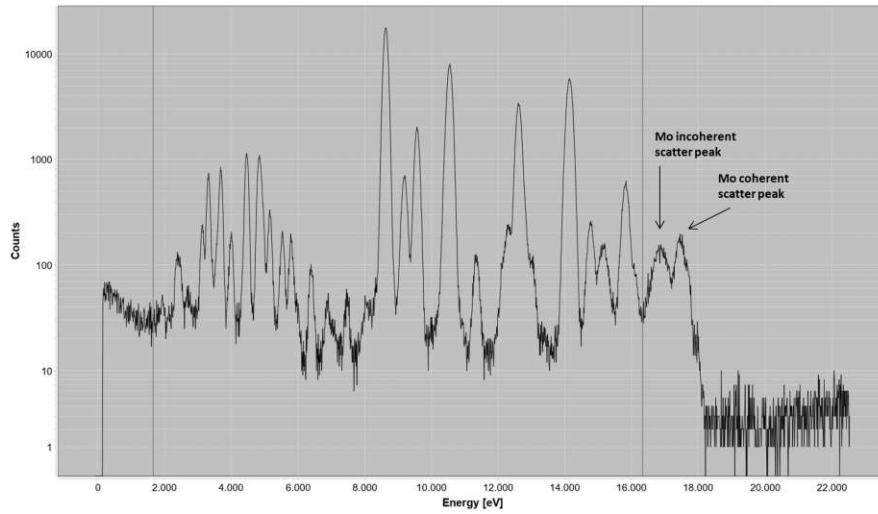


Figure 2.2.: Coherent and incoherent scatter peak Mo KL line.

it is possible for the resulting Si or Ge photon — depending on which material is used in the detector — to escape the detector and therefore reduce the collected charge energy by that amount. This leads to a separate peak that is shifted down by the energy of the Si-KL3 (1.74 keV) or Ge-KL3 (9.88 keV). Figure 2.3 shows a schematic of escape peaks. [6]

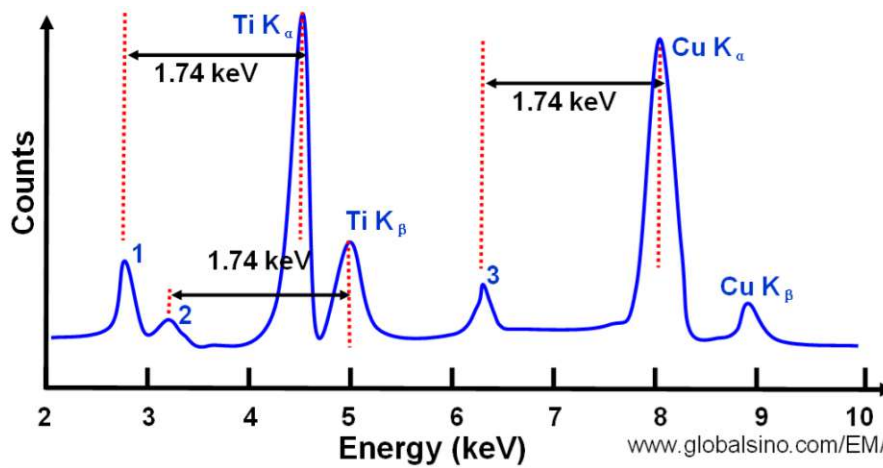


Figure 2.3.: Escape peaks in EDXRF spectra. 1 is the Si escape peak of Ti-K α , 2 is the Si escape peak of Ti-K β and 3 is the Si escape peak of Cu-K α . [12]

2.1.5. Sum peaks

Sum peaks or pileup peaks are again exclusive to energy discriminating detectors. They occur by two X-rays striking the detector in a time interval that is too short to be distinguished as two separate events. The measured energy of this event will be registered at the sum of the individual photon energies. Figure 2.4 shows a schematic of sum peaks. [6]

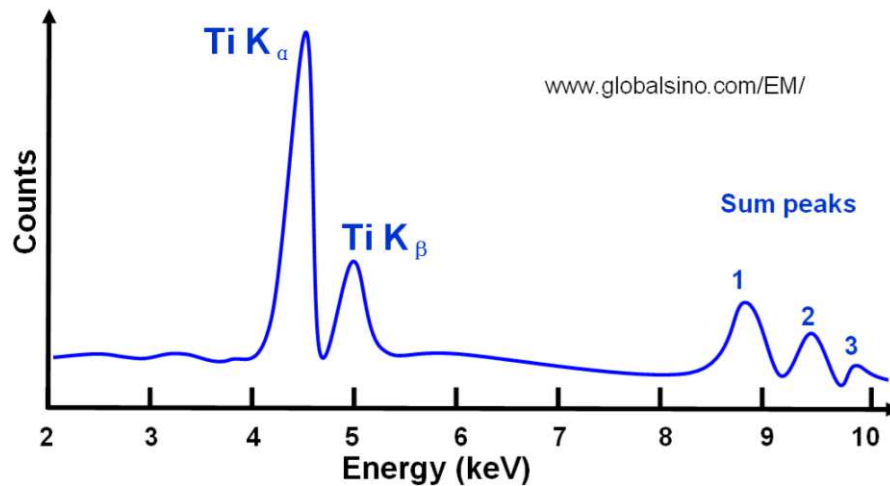


Figure 2.4.: Sum peaks in EDXRF spectra. 1 is the sum peak of two Ti-K α , 2 is the sum peak of Ti-K α and Ti-K β and 3 is the sum peak of two Ti-K β . [13]

2.1.6. Sample self absorption

As mentioned above, transitions with the same final shell have a fixed intensity ratio. For instance if a silicon atom has a vacancy in the K shell there is a probability of $\approx 59\%$ that an electron from the L3 shell fills it, resulting in a K-L3 line. The probability is $\approx 30\%$ for K-L2, $\approx 7\%$ for K-M3 and $\approx 4\%$ for K-M2. These ratios can be used in evaluating a spectrum. The theoretical values are however only valid for thin samples. If the exciting X-rays from the tube penetrate into the sample the produced fluorescence X-rays have to pass through the sample again to reach the detector to be registered. It is then possible for those X-rays to be absorbed by the sample. The absorption rate is energy dependent, which skews the intensity ratios. [6]

2.2. Spectrum processing

The term spectrum processing is used to refer to mathematical techniques that are used to alter the outlook of spectral data. Often this is accomplished by the use of some digital filter, to reduce noise, locate peaks or to suppress the continuum. This section will look at some methods of filtering a spectrum. [6]

2.2.1. Smoothing

Statistical fluctuations lead to an uncertainty \sqrt{y} on each channel, which in turn can result in fictitious maxima on the spectrum. During peak search and continuum estimation it can be useful to remove or suppress these fluctuations. Smoothing can also be used for qualitative analysis of spectra, but one has to be careful when doing quantitative analysis, since smoothing distorts the peaks. Following will be a description of some algorithms used for smoothing. [6]

Moving-average filter

A very simple algorithm for smoothing is the moving-average technique. Using a width m the spectrum is traversed and each channel is assigned the average of itself and the m channels left and right of it:

$$y_i^* = \frac{1}{2m + 1} \sum_{j=-m}^m y_{i+j} \quad (2.1)$$

While preserving the total counts in a peak, a considerable amount of peak distortion is introduced (figure 2.5). [6]

2.2.2. Savitzky-Golay filter

This filter is based on drawing a best-fitting curve through the data points and was developed by Savitzky and Golay in 1964 [14]. This approach works, since nearly all experimental data, confined to a sufficiently small interval, can be modeled by a polynomial of order r : $a_0 + a_1x + a_2x^2 + \dots + a_r x^r$. If we consider a few data points around a central channel i_0 and take $r = 2$, we can use this function for a least-squares fit:

$$y(i) = a_0 + a_1(i - i_0) + a_2(i - i_0)^2. \quad (2.2)$$

After determining the coefficients the value of the polynomial at the channel i_0 can be used as a smoothed value:

$$y(i_0) = a_0. \quad (2.3)$$

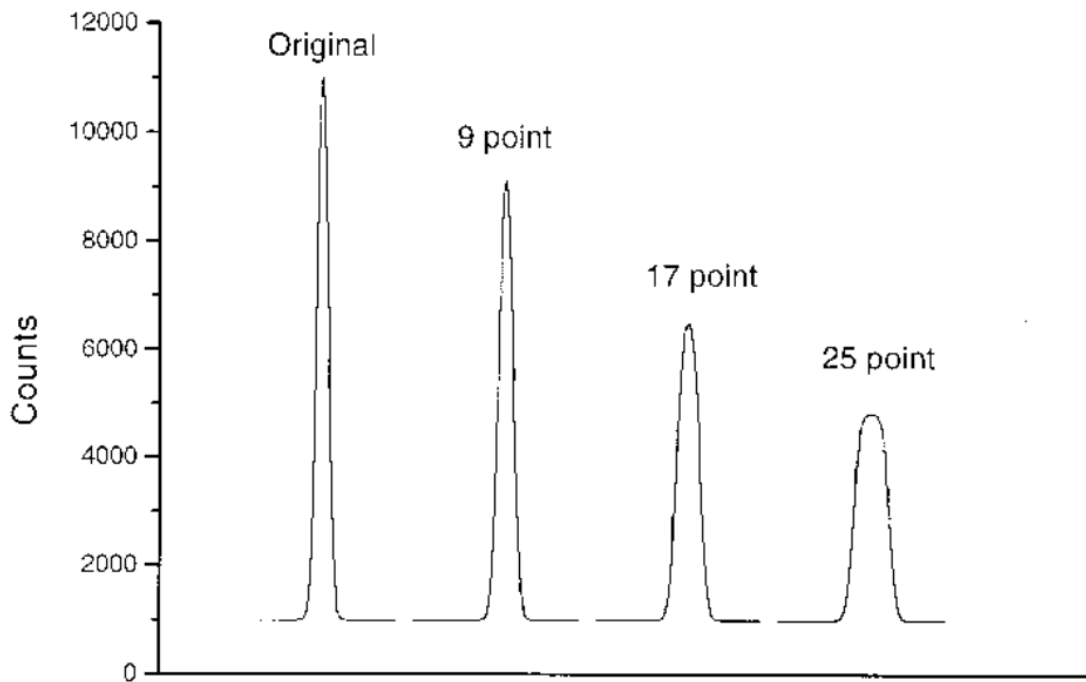


Figure 2.5.: Peak distortion by smoothing with a moving-average filter of various widths. The FWHM of the original peak is nine channels. [6]

Figure 2.6 shows a schematic illustration of this procedure. Smoothing the entire spectrum requires this process to be repeated for all channels. [6]

Performing a polynomial fit for every channel of a spectrum would require a lot of computational power. Since the x values are equidistant however, a linear combination involving only the y_i values can be used to calculate the coefficients:

$$a_k = \frac{1}{N_k} \sum_{j=-m}^m C_{k,j} y_{i+j}. \quad (2.4)$$

The exact polynomial coefficients of a least-squared-fitting procedure can also be calculated by this convolution of the spectrum with a filter of appropriate weights. The bounds m used in the summation represent the length of the filter to each side. $m = 2$ would lead to a 5-point filter ($2m + 1 = 5$). The only coefficient to be calculated is a_0 since we are only interested in the value of the polynomial at

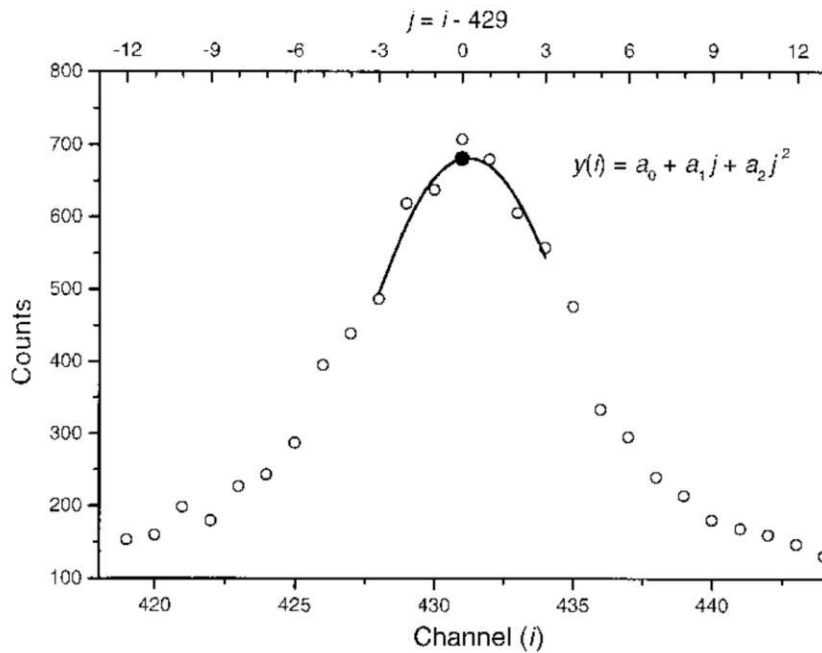


Figure 2.6.: A smoothed value is calculated by performing a polynomial fit through i_{-3} to $i_0 + 3$. [6]

position i_0 . For a second-order polynomial the coefficients are given by: [6]

$$\frac{C_{0,j}}{N_0} = \frac{3(3m^2 + 3m - 1 - 5j^2)}{(2m - 1)(2m + 1)(2m + 3)}, \quad (2.5)$$

$$y_i^* = a_0 = \frac{1}{N_0} \sum_{j=-m}^m C_{0,j} y_{i+j}. \quad (2.6)$$

The derivation that the presented convolution is equivalent to the least-squares-fitting procedure is shown in [14] in Appendix I.

A comparison to moving-average filters shows that polynomial filters are less effective in removing noise, but cause less peak distortion. Figure 2.7 shows the distortion effect as a function of the filter width to peak width ratio. When the width of the filter becomes wider than the peak, oscillations start to occur in the smoothed spectrum near the peak boundaries (figure 2.8). This should be considered when choosing the width for this filter. [6]

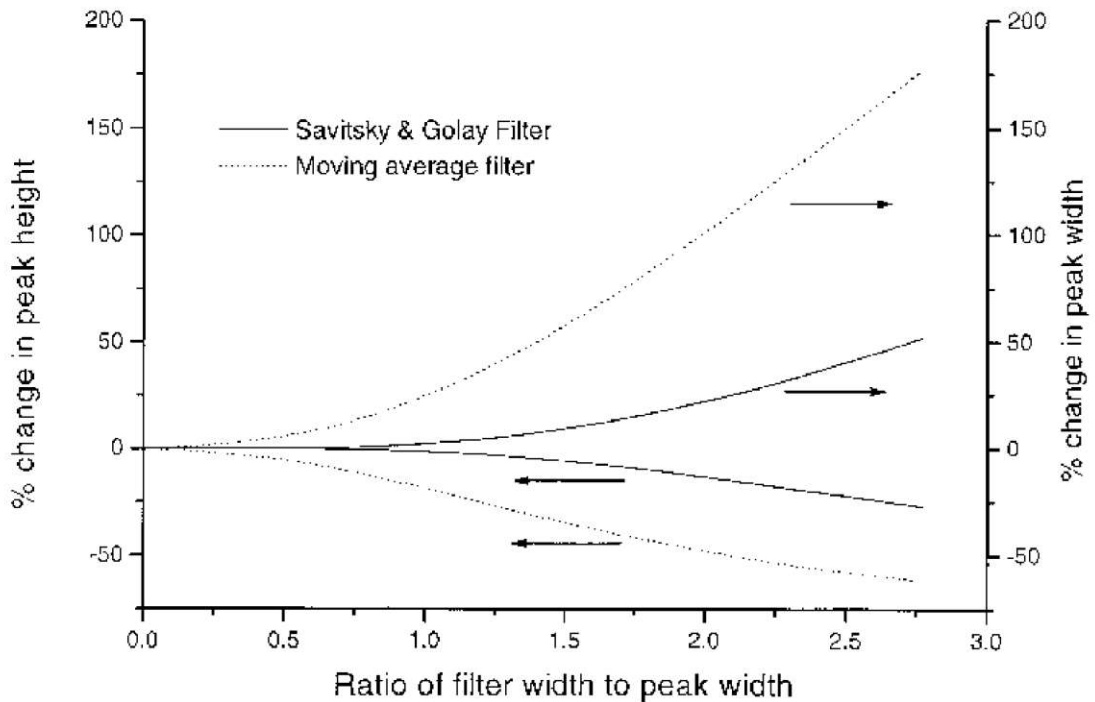


Figure 2.7.: Change of peak height and width for a moving-average filter and a Savitzky-Golay filter. [6]

2.2.3. Low statistics digital filter

The low statistics digital filter was developed by Ryan et al. in 1988 [15]. The concept of this filter is to split the spectrum into two parts that are treated differently. The "low statistics" part, where the accumulated counts are low and the statistical fluctuations have a high impact. And the "high statistics" part, where the accumulated counts are high and statistical fluctuations are insignificant. An adaptive n -point moving average filter is applied, which smooths the "low statistics" part while leaving the "high statistics" part unaffected. For every channel x with counts $y(x)$ the sum of two windows the size of $f \cdot F(E)$ are formed, a left sum L and a right sum R . $F(E)$ is the FWHM of the spectrometer at energy $E(x)$. The size of both windows is reduced simultaneously until the sum:

$$S = y + L + R \quad (2.7)$$

is smaller than a minimum M or until two conditions are met:

1. S is lower than $N = A\sqrt{y}$. This ensures that N/y reduces as $1/\sqrt{y}$ with increasing counts, so that smoothing is confined to the low-statistics regions.

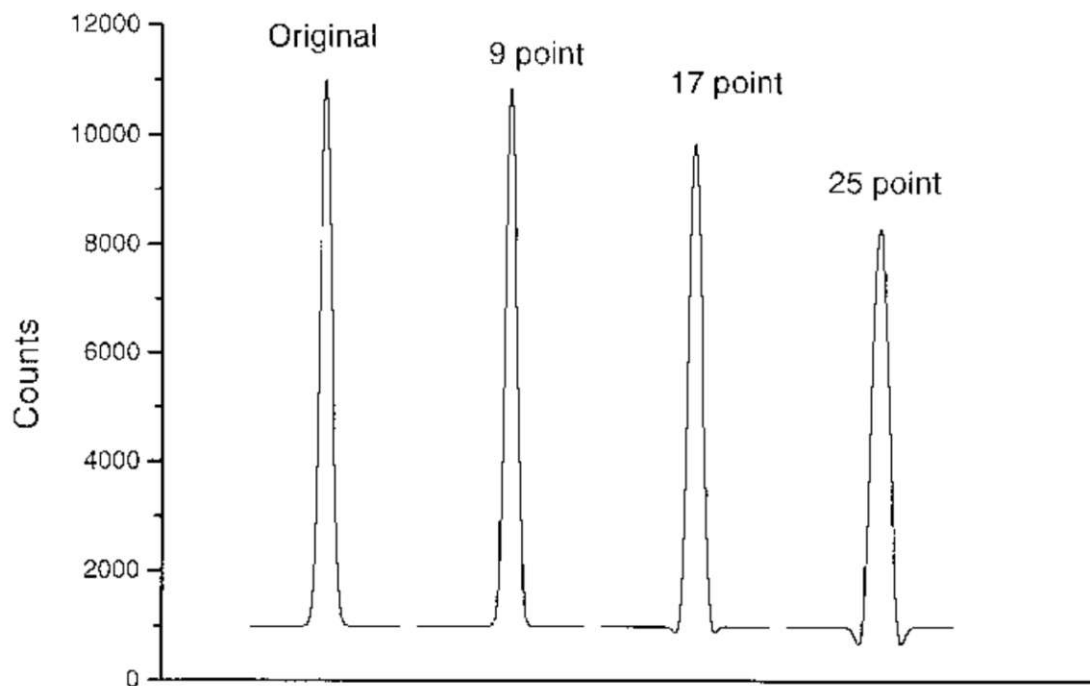


Figure 2.8.: A Savitzky-Golay filter applied with different widths. The FWHM of the original peak is nine channels. [6]

2. The slope $(R + 1)/(L + 1)$ is within the range of $1/r$ and r , to avoid the incorporation of peak tails in the average.

When these conditions are met, the smoothed value for x becomes the average of S . The parameters suggested by Ryan et al., which were successful for all spectra they had encountered, are: $f = 1.5$, $A = 75$, $M = 10$ and $r = 1.3$. Figure 2.9 shows a comparison between the low statistics digital filter and a 7-point moving-average filter. The latter clearly distorts the peaks, while the former leaves them mostly unaffected. For the "low statistics" regions both perform very similarly. [15]

2.2.4. Peak search

There are several methods for the automatic detection and localization of peaks in a spectrum. Usually the spectrum is transformed in a way to emphasize peak like structures, followed by a determination if the detected structures are significant. The sensitivity of the latter involves adjustable parameters. Three steps are usually involved in peak search procedures:

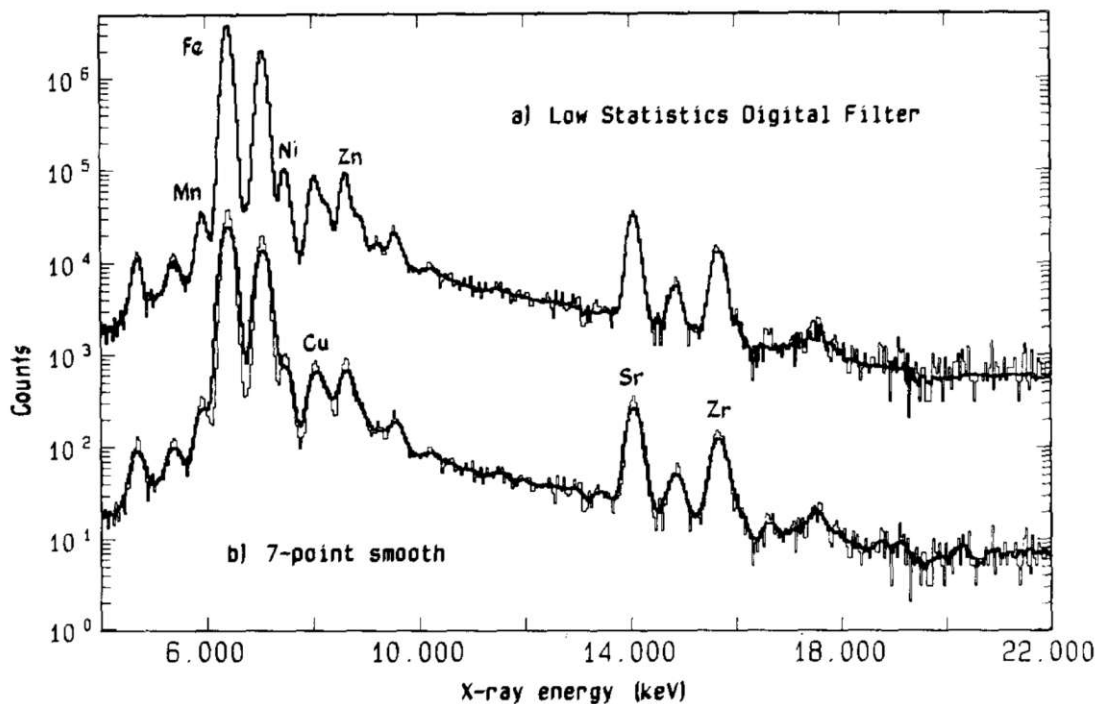


Figure 2.9.: Comparison of a spectrum processed with a) the low statistics digital filter and b) a 7-point moving-average filter. [15]

1. Transformation of the original spectrum, so that peaks are readily locatable and the continuum contribution is removed.
2. A test of significance and the approximate location of the peak maximum.
3. A more accurate peak position in the original spectrum.

In some methods the first and second smoothed derivative are used. Figure 2.10 shows those derivatives for a spectrum. The zero crossing of the first derivative and the minimum of the second derivative can be use quite effectively to locate peaks. One method for peak searching will be presented here. [6]

The first step of this method is to derive and smooth the spectrum. The algorithm then looks for downward zero crossings in the derivative to find possible peaks. At each crossing the slope of the derivative at that location is calculated and compared to a slope threshold. Large values for the slope threshold will neglect broad features of the spectrum. If the slope threshold is met, all points within a given width of the original spectrum are considered to estimate the peak height.

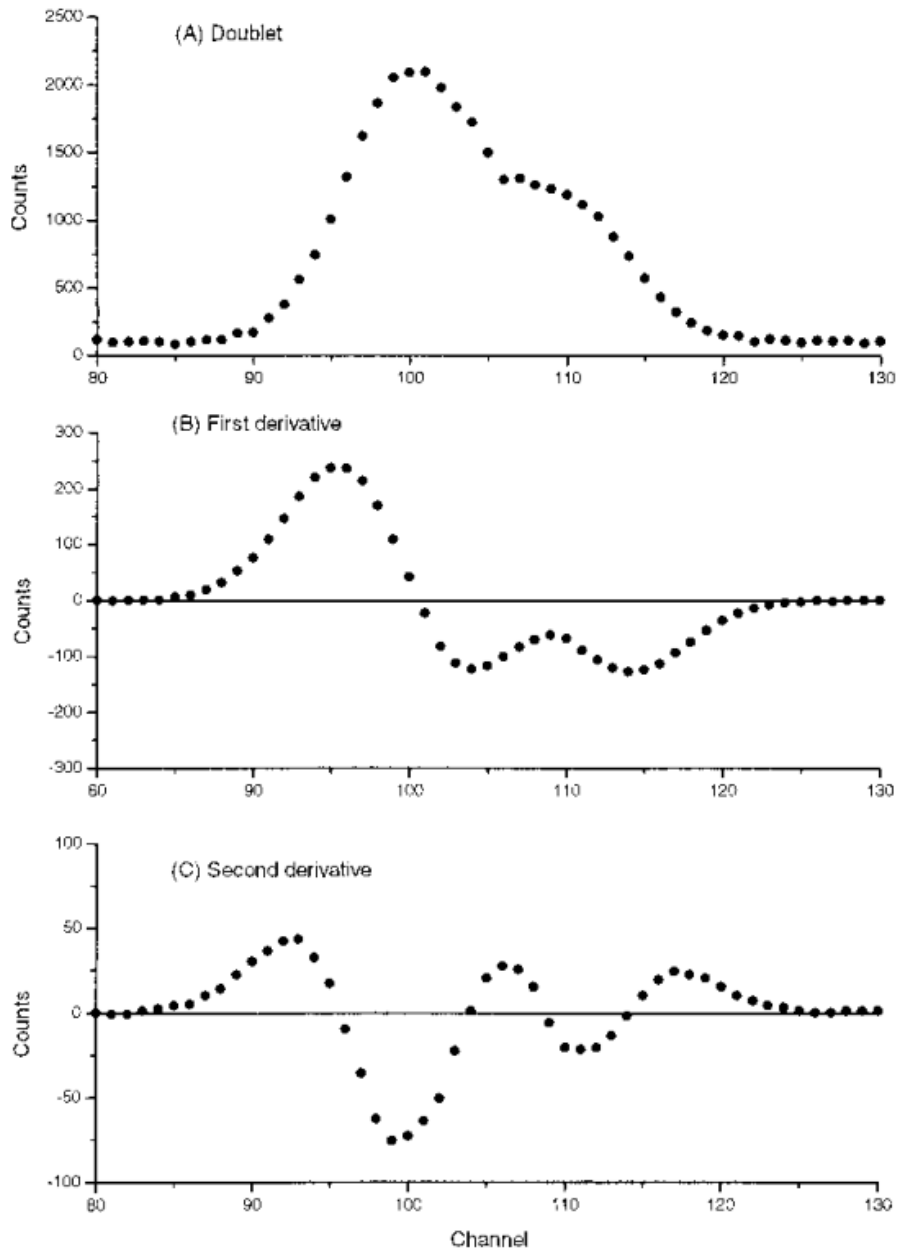


Figure 2.10.: (A) A doublet with peak width (σ) of four channels and a separation of 8 channels. (B) First derivative and (C) second derivative smoothed with a five-point Savitzky-Golay filter. [6]

Smaller values of the width are good for very narrow peaks, while larger values are

good for broad or noisy peaks. Within all the considered peaks, the one closest to the estimated peak height is chosen as the location of the peak. A last check is performed to see if the height of the peak is larger than some amplitude threshold. When the whole spectrum has been scanned, all the peaks that have been found are returned. [16]

2.3. Continuum Estimation

Usually the relevant information of a spectrum is found in the net peak area and the continuum is considered a nuisance. In principle there are three ways to deal with the continuum:

1. A filter can be used to suppress or eliminate the continuum.
2. The continuum can be estimated prior to the net peak estimation and subtracted.
3. The continuum can be estimated simultaneously with the net peak estimation.

This section will present the second approach, while the simultaneous estimation will be displayed in the next section.

2.3.1. Peak stripping

The goal of this method is to remove rapidly varying structures, by comparing a channel content y_i with that of its neighbours. Clayton et al. [17] proposed a method that compares channel i with the mean content of its direct neighbours:

$$m_i = \frac{y_{i-1} + y_{i+1}}{2}. \quad (2.8)$$

If m_i is smaller than y_i , then the content of channel i is set to the mean. Doing this for the whole spectrum will reduce the peaks slightly, while leaving the continuum mostly unaffected. Doing this for many iterations will "strip" the peaks from the spectrum. This method connects local minima, which is why it is crucial for the spectrum to be smoothed beforehand. To get a smooth continuum approximately 1000 cycles are needed. To reduce this number a root or log transform can be applied before applying the algorithm, which can then be reverted to receive the smoothed original continuum. Overlapping peaks are merged into one broad peak after some iterations, which takes much longer to be removed. This is a slight drawback of this method. [6]

SNIP algorithm

Ryan et al. [15] introduced the SNIP algorithm (Statistics-sensitive Non-linear Iterative Peak-clipping), to improve the efficiency of the peak stripping algorithm. The low statistics digital filter, as described above, was applied for smoothing. Instead of the mean of the direct neighbours, the channels a width w away from the current channel are taken for the mean calculation:

$$m_i = \frac{y_{i-w} + y_{i+w}}{2}. \quad (2.9)$$

The width was set to the FWHM of the spectrometer at channel i . To suppress the dynamic range, a double log transformation $G(y)$ is applied on the spectrum:

$$G(y) = \log(\log(y + 1) + 1). \quad (2.10)$$

Doing this only 24 iterations were necessary to get acceptable continuum estimations on all their test data. Reducing the width by a factor of $\sqrt{2}$ also eliminated the need to smooth the spectrum after processing. All that is left to do is to perform the inverse log transformation on the channels:

$$G^{-1}(y) = \exp(\exp(y) - 1) - 1. \quad (2.11)$$

2.4. Net peak area determination

The counts under a characteristic X-ray peak are proportional to the concentration of the respective element. The net area determination of the peaks is therefore the ultimate goal of the spectrum evaluation, since the peak area corresponds directly with the counts measured by the detector. This section will describe a widely used and very flexible procedure to do that. [6]

2.4.1. Least-squares fitting using analytical functions

This method uses an algebraic function to model the measured spectrum. As object function χ^2 is used, which is defined as the weighted sum of the differences between the measured spectrum y_i and the model $y(i)$ over a region of the spectrum ($n_1 - n_2$):

$$\chi^2 = \sum_{i=n_1}^{n_2} \frac{1}{y_i} (y_i - y(i, a_1, \dots, a_m))^2 \quad (2.12)$$

where a_j are the parameters of the model and $1/y_i$ is used as the weight for the summands. The optimum parameters can be found by minimizing χ^2 , which can

be done by setting the partial derivatives of χ^2 to zero:

$$\frac{\partial \chi^2}{\partial a_j} = 0, \quad j = 1, \dots, m. \quad (2.13)$$

If the model is linear in all the parameters a_j , the resulting equations can be solved algebraically. In the general case, at least some parameters are non-linear in which case the optimum value of the parameters must be found by iteration.

Non-linear least squares fitting can be seen as the problem of finding the minimum of a function in an m -dimensional space. An algorithm performing this task will look like the following:

1. With some initial values for the parameters calculate χ^2 : $\chi_{old}^2 = \chi^2(a_{ini})$.
2. Find a new set of values a_{new} so that $\chi_{new}^2 < \chi_{old}^2$.
3. If χ_{new}^2 is the minimum of the function, a_{new} are the optimum values of the fit, otherwise set $\chi_{old}^2 = \chi_{new}^2$ and repeat from step 2.

A key problem to solve when applying this least-squares procedure is to construct an analytical function that describes the spectrum accurately. This includes the description of the continuum, the characteristic lines and all other features like escape and sum peaks. The response function of an energy-dispersive detector is almost Gaussian, but deviations from the Gaussian shape should also be taken into account. On the other hand the number of the parameters should be kept as low as possible to make it easier to locate the minimum of χ^2 function.

Description of the continuum

Usually it is virtually impossible to construct a precise physical model to describe the continuum, because there are many processes that contribute to it. That is why very often some type of linear polynomial expression is used:

$$y_b(i) = a_0 + a_1(E_i - E_0) + a_2(E_i - E_0)^2 + \dots + a_k(E_i - E_0)^k, \quad (2.14)$$

where E_i is the energy of channel i in keV and E_0 is a suitable reference energy. This linear polynomial is useful to describe the continuum over a region 2-3 keV wide. The reason why this polynomial is expressed as a function of $(E_i - E_0)$ is that i^3 can get as high as 10^9 , whereas $(E_i - E_0)^3$ is at most 10^3 . Values for k are usually in the range of 0 to 2. Polynomials of order higher than 4 tend to have physically unrealistic oscillations.

A polynomial that can be used to model the continuum over the entire spectrum is an exponential polynomial:

$$y_b(i) = a_0 \exp [a_1(E_i - E_0) + a_2(E_i - E_0)^2 + \dots + a_k(E_i - E_0)^k]. \quad (2.15)$$

Values for k as high as 6 can be appropriate to describe a continuum from 2 to 16 keV. [6]

Description of fluorescent lines

The simplest way to describe the profile of a peak is a single Gaussian, since the response function of a semiconductor detector is mostly Gaussian. It can be completely characterized by the three parameters position μ , width σ and area A :

$$\frac{A}{\sigma\sqrt{2\pi}} \exp\left[-\frac{(x_i - \mu)^2}{2\sigma^2}\right]. \quad (2.16)$$

The peak area is a linear parameter, but the width and the position are non-linear. The often used FWHM for a Gauss peak is given by:

$$\text{FWHM} = 2\sqrt{2 \ln 2} \sigma \approx 2.35\sigma. \quad (2.17)$$

To describe a whole spectrum with single Gaussian requires a lot of parameters. 10 elements with 2 peaks each ($K\alpha$ and $K\beta$) gives already 60 parameters to be optimized. This gets unmanageable very quickly, there are ways that the fitting function can be written differently.

The most obvious step is to stop optimizing the position and width of each peak individually, since the energies of the fluorescent lines are very well known. The peak function can be rewritten in terms of energy, by first defining the energy of channel 0 as *Zero* and expressing the spectrum *Gain* in electron-volts per channel, which gives the energy of channel i as:

$$E(i) = \text{Zero} + \text{Gain} \cdot i. \quad (2.18)$$

The Gaussian peak can then be written as:

$$G(i, E_j) = \frac{\text{Gain}}{s\sqrt{2\pi}} \exp\left[-\frac{(E_j - E(i))^2}{2s^2}\right]. \quad (2.19)$$

with E_j being the energy of the X-ray line in eV and s the peak width given by:

$$s^2 = \left(\frac{\text{Noise}}{2.3548}\right)^2 + 3.58 \cdot \text{Fano} \cdot E_j. \quad (2.20)$$

The *Noise* in this equation is the electronic contribution to the peak width (about 80-100 eV FWHM) and the factor 2.3548 to convert to σ units. *Fano* is the Fano factor (~ 0.114), and 3.58 is the energy required to produce an electron-hole pair in silicon. $\text{Gain}/s\sqrt{2\pi}$ in equation (2.19) is required to normalize the Gaussian so

the sum over all channels is unity. The transition from fitting the peak position individually to describing the whole spectrum with *Zero*, *Gain*, *Noise* and *Fano* drastically reduces the dimensionality of the fitting problem.

Another modification to the fitting function is to move away from fitting the fluorescence line of each transition from an element separately, but to model the whole response function of an element. As already mentioned above, there is a fixed intensity ratio between all transitions ending in the same shell. The spectrum of an element can then be represented as:

$$y_p(i) = A \sum_{j=1}^{N_p} R_j G(i, E_j), \quad (2.21)$$

where G is the Gaussian defined in equation (2.19) with energy E_j and R_j being the relative intensities of the lines. The summation over all lines in the group N_p will give $\sum R_j = 1$. This not only drastically reduces the number of parameters, but also improves the ability of the method to resolve overlapping peaks. If for instance the $K\alpha$ peak of one element overlaps with some other line, it can be hard to determine how much of the area belongs to which peak. If the $K\beta$ peak of the same element is not interfered with however, the area of the $K\alpha$ peak is known as well. This leaves the rest of the area for the overlapping line. [6]

3. GUI

JPeakFit is a peak-deconvolution software for X-ray fluorescence spectra developed in Java. It features a graphical user interface (GUI) with multiple tabs. The program was written with ease of use in mind and the layout is designed to streamline the process of fitting a spectrum. This chapter will describe how to use all the components in each tab. The explanation how the program is structured programmatically is given in chapter 4.

3.1. File Tab

When starting JPeakFit this tab will be selected first. It provides access to some general functionality like file IO and starting the fit routine (figure 3.1).

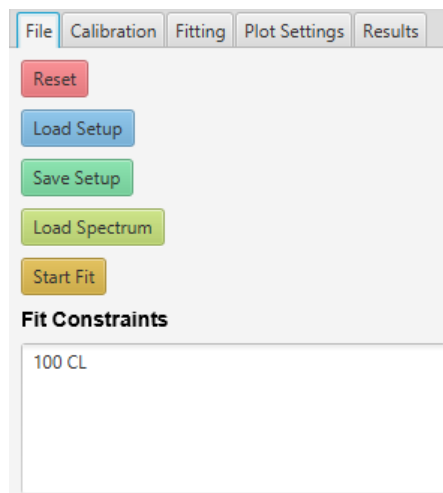


Figure 3.1.: The *File Tab* in JPeakFit.

The button ‘Save Setup’ can be used to save the settings of the current session, which can later be loaded with the button ‘Load Setup’. The result calculated through the fit routine is not saved, but can easily be recalculated since all the settings are restored when loading. Files created when saving use the ending ‘.jpf’.

The first step of fitting a spectrum is to load it into JPeakFit. This can be done by pressing ‘Load Spectrum’ and selecting a spectrum file with the file-format ‘.spe’. This should be the first step of the fitting process, since a number of functions require a spectrum to be loaded. After the spectrum has been imported successfully, it will be visible in the Plot window on the right (see figure 3.2).

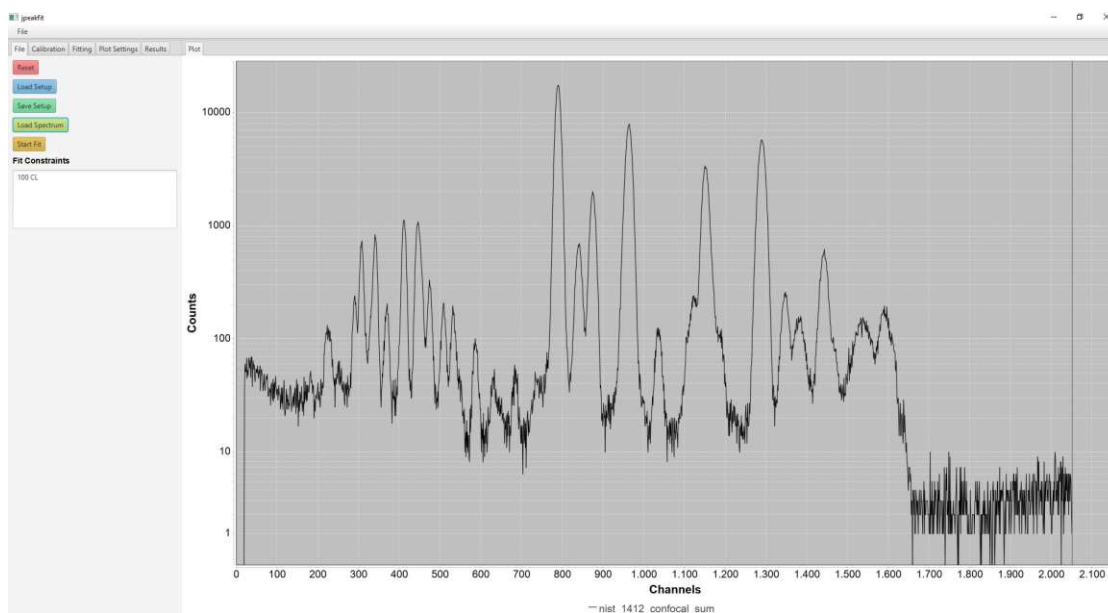


Figure 3.2.: A spectrum has been loaded.

The last button in the *File Tab* is labeled ‘Fit’. Pressing it will start the fit routine according to the *Fit Constraints* given in the text field below. A description of how the fit routine works will be given in the next chapter (4.5.1). The result will be calculated in a number of steps equal to the number of constraints given, which tell the fit algorithm what should be optimized during each step. Every row can contain one constraint which consists of at least two parameters separated by spaces. The first parameter has to be the number of maximum iterations for this step followed by at least one of the following fit parameters:

- **CL:** This stands for *ChemLibrary* and is the most important fit parameter. When this is given the fit routine will adapt the area for each element peak, which is ultimately the wanted information. Therefore it is sensible to include this at least in the first and the last constraint in the list.
- **BG:** When this parameter is given, the *Background* will be adapted in this step. This will only have any effect on the result if a *Background* other than

NullBackground is selected (see section 3.3.4)¹.

- **EC:** This is for adapting the *Energy Calibration*. It will fine tune the energy axis calibration and adapt the parameters *Fano* and *Noise* (see chapter 3.2.2). Including this option will result in a prolonged fitting time, since more computations are required.

The *Fit Constraints* could look like this:

```
100 BG CL
20 EC CL
```

This would start the fitting routine with at most 100 iterations where both the background and the peak areas are adapted in each iteration, followed by a maximum of 20 iteration where the energy calibration and the peak areas are altered.

3.2. Calibration Tab

The second tab is the *Calibration Tab*, which allows setting the *Region of Interest (ROI)* and calibrating the energy of the channels. It is also useful in identifying unknown peaks with the *KLM-Marker* feature (figure 3.3).

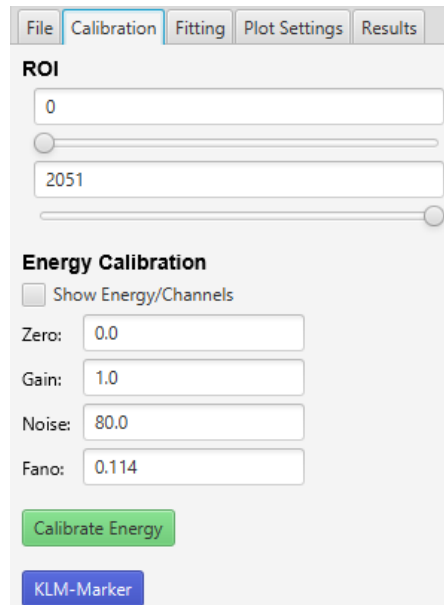


Figure 3.3.: The *Calibration Tab* in JPeakFit.

¹This does not affect the *Filter-Background* (see section 3.3.4).

3.2.1. ROI

The *ROI* will affect a lot of functions like the *Filter-Background*, the *KLM-Marker* and the fit itself. The bounds of the *ROI* can either be set by directly entering the desired number, or by dragging the slider. If the slider is selected the arrow keys can also be used to move the *ROI* by one channel at a time.

3.2.2. Energy Calibration

This section of the tab is for the energy calibration of the channels. On top there is a checkbox, to switch the x-axis from showing channels or energy in eV. The energy for channel i is calculated with the values for *Zero* and *Gain* from the text boxes below with the formula (equation (2.18)):

$$E(i) = Zero + Gain \cdot i.$$

JPeakFit assumes the peaks in the spectrum to be Gaussian (see section 2.4.1). The values for *Noise* and *Fano* have an impact on the standard deviation of the Gauss peaks (see equation (2.20)). They can be set manually or calculated with the use of the *EC* constraint during fitting.

Zero and *Gain* can either be set manually or calculated by assigning two peaks in the spectrum to element lines. This can be done by pressing the ‘Calibrate Energy’ button, which opens the menu seen in figure 3.4. Additionally they are also adjusted if the *EC* constraint is used during fitting.

The menu in figure 3.4 can be used to detect peaks in the spectrum and match them to known element peaks. Pressing ‘Search peaks’ will scan the spectrum inside the *ROI*, highlight and number the found peaks. Below the button is a text box that can be used to select the wanted peak. This can either be done by entering the number by hand into the text box, using the up and down buttons or using the up and down arrow keys on your keyboard, while the text box is selected. The currently selected peak will be marked with a red vertical line in the plot. JPeakFit uses the algorithm presented in section 2.2.4 with some alterations. There are only 2 parameters that are used to decide if a found peak is valid, the *Search width* w and the *Sensitivity* s . The former will only allow peaks that are decreasing monotonously to either side from the peak top for at least $\frac{w}{2}$ channels rounding down. The later requires the channel counts at the edges of the *Search width* to not be higher than $s \cdot peakheight$. To ensure that statistical fluctuations don’t interfere with the monotony of the peaks, the spectrum is smoothed with a Savitzky-Golay filter with a smooth width of 14. Information on this smoothing algorithm can be found in section 2.2.2.

Once a peak is selected, the button ‘Set energy for selected peak’ can be pressed,

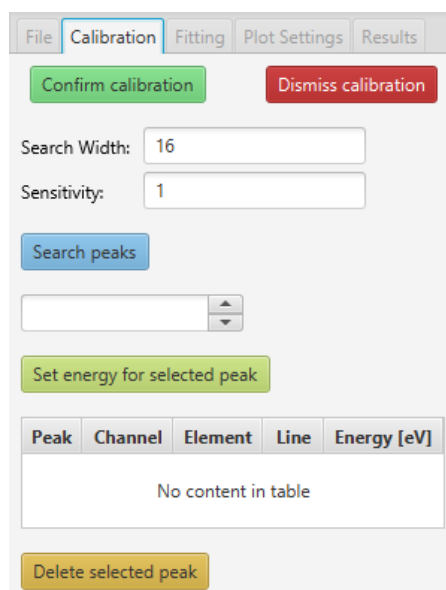


Figure 3.4.: The *Calibrate Energy* menu in JPeakFit.

which opens the window seen in figure 3.5. To choose the line corresponding to

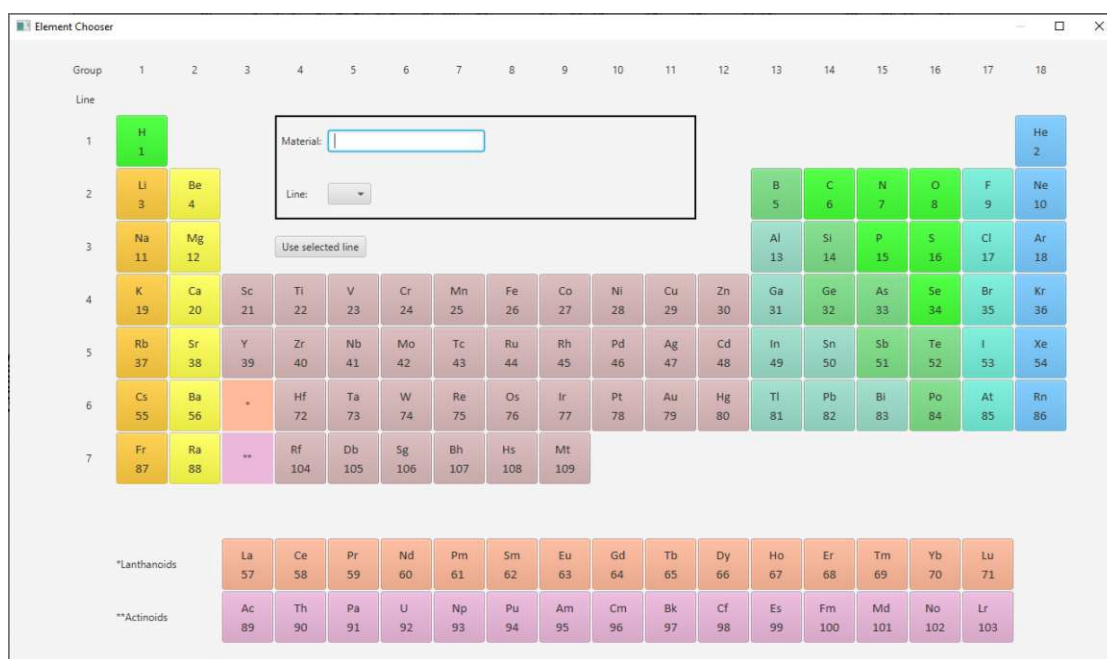


Figure 3.5.: Window to set the energy of a peak.

the peak, an element has to be selected either by pressing the elements button in the periodic table or by typing the chemical symbol of the element in the text box next to 'Material:' and pressing enter. Once an element is selected the drop down box next to 'Line:' will contain all the transitions found in the database, with the KL3 line being preselected. After the line has been picked, pressing 'Use selected line' will close the window and add the line-peak-pair into the table below the 'Set energy for selected peak' button. To delete a line-peak-pair from the table the corresponding entry has to be selected in the table and the button 'Delete selected peak' has to be pressed.

To complete the energy calibration exactly two line-peak-pairs have to be entered into the table. When the button 'Confirm calibration' at the top is pressed, the energy calibration is closed and the two pairs in the table are used to calculate the *Zero* and *Gain* for the spectrum. Pressing the 'Dismiss calibration' Button at any time will exit the energy calibration and discard all changes.

3.2.3. KLM-Marker

After performing the energy calibration it can be useful to open the *KLM-Marker* menu by pressing the button with the same name (figure 3.6). This menu will have

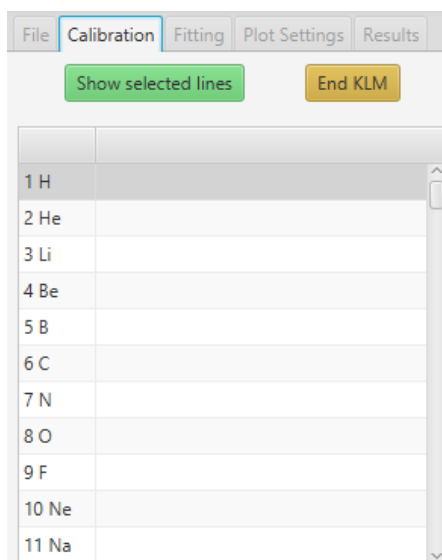


Figure 3.6.: The *KLM-Marker* menu in JPeakFit.

a list of all elements on the left hand side and a plot of the smoothed spectrum within the *ROI*. Selecting an element in the list on the left will show markers for

where these elements K-, L- and M-lines would be with the current energy calibration. Markers for the K-lines are blue, L1-lines are red, L2-lines are green, L3-lines are magenta and M-lines are cyan. When there is more than one transition in a group, the marker for the most probable one will have a height exactly matching the shown spectrum, whereas the height of markers for other transitions is calculated based on the intensity ratio of that transition compared to the most probable one. This should give a rough estimate if different peaks could stem from the same element. It should be kept in mind, that a high background and overlapping peaks will interfere with the suggested peak height ratios.

At the top of this menu is the button ‘Show selected lines’. Pressing it will draw a marker of every selected element into the plot. This can be used to see which peaks are not yet accounted for. Escape and sum peaks are also included. The height of every marker is set to fit exactly the height of the shown spectrum at its location and probabilities of transitions are ignored. An example of this can be seen in chapter 5 in figure 5.8.

3.3. Fitting Tab

The *Fitting Tab* is used to enter which elements the algorithm is looking to fit to the spectrum and also to set the background and the detector material (figure 3.7).

3.3.1. Element Chooser

Before starting the fit routine, the elements present in the spectrum have to be selected. This can be done by pressing the button ‘Element Chooser’ which opens a window with a periodic table (figure 3.8). After an element is selected, the buttons in the black rectangle - the transition buttons - are activated. In the left corner, the currently selected element can be seen. The active transition buttons correspond to the transitions for that element, which are available in the database. Pressing one of the transition buttons once gives it a red border, which indicates that this transition group has been selected for the selected element. Pressing it again deletes the border again. If an element has at least one transition button selected it will also have a red border.

There are eight transition buttons with the following labels:

- **K:** Choosing this transition button, will enable all tabulated transitions that end in a K-shell for the fit. Inter-transitional probabilities are used for the fit. Selecting this button will deactivate the *KL* and *KM* buttons.

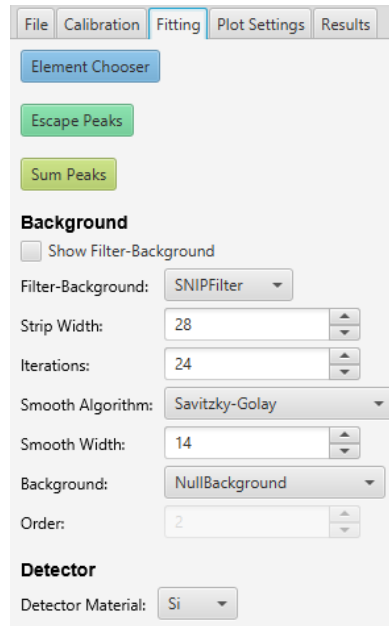


Figure 3.7.: The *Fitting Tab* in JPeakFit.

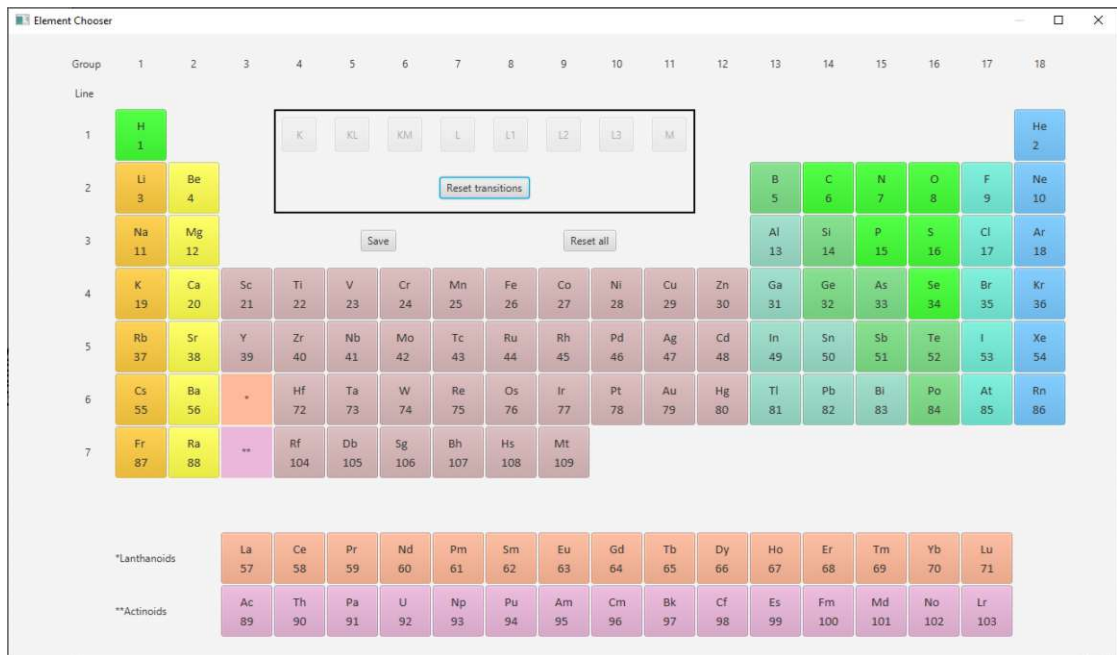


Figure 3.8.: The *Element Chooser* window.

- **KL:** When this transition button is selected all tabulated transitions from an L- to a K-shell are subject to be fitted. Inter-transitional probabilities are not considered in this case.
- **KM:** Similar to the previous button, this enables all tabulated transitions from an M- or N- to a K-shell and inter-transitional probabilities are again ignored. Selecting both *KL* and *KM* yields the same transitions being fitted as just selecting *K*, while not considering inter-transitional probabilities.
- **L:** Unlike to selecting *K*, choosing the *L* buttons is exactly the same as choosing all three of *L1*, *L2* and *L3*. This button is just for convenience to reduce the number of clicks.
- **L1/L2/L3:** Selecting one of those transition buttons will enable all tabulated transitions that end in the L1-, L2- or L3-shell respectively.
- **M:** Finally the *M* button, will enable all tabulated transitions that end in the M-shell.

After all wanted transitions for every element have been selected, pressing the ‘Save’ button will close the *Element Chooser* window and save the selection. The ‘Reset transitions’ button will reset all selected transition buttons for the current element, while pressing the ‘Reset all’ button will reset all transitions for all elements.

3.3.2. Escape Peaks

Every element that was selected in the *Element Chooser* is available in the menu that opens up when the ‘Escape Peaks’ button is pressed (figure 3.9). The table

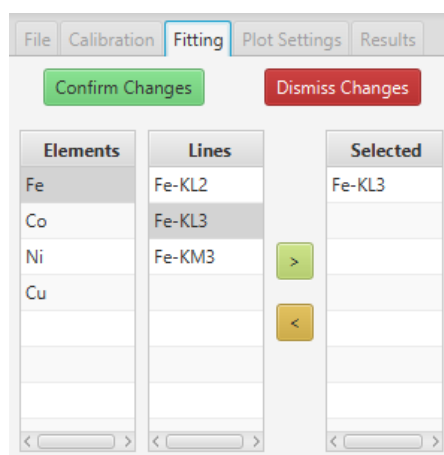


Figure 3.9.: The *Escape Peaks* menu.

‘Elements’ lists them all and once one entry is selected, the table ‘Lines’ shows all the lines that have been chosen in the *Element Chooser* for the selected element. When a line is selected, a marker at the position of where the escape peak for that line would be is drawn into the plot. If the marker is outside the ROI nothing happens. The energy calculation for the escape line is based on the formula:

$$E_{Esc} = E_{El} - E_K,$$

where E_{El} is the energy of the selected line and E_K is the energy of the KL3 line of the selected detector material.

When a selected line should be added to be considered by the fit algorithm, pressing the button ‘>’ will add it to the ‘Selected’ table, from where it can be removed again with the button ‘<’. Once every wanted line has been added to the ‘Selected’ table, the ‘Confirm Changes’ button will accept all changes made and close the menu, while the button ‘Dismiss Changes’ will close the menu without saving.

3.3.3. Sum Peaks

All the lines that are available in the *Escape Peaks* menu are also available in the *Sum Peaks* menu (figure 3.10), which can be opened by pressing the ‘Sum Peaks’ button. To add a sum peak, choose one line in both the top and the bottom ‘Lines’ table by first selecting an element in the ‘Elements’ table and pressing the ‘>’ button. This again adds it to the ‘Selected’ table, from where it can be removed with the ‘<’ button. When two lines in the ‘Lines’ table or a sum peak in the ‘Selected’ table is selected, the combined energy of the respective lines is displayed in form of a marker in the plot. The ‘Confirm Changes’ and the ‘Dismiss Changes’ buttons close the menu with and without saving the changes respectively.

JPeakFit doesn’t automatically add all possible sum peaks to the spectrum. Instead the user is given control of which sum peaks should be considered by the algorithm. Other modern deconvolution software usually only leave the option to calculate sum peaks for all lines of the fit. The individual selection of lines responsible for a sum peak can reduce the optimization time, due to a smaller number of free fit parameters.

3.3.4. Background Settings

This section of the *Fitting Tab* is to manipulate the shape of the *Filter-Background* and the *Background* (figure 3.7). The *Filter-Background* is calculated by smoothing the spectrum and then filtering it. The smoothing and filtering parameters

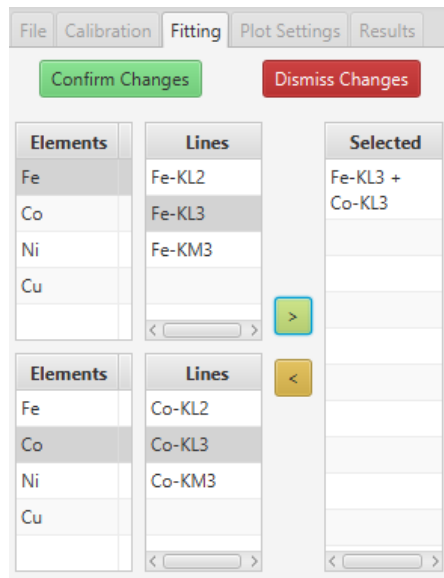


Figure 3.10.: The *Sum Peaks* menu.

can be adjusted in this section. This background can be calculated before the fit starts and can therefore be drawn into the plot before fitting. The *Background* however is fitted parallel to the elements, by varying it's parameters and trying to minimize the deviation between the result and the original spectrum and can therefore not be drawn into the plot.

Right at the top of the *Background Settings* section is the option to show and hide the *Filter-Background* via a checkbox. Next is a drop down menu to select how the filtering should be done. Right now there is only the option of choosing the *SNIPFilter* or turning filtering off completely by selecting *NullFilter*. The SNIP (**S**tatistics-sensitive **N**on-linear **I**terative **P**eak-clipping) filter is a variation of the one developed by Ryan et al [15] (for more information see chapter 4.6). When filtering is active the 'Strip Width' determines the amount of channels the *SNIPFilter* considers at a time, while the 'Iterations' determine the number of times the filter is run on the spectrum.

For the 'Smooth Algorithm' there are two options, the *Savitzky-Golay* filter and the *Low Statistics Digital Filter* (see chapter 2.2.1). For both the parameter 'Smooth Width' can be chosen, to determine the number of channels that are used to smooth.

The drop down menu right of 'Background' determines the algorithm used to calculate the background during the fit. It can either be deactivated by selecting 'NullBackground', or use a polynomial by selecting 'PolynomialBackground'. When the latter is selected, the order of the polynomial can be chosen via the text

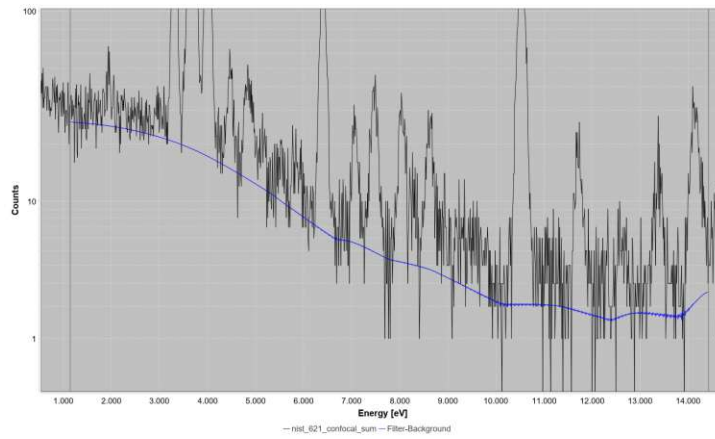


Figure 3.11.: A *SNIPFilter* background in blue. Used parameters: Strip width: 28, Iterations: 24, Smoothing: Savitzky-Golay, Smooth width: 14.

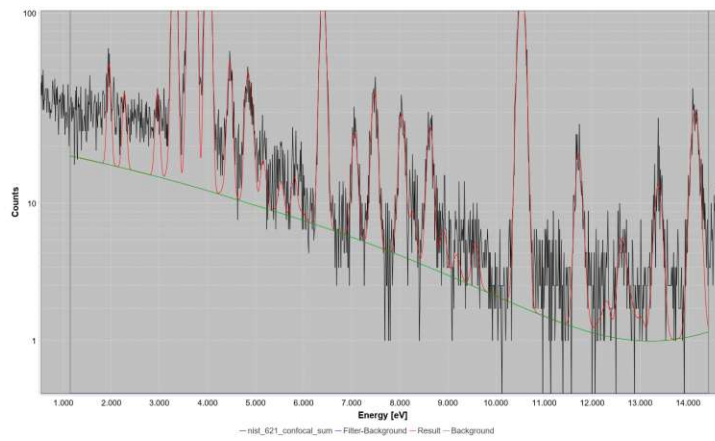


Figure 3.12.: A *PolynomialBackground* of order 3 in green.

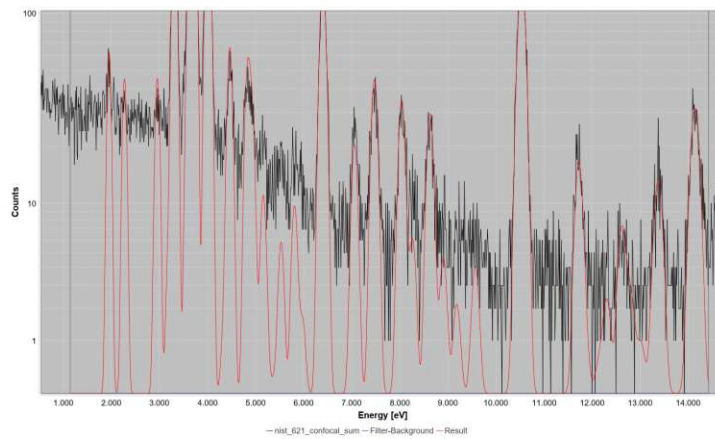


Figure 3.13.: A *NullBackground*.

box right of ‘Order’. The *Background* is also automatically deactivated if a *Filter-Background* other than *NullFilter* is used, since in that case the continuum is already estimated. Figures 3.11-3.13 show the output of the different backgrounds on a spectrum.

3.3.5. Detector

This allows the selection of the detector material and can either be silicon or germanium by selecting ‘Si’ and ‘Ge’ respectively. This setting is important to correctly calculate the energy of escape peaks (see chapter 2.1.4).

3.4. Plot Settings Tab

The *Plot Settings Tab* allows the customization of what is shown in the plot window via the following check boxes (figure 3.14):

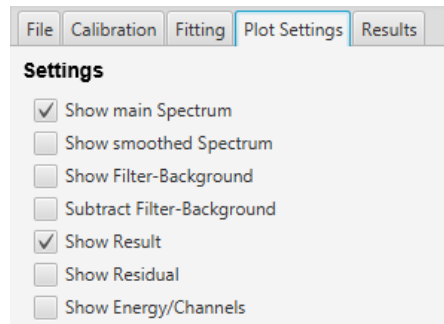


Figure 3.14.: The *Plot Settings Tab* in JPeakFit.

- **Show main Spectrum:** Shows the original spectrum as it was loaded from the .spe file when checked.
- **Show smoothed Spectrum:** When this checkbox is chosen, the smoothed version of the loaded spectrum is shown. The smoothing can be adjusted within the *Fitting Tab*.
- **Show Filter-Background:** This toggles the *Filter-Background* on and off. This checkbox is also featured in the *Fitting Tab* from where the *Filter-Background* can also be altered, to best describe the background. Figure 3.15 shows the plot with the first three check boxes checked.
- **Subtract Filter-Background:** With his checked, the *Filter-Background* is subtracted from the main, the smoothed and the result spectrum. The resulting spectra are only shown inside the *ROI*, since the *Filter-Background* is only defined within that region.

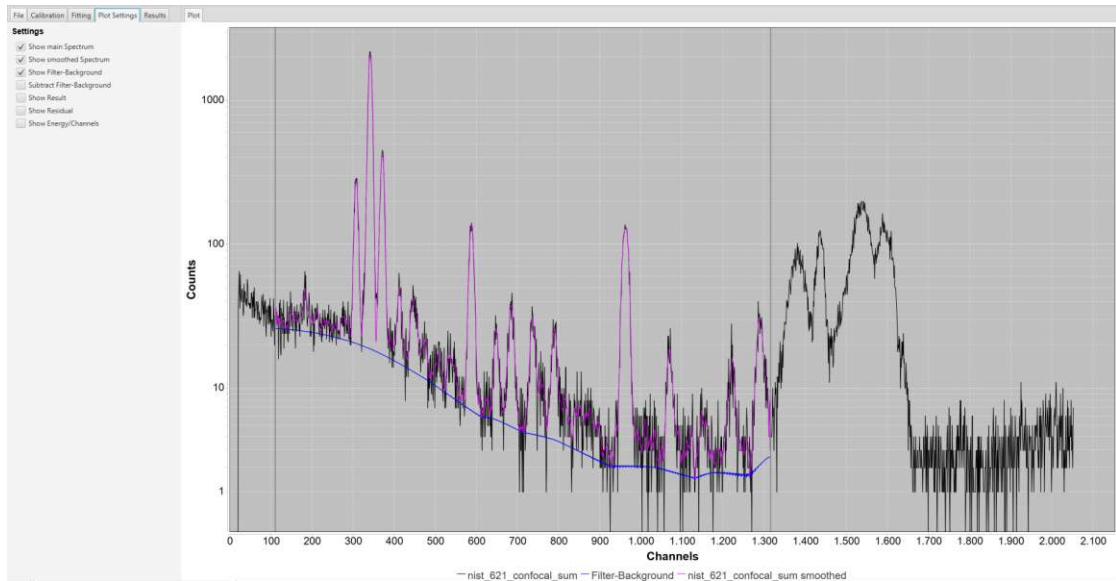


Figure 3.15.: The Plot when main spectrum, smoothed spectrum and filter-background are shown with axis set to channels.

- **Show Result:** When this is selected, the result from the fit will be drawn in the plot, if it is available. Before a fit has been performed, this checkbox will not change anything in the plot.
- **Show Residual:** Shows the standard residual of the fit and the main spectrum, which is calculated per channel and defined as $\frac{m-r}{\sqrt{r}}$, where m is the count in a measured spectrum channel and r in the result channel. This feature can be very useful in determining the quality of a fit but is missing in some modern software packages.
- **Show Energy/Channels:** This can be used to toggle the units of the x-axis, where not checked shows the channels and checked shows the energy in eV. The same checkbox can be found in the *Calibration Tab*. Figure 3.16 shows the plot with the last four and the first check boxes checked.

3.5. Results Tab

When starting the program, the *Results Tab* is empty, but it will be populated once a fit is complete (figure 3.17). The table shows the counts, the statistical uncertainty and the background counts for each previously selected element and line. If the counts for one line group is zero, the lines in that group will not be listed. Selecting a line, will show a marker at the corresponding position in the plot. On the top left of this tab the reduced chi-square score of the fit is shown,

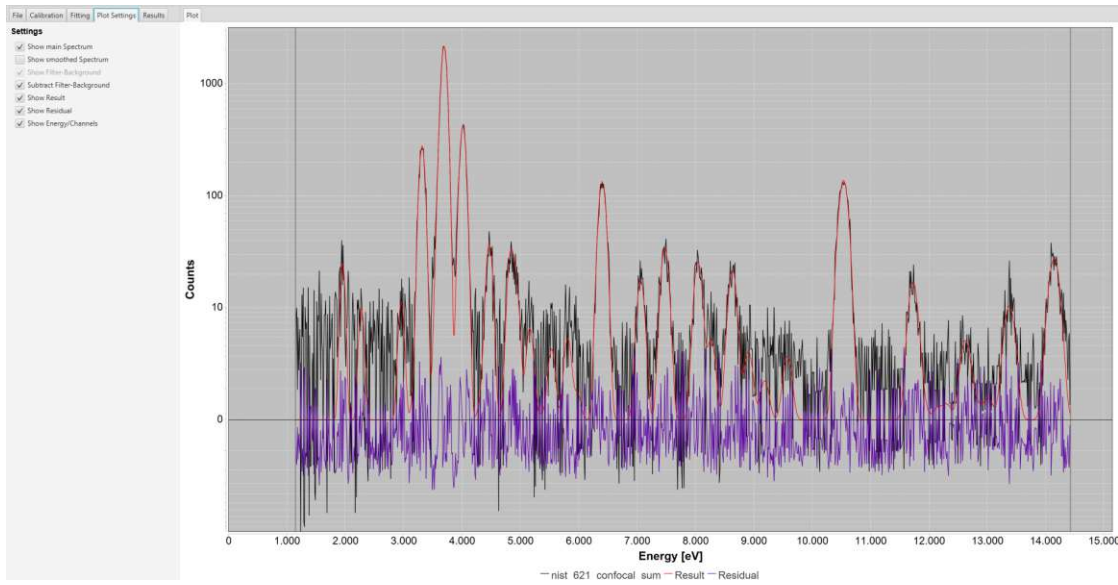
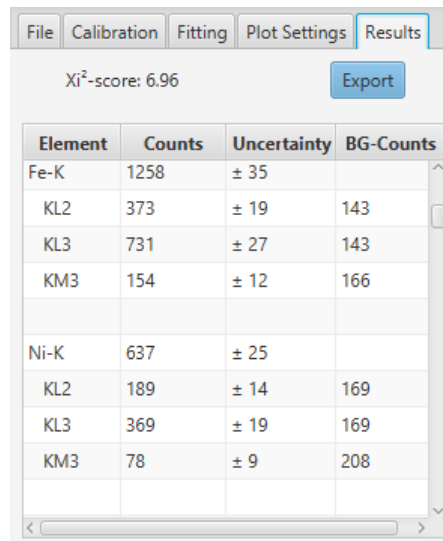


Figure 3.16.: The Plot when the filter-background is subtracted and residual and main spectrum are shown with axis set to energy.



File Calibration Fitting Plot Settings **Results**

χ^2 -score: 6.96 Export

Element	Counts	Uncertainty	BG-Counts
Fe-K	1258	± 35	
KL2	373	± 19	143
KL3	731	± 27	143
KM3	154	± 12	166
Ni-K	637	± 25	
KL2	189	± 14	169
KL3	369	± 19	169
KM3	78	± 9	208

Figure 3.17.: The *Results Tab* in JPeakFit.

which is calculated by the following formula:

$$\chi^2 = \frac{1}{m-p} \sum_i \frac{(R_i - S_i)^2}{S_i},$$

where R_i are the counts in the channels of the result spectrum and S_i are the counts of the channels of the original spectrum. $m - p$ are the degrees of freedom, with m being the number of channels and p the number of fitted parameters.

3.5.1. Export Results

To save the results the ‘Export Results’ button can be pressed. A file save dialog will open up with the option of 2 formats. The results can be saved in exactly the same way as they are presented in the table as a .csv file. The other option is to choose a .ASR file. This format is needed for the fundamental parameter based quantification software package ATI-QUANT, which was developed by Grossmayer[18], Necker[19] and Holub[20] at the Atominsitut of TU Wien. Not every transition is listed, but the K-, L- and M-lines are grouped together. JPeakFit adds the sum of the peak areas of the two most dominant peaks of each group as the total, which is KL3+KL2, L3M5+L2M4 and M5N7+M5N6 for K, L and M respectively. The file has an entry of one such group in every row, with multiple columns. The first column contains the atomic number of the element. The second column marks which group is considered with numbers, where ‘1’ stands for K, ‘2’ for L and ‘3’ for M. In the third column the energy of the peak is recorded, which is simply the energy of the most dominant line. Columns four and five contain the peak area and the standard deviation. The final column contains the chi-square value for the peak group of the column, but since this information is not available in JPeakFit, ‘0’ is put into every row.

3.6. Plot

The plot is always visible at the right side (figure 3.18). The plot can be zoomed, by dragging a rectangle over the area that should be zoomed into. The rectangle has to be drawn from the top left corner to the bottom right corner. A rectangle drawn in any other way will result in the plot being restored to the original zoom level. Right clicking anywhere on the plot will open a menu at that position with two options. The first is to export the current view of the plot to a .png or .jpg by hovering over ‘Export As’ and then choosing the desired file format. The second option is to toggle the y-axis of the plot between a logarithmic and a linear scale. Depending on what the axis is currently set to, this point will read either ‘Set Y Axis Lin’ or ‘Set Y Axis Log’.

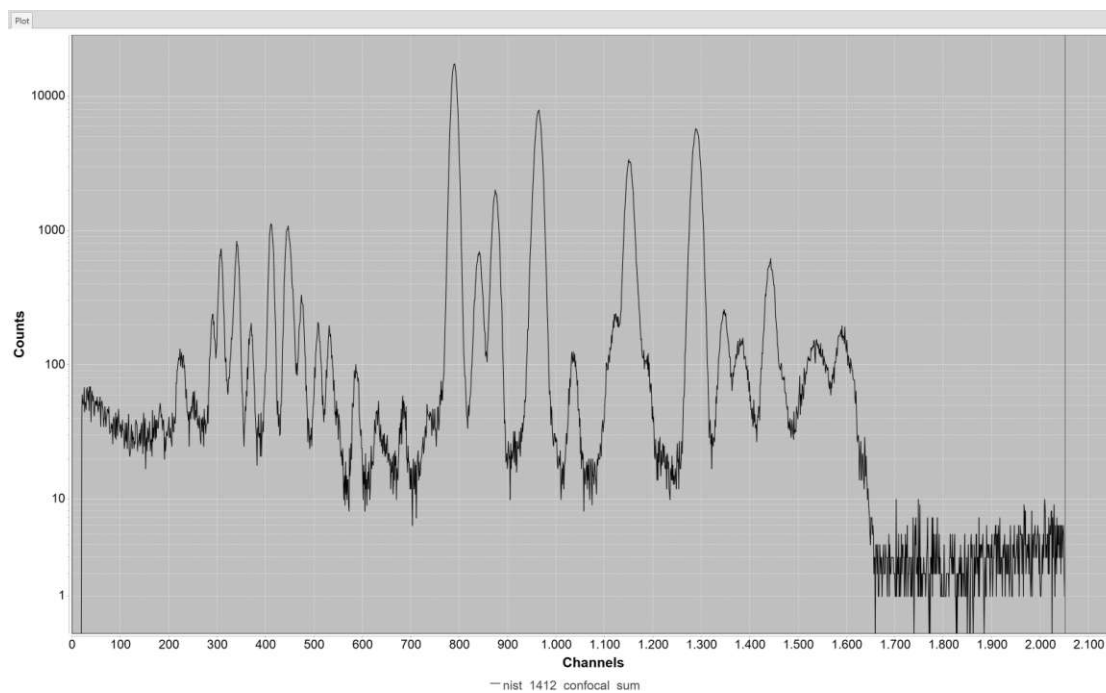


Figure 3.18.: The *Plot Tab* in JPeakFit.

4. Description of classes

This chapter will explain how JPeakFit is structured programmatically, which is meant as a short overview to simplify the further development of the application. Furthermore the algorithms used will be described here.

4.1. Model-view-presenter

The structure of this application is based on the state-of-the-art model-view-presenter (MVP) design pattern. The idea of this approach is to split the program into three different parts with specialised responsibilities. The model contains the information about the current settings and selections the user has made. The view is responsible for displaying the user interface and presenting the wanted information to the user. The presenter handles the user inputs and changes the model and the view accordingly.

There are different variations of the MVP pattern [21], the one used here is best described as Passive View [22]. That means that the view and the model are not connected at all and everything is handled directly by the presenter. This concept is broken in a few select places, which will be discussed below.

4.2. Model

The *Model* class contains information about the current state of the settings made by the user. Whenever some value is changed in the view, the presenter changes the corresponding value in the *Model*. This is useful when saving the current setup, as all the information that has to be saved is stored inside this class. The *Model* is saved into a file using the JAXB library, which allows easy conversion of Java classes into XML and the other way around. Using the XML format also has the advantage of the saved files being human readable. [23]

4.3. View

To make the *View* class more manageable it is split up into multiple sub-*Views*. There is a separate class for every tab, the menu, the pop-up windows and one

to handle the plot. The *View* class is responsible for creating the user interface using the sub-*View* classes and to provide the presenter with functions to alter what is displayed to the user. As the *Presenter* is unaware of the sub-*Views*, the main *View* has to handle all the requests and delegate them to the corresponding sub-*Views*.

On the flip side, the *Presenter* provides functions to the *View* to handle user input. Almost all of the program logic is handled in the *Presenter*. The only exceptions to this are in the *FittingTab* class - when selecting the lines in the Escape and Sum Peaks menu - and in the *PeriodicTable* class - when selecting the elements in the table. Even though it would have been possible to let the *Presenter* handle those tasks, the author felt it would simplify the code enough to justify letting the *View* handle some of the program logic, which doesn't directly affect the *Model*.

4.3.1. Spectrum Chart

The plot on the right side of the program is generated with the help of the *SpectrumChart* class. It was created to allow simple plotting and manipulation of X-ray spectra [24]. It functions as a wrapper class to the JFreeChart library [25], to make it easier for the plot to be changed from other classes.

4.4. Presenter

Similar to the *View*, the *Presenter* is split into multiple sub-*Presenters*. Each one of the latter provides functions for the respective sub-*View*, which are called when the User takes certain actions on the interface. With the given data, these functions do some calculations and then change the *Model* and the *View* accordingly.

4.5. JPeakFit CLI

The JPeakFit GUI is based on a command line interface (CLI) also named JPeakFit, which was developed by Christian Hofstadler [26]. The GUI takes the user input, transforms it into the required format and passes it to the CLI. When the CLI is finished with the calculation, the data is read out by the GUI and presented to the user.

4.5.1. Description of the fit routine

The CLI will start to do the fitting according to the fit constraints given by the user (see section 3.1). As mentioned above there are 3 constraints to be chosen, CL, EC and BG. Each one of those constraints has parameters, used in the fit function

that can be adapted by the fitting algorithm. The implementation follows the theory described in 2.4.1.

4.5.2. Fit function

The fit function that is minimized during the fit is the χ^2 function from equation (2.12).

CL - ChemLibrary

This is the heart of the fitting routine, where the counts for the chosen elements are fitted. All chosen sum and escape peaks are fitted individually, as well as all the transitions chosen with the **KL** and **KM** buttons in the *Element Chooser*. All the transitions chosen with the **K**, **L1**, **L2**, **L3** and **M** buttons, are fitted using the intensity ratios of all the transitions ending in the same final shell.

Every individual peak and every peak group is represented as one parameter in the fit function. This parameter represents the counts for the peak/peaks. Increasing one of these parameters will make the corresponding fitted peak larger.

4.5.3. EC - EnergyCalibration

This adapts the position and the width of all the peaks together, following the theory found in the same section 2.4.1 ‘Description of fluorescent lines’.

The energy calibration is represented with four parameters for *Zero*, *Gain*, *Fano* and *Noise* in equations (2.19) and (2.20).

4.5.4. BG - Background

This will calculate the *Background* using the background model given by the user. Currently there is only the option for a linear polynomial by choosing *PolynomialBackground* or choosing no background by choosing *NullBackground*.

When choosing a *PolynomialBackground* it will be represented with a number of parameters equal to the order of the polynomial.

4.5.5. Fit algorithm

The fit algorithm used to find the minimum of the fit function is an implementation of Newton’s method. Newton’s method can be used to find the solution to the following equation with the differentiable function $F(x)$:

$$F(x) = 0. \quad (4.1)$$

Starting from some initial value x_0 we can construct a linear approximation of $F(x)$ near x_0 with $F(x_0 + h) \approx F(x_0) + F'(x_0) \cdot h$, and solve for $F(x_0) + F'(x_0) \cdot h = 0$ which gives:

$$h = -\frac{F(x_0)}{F'(x_0)}. \quad (4.2)$$

We therefore arrive at the iteration:

$$x_{k+1} = x_k - \frac{F(x_k)}{F'(x_k)}, \quad k = 0, 1, \dots \quad (4.3)$$

This method can be used for optimization if we consider that we have to solve the following equation to find the minimum of a function $G(x)$:

$$G'(x) = 0. \quad (4.4)$$

This is very similar to our original equation (4.1) so we can replace $F(x_k)$ in equation (4.3) with $G'(x_k)$ to arrive at [27]:

$$x_{k+1} = x_k - \frac{G'(x_k)}{G''(x_k)}, \quad k = 0, 1, \dots \quad (4.5)$$

The χ^2 function has more than one parameter, which extends the iteration process, but at its core it is the same. We want to find the solution to equation (2.13) which can be done with the following iteration:

$$a_{j,k+1} = a_{j,k} - \frac{\partial \chi^2(a_{j,k})}{\partial a_{j,k}} \cdot \left(\frac{\partial^2 \chi^2(a_{j,k})}{\partial a_{j,k}^2} \right)^{-1}, \quad k = 0, 1, \dots, \quad j = 1, \dots, m. \quad (4.6)$$

The implementation of the algorithm used in JPeakFit looks at each parameter to be fitted separately. At the beginning the value for χ^2 is calculated using the initial values for each parameter. Then the first parameter is considered and using equation (4.6) $a_{1,1}$ is calculated from $a_{1,0}$. If this change improved χ^2 the parameter is chosen as the currently best value for this parameter and the next parameter is considered. If the χ^2 value did not improve, the step size ($a_{1,1} - a_{1,0}$) is reduced by a factor of 10 and the χ^2 value is checked again. This will be repeated until some parameter specific threshold is passed or the χ^2 value improved. This has to be done in order to prevent the iteration process to jump past the minimum, which can happen if the gradient for the current parameter is steep. After every parameter has been adapted once in this fashion, one iteration is complete and the process starts anew with the new set of parameter values. This is continued until either the iteration limit set by the user is reached, or χ^2 did not improve over the course of one iteration.

4.5.6. Data bank

JPeakFit uses an SQLite data bank composed by Giancarlo Peponi with the data from [28] and [29]. All of the transitions and intensity ratios are pulled from this data bank.

4.6. SNIP filter

To estimate the *Filter-Background* JPeakFit reuses an algorithm that has already been developed earlier. The filter was implemented in line with the filter described in chapter 2.3.1, with two changes. The filter width is fixed for the entire spectrum, chosen by the user, instead of being variable and on top of the low statistics digital filter (2.2.3) the Savitzky Golay filter (2.2.2) is also offered. Details can be found in the project work “Implementation of a SNIP filter for continuum estimation of X-ray spectra for spectrum deconvolution” [24].

5. Example fit

This chapter will show how to use JPeakFit to evaluate a measured spectrum by going through all the steps with an example.

5.1. Example fit of NIST SRM 1412

The sample measured for this spectrum is the Standard Reference Material (SRM) 1412 from the National Institute of Standards and Technology (NIST), which is a multicomponent glass [30]. It was measured with a monochromatic confocal micro-X-ray fluorescence spectrometer [31].

After starting JPeakFit, the first thing to do is to load a spectrum, by clicking ‘Load Spectrum’ and selecting a .spe file with the wanted measured spectrum. Before the program knows which energy corresponds to which channel, the elements won’t line up with the correct peaks. Therefore a sensible next step is to perform an energy calibration. To do that one has to select the *Calibration Tab* at the top and press the ‘Calibrate Energy’ button. Doing so will change the layout of the tab to the one shown in figure 5.1. Pressing the ‘Search peaks’ button will place the markers seen on the same figure in the *Plot Tab*, at the positions of the peaks.

If a wanted peak is not selected, the ‘Search width’ and the ‘Sensitivity’ can be adjusted to achieve the required result (see chapter 3.2.2). Preferably two well defined peaks that are not next to each other are chosen, to improve the accuracy of the calibration. In this case the peaks for Zn-KL3 and Sr-KL3 are a good choice, which are the peaks labeled 12 and 19 respectively. To set the energy for a peak, it has to be selected with the text box below the ‘Search peaks’ button. Once the correct peak is selected, indicated by the red marker, pressing the ‘Set energy for selected peak’ button will allow choosing the corresponding X-ray line for that peak (see figure 5.2). When both peaks have been identified, the energy calibration can be applied by pressing ‘Confirm calibration’, which will calculate the right values for Zero and Gain. To check if this calibration is correct, the KLM-Marker is very handy. Pressing the button with the same name will show a list of elements on the left, which when selected will show their X-ray lines on the plot. If some expected or frequently occurring elements align nicely with the peaks it can be assumed that the calibration is correct.

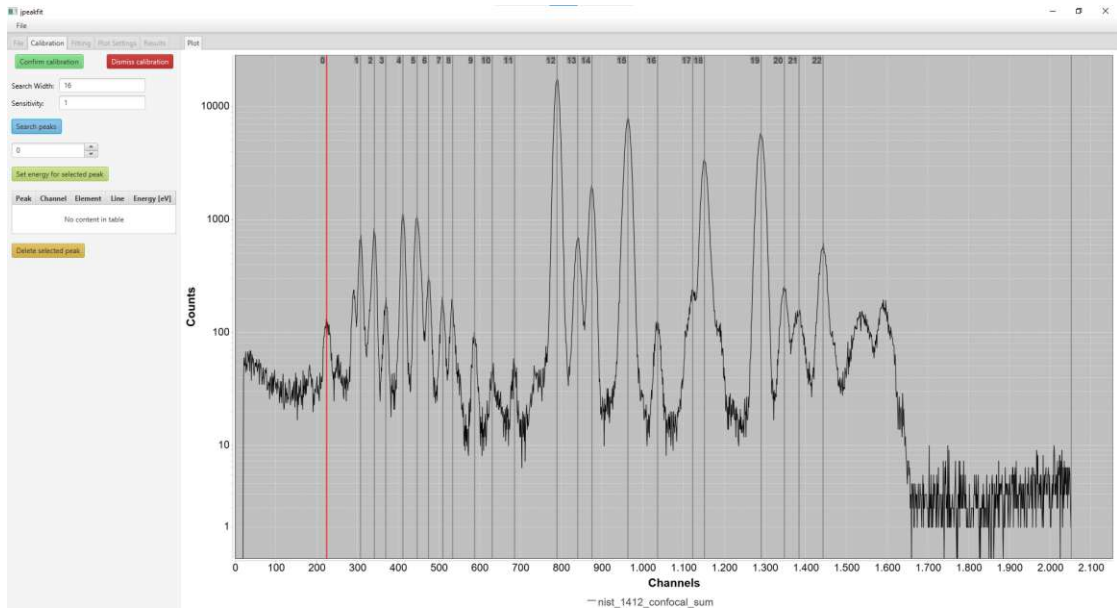


Figure 5.1.: Peaks in the spectrum have been marked

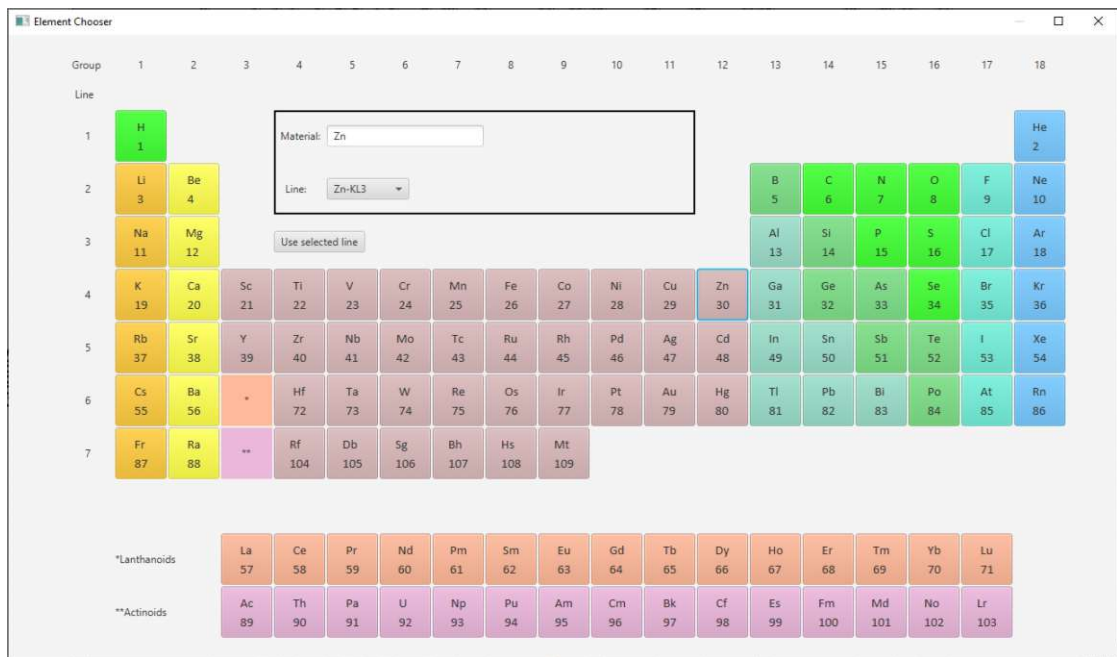


Figure 5.2.: Menu to appoint an X-ray line to a peak

The next step is to set the region of interest or ROI. Since the ROI affects the Filter-Background it can be useful to set the checkbox to show it in the *Plot Settings Tab*. The ROI should be set in a way to exclude the areas that are dominated by noise. For this spectrum a good setting is the region between 157 and 1488.

Once this is done, the elements which are present in the spectrum have to be identified. This process demands some experience from the user, as it is for instance not always easy to distinguish the peaks of some elements that overlap. A great tool for the identification is the KLM-Marker. It shows exactly where an element's lines are positioned with the set calibration and also the relative intensities for transitions with the same final shell. There is no relation between the intensities of the three L line groups in JPeakFit. To make identifying the peaks easier, the numbers from the peak search will be used to name the peaks (figure 5.1).

Going through the element list in order of increasing Z numbers, the first elements that show a good fit are potassium for peak 1 and calcium for peaks 2 and 3, followed by iron, nickel and copper for peaks 9, 11 and the peak between 11 and 12 respectively (figure 5.3).

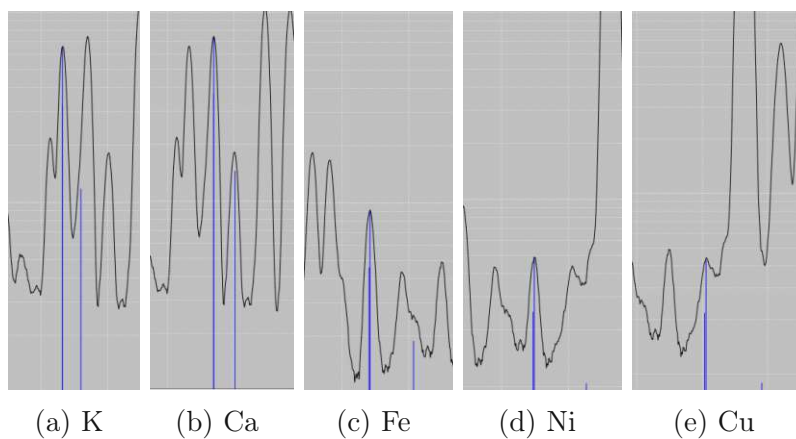


Figure 5.3.: KLM-Marker for elements of K, Ca, Fe, Ni and Cu

The next good fit is zinc for peaks 12 and 14. Arsenic looks like a good fit for the KL3 line at peak 15, but the KM3 line is completely missing, which means that peak 15 is not produced by arsenic. Krypton also looks good, but since it is a gas at room temperature and very rare in the atmosphere, this is highly unlikely. The last peak for a K transition inside the ROI comes from strontium with peaks 19 and 22 for KL3 and KM3 respectively (figure 5.4).

Since the K peak produced by the molybdenum anode was removed when setting

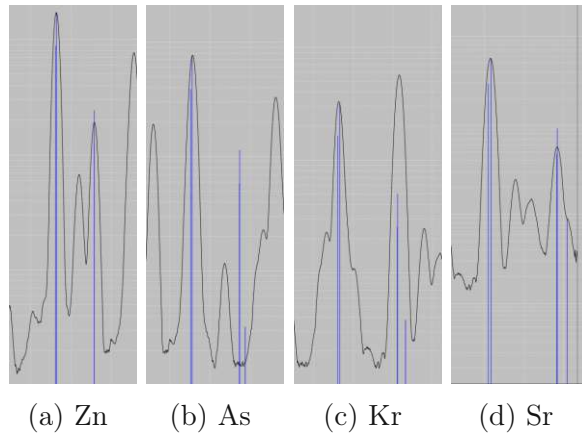


Figure 5.4.: KLM-Marker for elements of Zn, As, Kr and Sr

the ROI, this concludes all the peaks from transitions to the K shell. The strontium L lines have high enough energy to be also visible on the spectrum, left of peak 0. Peak 1 and the one left to it can be contributed to cadmium and peaks 4-8 fit nicely for barium. The final element, that covers almost all of the remaining peaks is lead, with peaks 13, 15-18, 20 and 21 with the L lines. Since the L lines are that intense, leads M lines have also to be considered, which make up peak 0. (figures 5.5 and 5.6).

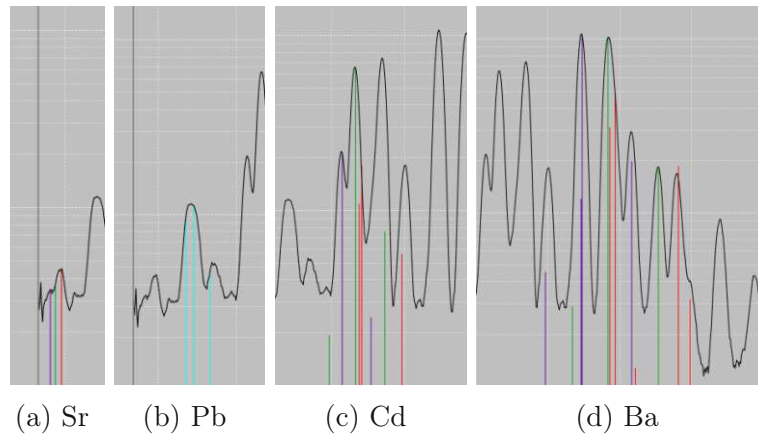


Figure 5.5.: KLM-Marker for elements of Sr, Pb, Cd and Ba

The only pronounced peak that couldn't be matched with any K, L or M lines is peak 10. What hasn't been looked at by now are escape and sum peaks. Since the most intense peak is the Zn-KL3 peak it is sensible to start looking at the escape

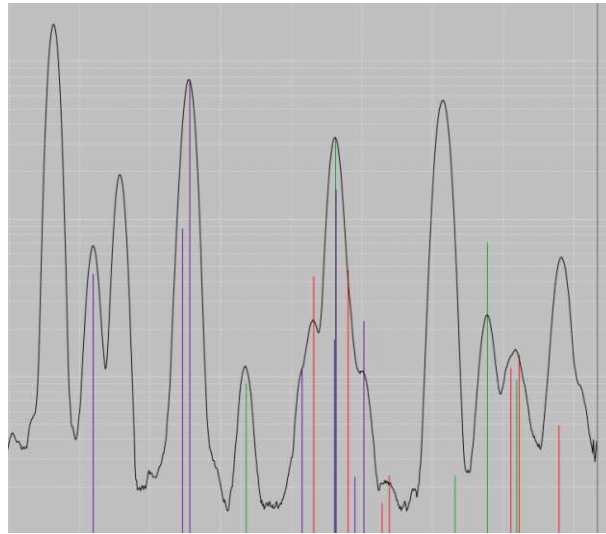


Figure 5.6.: KLM-Marker for Pb

lines of it and it does indeed match well with peak 10 (figure 5.7). Sum peaks are not relevant for this spectrum, since the energy of Zn doubled is already outside of the ROI and there are no intense peaks before it.

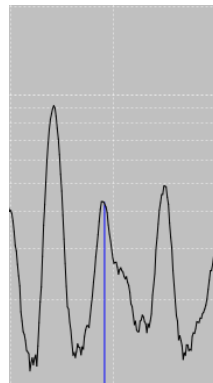


Figure 5.7.: KLM-Marker for Zn escape peak

This concludes the element selection since all distinct peaks could be accounted for. Pressing the ‘Show selected lines’ button in the KLM-Marker menu is a good way to check if no peak has been forgotten (figure 5.8).

The next step is to do the actual fitting. For a first fit the preset ‘100 CL’ has proven to be appropriate (see chapter 3.1). Although the resulting fit will not be ideal in most cases, it will finish quickly and if there has been an oversight in

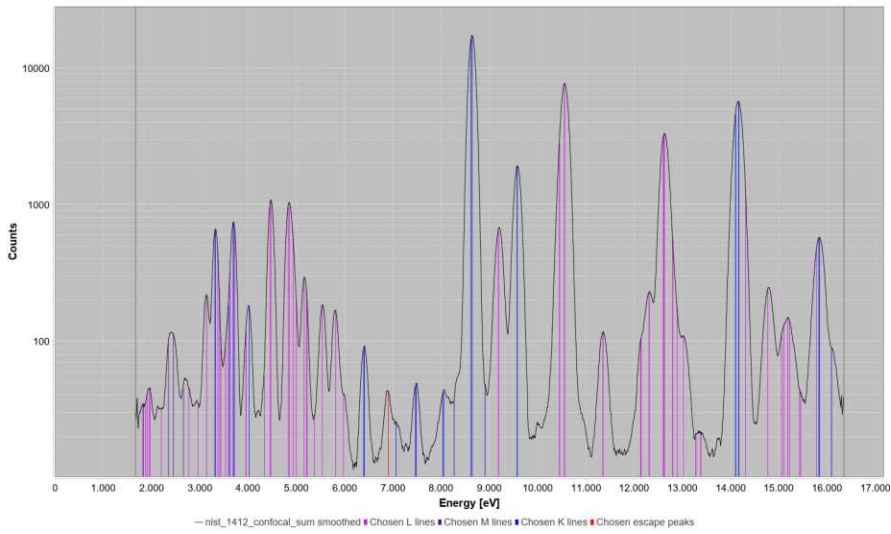


Figure 5.8.: KLM-Marker for all selected lines

element selection it will become apparent. Fitting with this setting leads to the result shown in figure 5.9. The calculated peaks seem to be slightly shifted to the

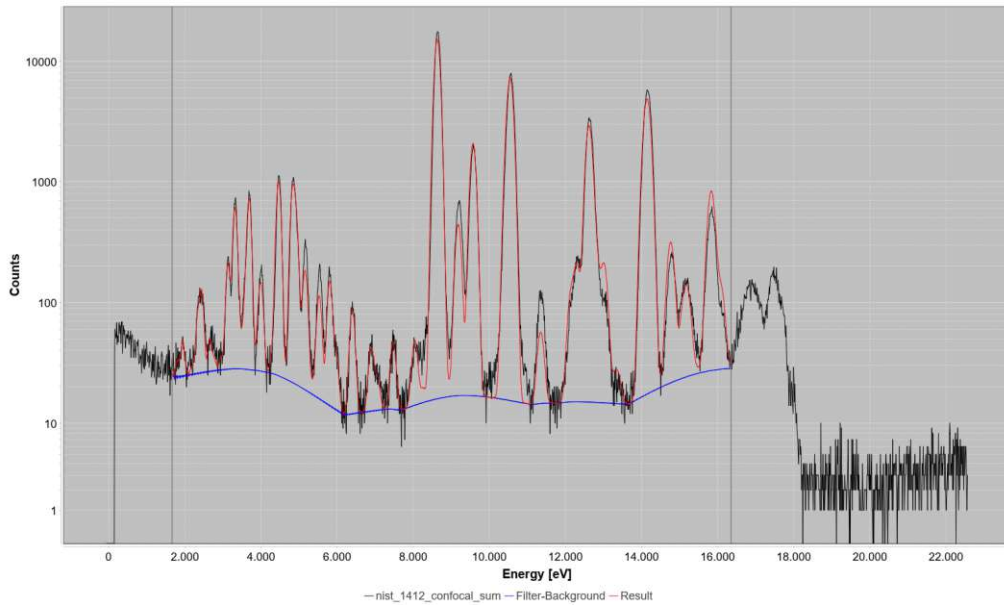


Figure 5.9.: First fit with all elements selected

left and seem a bit broader than in the measured spectrum. To fix this another

fit can be run with energy calibration. This will take a longer time to complete, since the calculations are more complex. To do that the line '100 EC' can be added to the fitting parameters. It is important to do the energy calibration after doing a basic fit for the elements, since otherwise there will be no peaks in the fitted spectrum to be adapted. After the energy calibration was done once, future fits can omit the energy calibration from the fitting parameters again, since the adaptations made will be saved in the parameters Zero, Gain, Noise and Fano. The results of the mentioned steps yield the fit seen in figure 5.10.

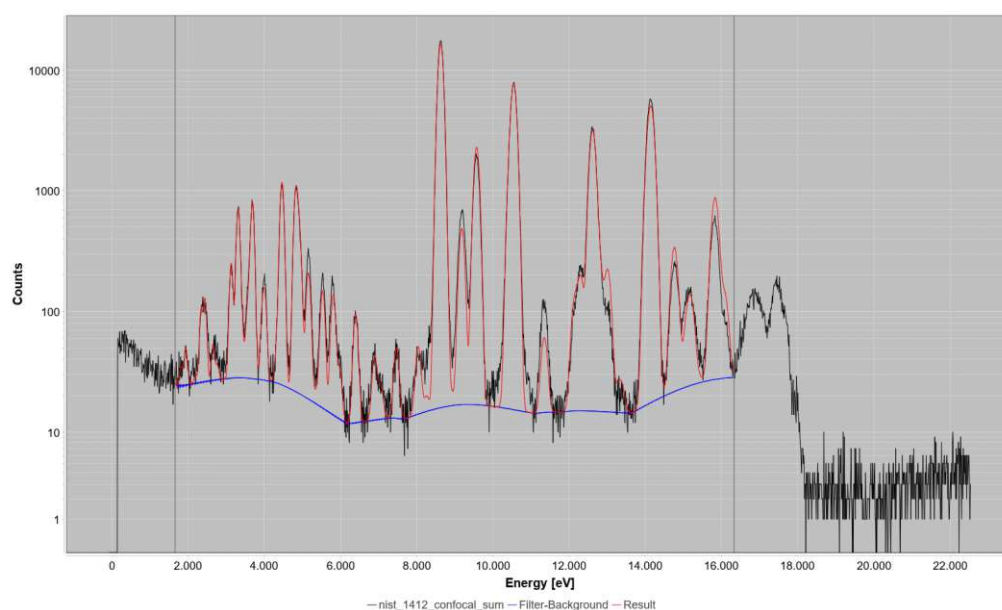


Figure 5.10.: Fit after energy calibration

Looking at this spectrum it can be seen, that some peaks are underestimated while others are overestimated. Figure 5.11 shows this happening for Ca-K and Ba-L. This is because of the fixed intensity ratios between lines which get skewed by sample self absorption (see chapter 2.1.6). For the K peaks this can be solved by choosing 'KL' and 'KM' separately in the 'Element Chooser'. For L lines there is no way to disregard intensity ratios in JPeakFit. To improve this fit the KL and KM lines will be selected separately for Ca and Sr. This will yield the final result for this example, which can be seen in figure 5.12.

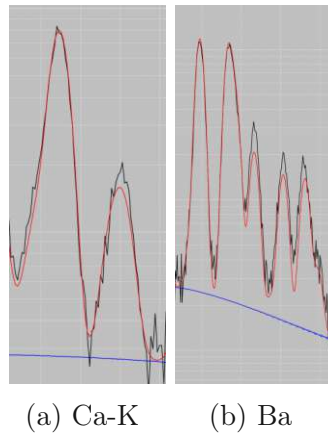


Figure 5.11.: Ca-KM and Ba-L underestimated due to sample self absorption.

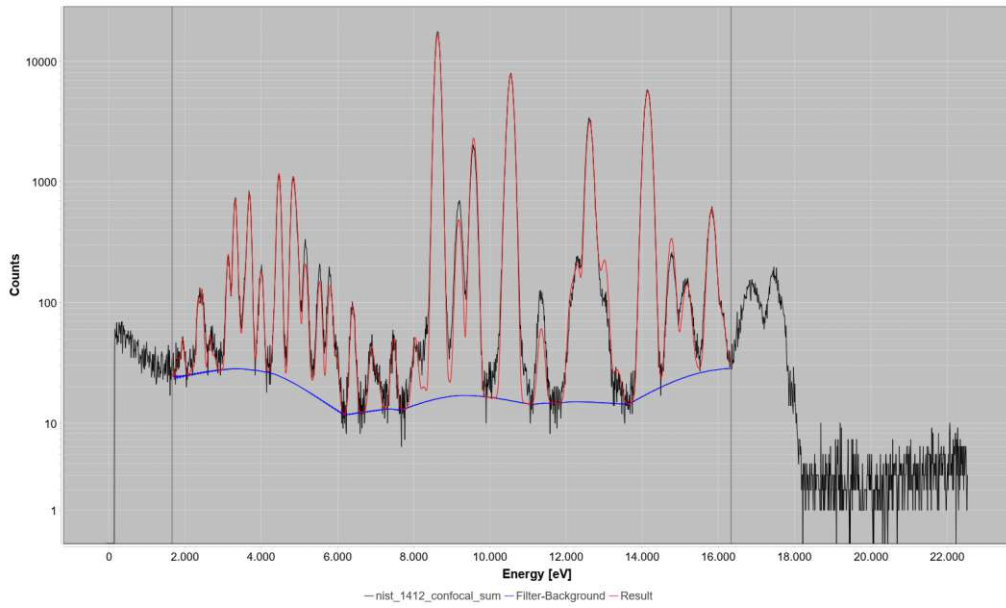


Figure 5.12.: Final fit

6. Results and Discussion

The results for the example spectrum in the previous chapter and four other spectra will be compared with the ones obtained with the established programs AXIL and PyMCA.

Four spectra are from NIST SRM samples, the data sheets of which can be found in appendix A. The NaMgAlCa25 is a sample containing sodium, magnesium, aluminum and calcium each as a mass fraction of 25 mg/kg.

The first two spectra being looked at (NIST 1412, NIST 621) were measured with a monochromatic confocal micro-X-ray fluorescence spectrometer [31]. The other three (NIST 1640A, NIST 1643F, NaMgAlCa25) were measured with WOBIS-TRAX, a TXRF spectrometer [32].

A table with the data and a picture of the fit results of JPeakFit, AXIL and PyMCA with all peaks labeled will be listed here. The tables with the peak areas also features a difference in percent between JPeakFit and AXIL/PyMCA, which uses ‘JPeakFit Peak Area’ as the base value. The obtained results will also be discussed.

6.1. Results NIST 1412

Table 6.1.: Comparison of calculated peak areas of NIST 1412 spectrum.

	Const.	Perc./ Weight	JPeakFit Peak Area	AXIL Peak Area	PyMCA Peak Area	AXIL Diff %	PyMCA Diff %
K-K	K ₂ O	4.14	7,541	7,921	7,830	5.04	3.83
Ca-K	CaO	4.53	9,172	8,995	9,368	-1.93	2.14
Fe-K	Fe ₂ O ₃	0.03	1,231	1,253	1,312	1.79	6.59
Ni-K		n/a	594	577	674	-2.86	13.48
Cu-K		n/a	615	562	684	-8.62	11.25
Zn-K	ZnO	4.48	289,257	289,804	290,098	0.19	0.29
Sr-K	SrO	4.55	125,213	124,076	125,150	-0.91	-0.05
Sr-L	SrO	4.55	360	251	171	-30.28	-52.43
Cd-L	CdO	4.38	3,264	2,373	3,217	-27.30	-1.44
Ba-L	BaO	4.67	35,592	35,507	35,854	-0.24	0.74
Pb-L	PbO	4.40	222,119	221,156	223,540	-0.43	0.64
Pb-M	PbO	4.40	1,800	1,472	1,689	-18.22	-6.16

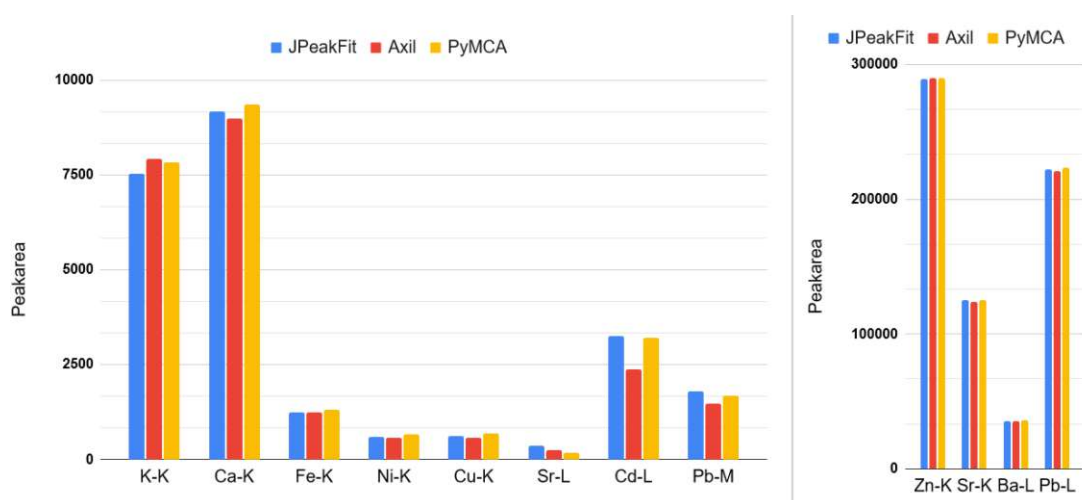


Figure 6.1.: Plot comparing calculated peak areas of NIST 1412 spectrum.

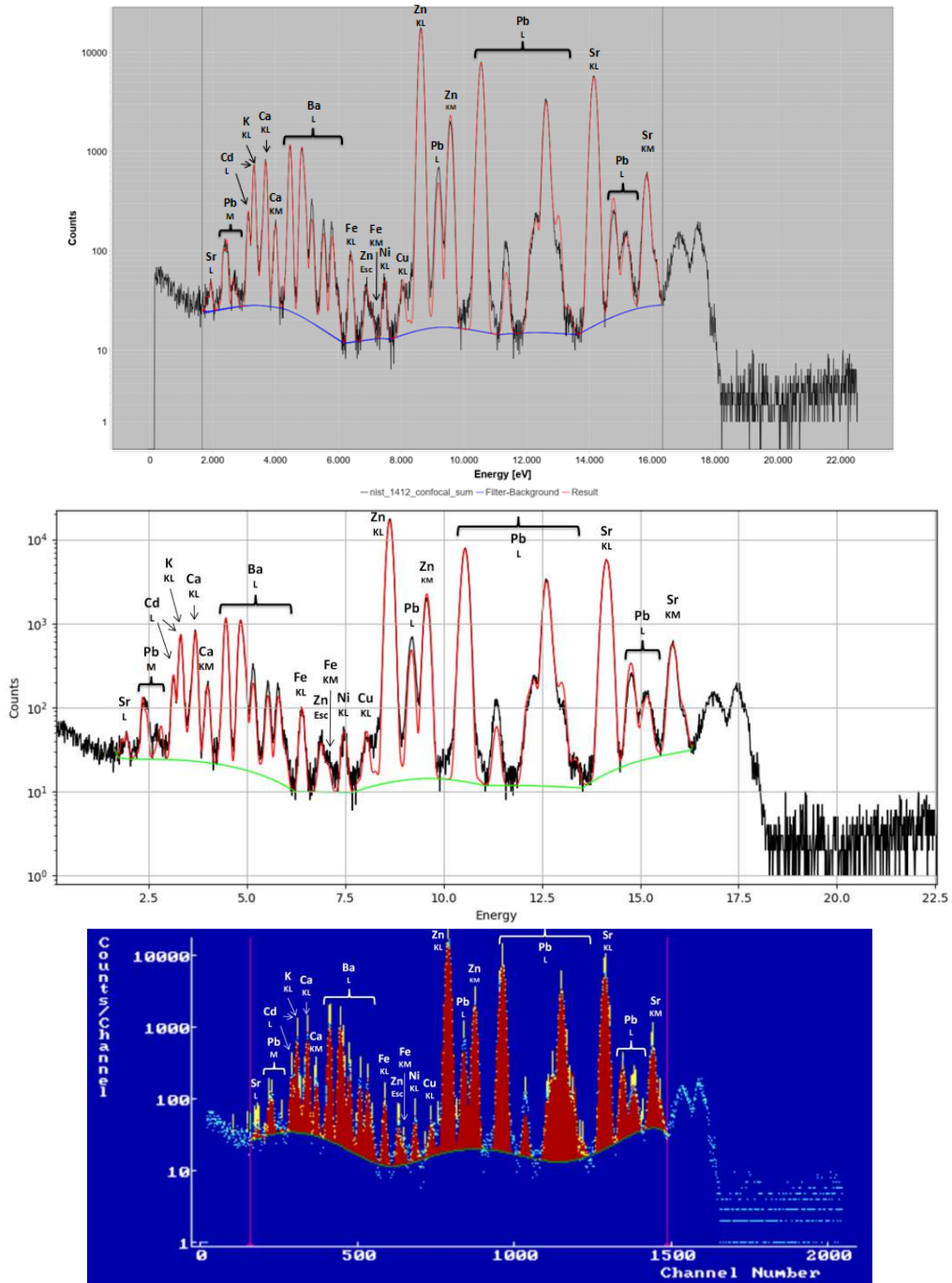


Figure 6.2.: Fitted spectra for NIST 1412 with labeled peaks. From top to bottom: JPeakFit, PyMCA, AXIL.

6.2. Discussion NIST 1412

This spectrum has a lot of intense peaks and also some overlapping lines. In the plots (figure 6.1) it can be seen that a few peaks are overestimated while others are underestimated. The reason for the intensity ratio differing from the book value is sample self absorption described in 2.1.6. This self absorption is currently not being included in JPeakFit. For the K lines the intensity ratios can be turned off in the Element Chooser, but for L-lines there is no such option. There are many lines in these line groups, which would increase the number of independently fitted parameters too much.

PyMCA and JPeakFit calculate very similar peak areas. The only case where the difference is bigger than 15% is for Sr-L (-52%) which is a very small peak. The difference stems in one part from PyMCA automatically considering even small escape peaks. In this case the Ca-KL3 Esc line overlaps with Sr-L1M3. The other part is from overlapping Pb-M lines which PyMCA has a fixed relation for but JPeakFit can choose freely, which in this case leads PyMCA to have a bigger Pb-M4N2 peak area than JPeakFit, which takes away counts from Sr-L.

The peak areas from AXIL are also very similar to JPeakFits. Sr-L is a bit lower too for AXIL than for JPeakFit (-30%). In this case the reason is that the background for AXIL is noticeably higher than for JPeakFit. The second big difference is for Cd-L (-27%). This stems in part from K-KL and Cd-L1 overlapping and AXIL favoring K-KL more than JPeakFit. The other part is again the background, which is higher for AXIL.

6.3. Results NIST 621

Table 6.2.: Comparison of calculated peak areas of NIST 621 spectrum.

	Const.	Perc./ Weight	JPeakFit Peak Area	AXIL Peak Area	PyMCA Peak Area	AXIL Diff %	PyMCA Diff %
Ar-K		n/a	123	75	171	-39.02	38.87
K-K	K ₂ O	2.01	3,177	3,128	3,238	-1.54	1.91
Ca-K	CaO	10.71	27,217	27,233	27,340	0.06	0.45
Fe-K	Fe ₂ O ₃	0.04	1,952	1,899	2,007	-2.72	2.83
Ni-K		n/a	545	520	564	-4.59	3.45
Cu-K		n/a	420	398	484	-5.24	15.25
Zn-K		n/a	371	332	431	-10.51	16.22
As-K	As ₂ O ₃	0.03	2,194	2,120	2,014	-3.37	-8.19
Rb-K		n/a	231	183	259	-20.78	12.23
Sr-K		n/a	643	548	607	-14.77	-5.66
Ba-L	BaO	0.12	1,158	999	1,234	-13.73	6.57
Pb-L		n/a	531	389	953	-26.74	79.53

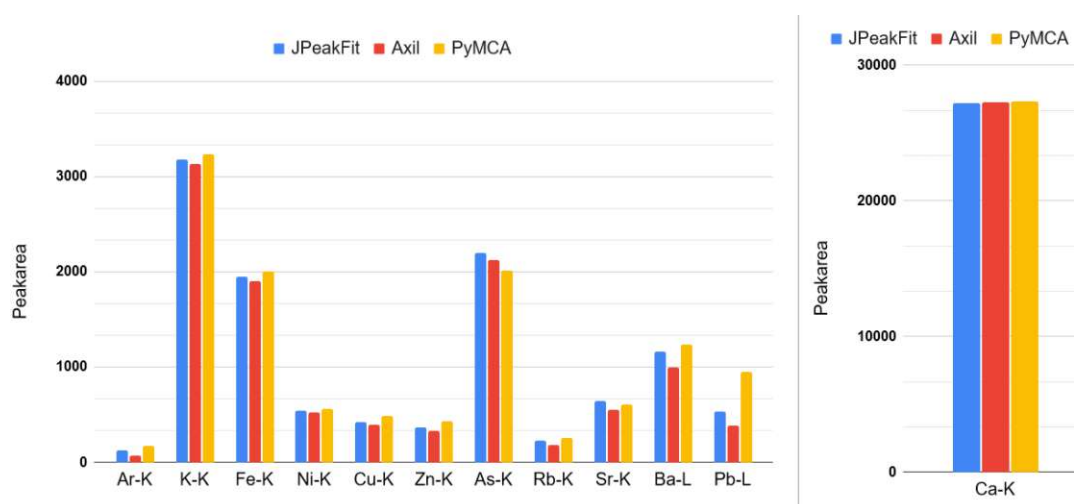


Figure 6.3.: Plot comparing calculated peak areas of NIST 621 spectrum.

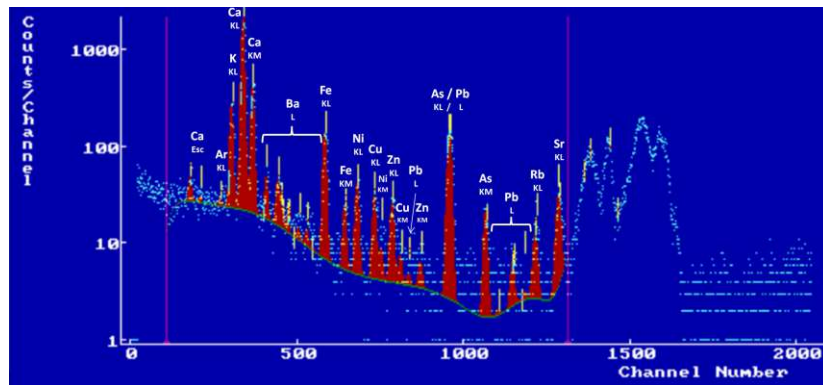
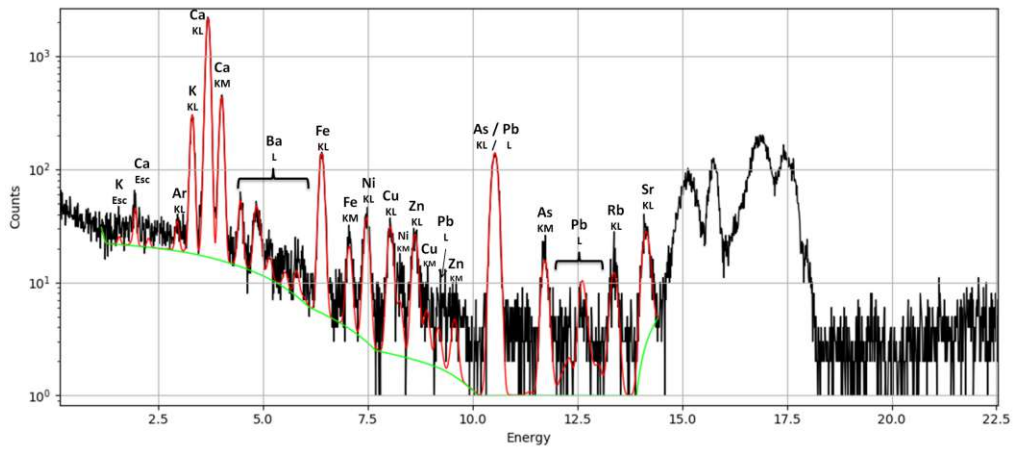
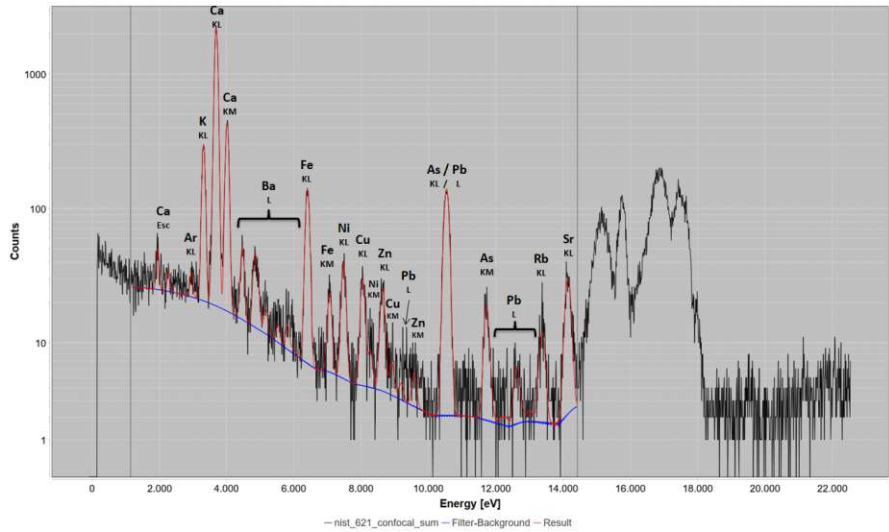


Figure 6.4.: Fitted spectra for NIST 621 with labeled peaks. From top to bottom: JPeakFit, PyMCA, AXIL.

6.4. Discussion NIST 621

Compared to the previous spectrum, in this one there are relatively smaller peaks, which means in percentage difference there are gonna be greater differences. In absolute values all 3 programs calculate similar peak areas.

Between PyMCA and JPeakFit the biggest difference in absolute values lies with the peak areas for As-K (-180) and Pb-L (+422). Since As-KL3 and Pb-L3M5 are nearly at the exact same energy (10.54 keV and 10.55 keV respectively), they are hard to differentiate. JPeakFit accounted the peak more to As than PyMCA did.

When comparing the AXIL results to JPeakFit it can be noticed that almost all values for AXIL are lower. This can again be attributed to AXIL calculating a higher background. For this spectrum the difference is especially noticeable. Accounting for that however, the results match well.

6.5. Results NIST 1640A

Table 6.3.: Comparison of calculated peak areas of NIST 1640A spectrum.

	Mass Fraction [$\mu\text{g}/\text{kg}$]	JPeakFit Peak Area	AXIL Peak Area	PyMCA Peak Area	AXIL Diff %	PyMCA Diff %
Si-K	5,169.00	6,267	6,139	6,225	-2.04	-0.68
Ar-K	n/a	141	124	162	-12.06	15.14
K-K	575.30	1,010	999	1,018	-1.09	0.82
Ca-K	5,570.00	11,943	12,027	12,002	0.70	0.50
Cr-K	40.54	238	219	221	-7.98	-7.17
Mn-K	40.39	291	271	312	-6.87	7.29
Fe-K	36.80	311	296	333	-4.82	7.14
Co-K	20.24	242	233	250	-3.72	3.31
Ni-K	25.32	348	341	328	-2.01	-5.80
Cu-K	85.75	1,388	1,386	1,406	-0.14	1.30
Zn-K	55.64	1,007	1,000	1,037	-0.70	2.96
Ge-K	n/a	31	12	41	-61.29	31.64
As-K	8.07	106	104	71	-1.89	-32.74
Se-K	20.13	463	450	471	-2.81	1.81
Rb-K	1.19	56	67	73	19.64	30.54
Sr-K	126.03	4,410	4,361	4,422	-1.11	0.27
Y-K	122.00	4,702	4,570	4,732	-2.81	0.64
Mo-K	45.60	1,720	1,559	1,759	-9.36	2.27
Mo-L	45.60	747	678	753	-9.24	0.86
Ba-L	151.80	477	415	550	-13.00	15.30
Tl-L	1.61	61	38	102	-37.70	66.48
Pb-L	12.10	334	319	417	-4.49	24.77
U-L	25.35	437	412	727	-5.72	66.30

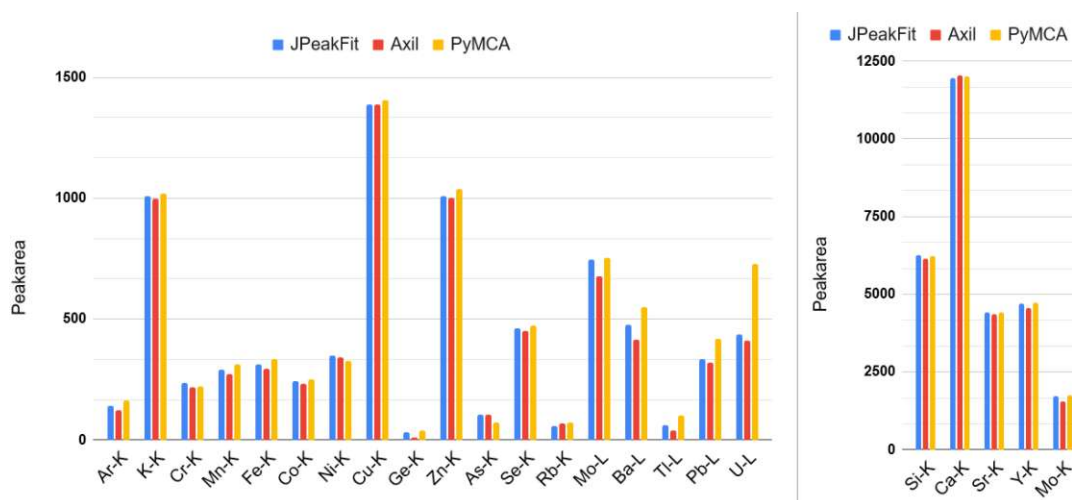


Figure 6.5.: Plot comparing calculated peak areas of NIST 1640A spectrum.

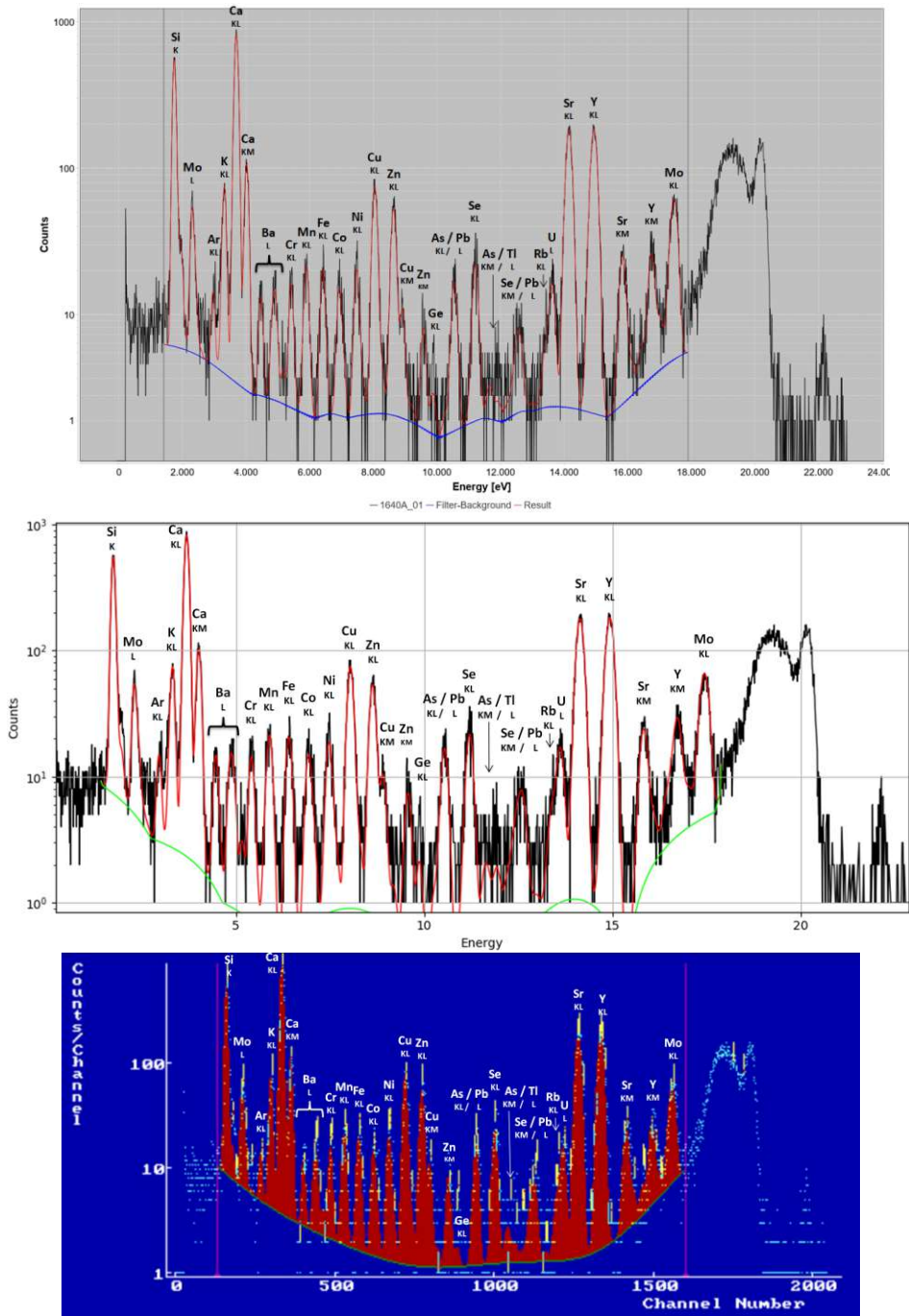


Figure 6.6.: Fitted spectra for NIST 1640A with labeled peaks. From top to bottom: JPeakFit, PyMCA, AXIL.

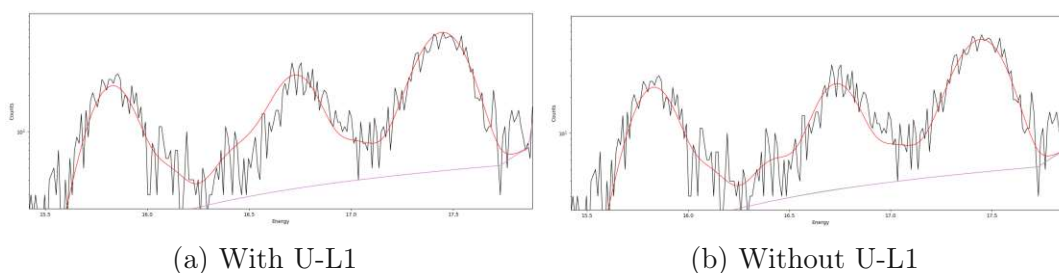


Figure 6.7.: Comparison of PyMCAs fit with and without U-L1.

6.6. Discussion NIST 1640A

This spectrum features a lot of elements and an even lower count rate which makes the percentage difference large again.

The biggest difference in absolute values between PyMCA and JPeakFit for this spectrum is U-L (+290). This is because PyMCA makes the U-L1 line big, even though this leads to a worse chi-square value of the fit. If the U-L1 line is turned off the chi-square value for the spectrum decreases from 1.32 to 1.25. Figure 6.7 shows how the affected region of the spectrum changes. Why this happens is unknown. Also PyMCA calculates the peak area for As-K a bit lower (-35) and the one for Pb-L a bit higher (+83). This is again due to the overlap of the lines.

The differences of JPeakFit and AXIL are again due to AXIL calculating a higher background, which makes almost all the peak areas smaller.

6.7. Results NIST 1643F

Table 6.4.: Comparison of calculated peak areas of NIST 1643F spectrum.

	Mass Fraction [$\mu\text{g}/\text{kg}$]	JPeakFit Peak Area	AXIL Peak Area	PyMCA Peak Area	AXIL Diff %	PyMCA Diff %
Na-K	18,640.00	1,905	1,947	1,853	2.20	-2.76
Mg-K	7,380.00	8,249	8,357	8,557	1.31	3.73
Al-K	132.50	2,074	2,210	2,356	6.56	13.61
Si-K	n/a	82,392	83,383	84,464	1.20	2.51
K-K	1,913.30	23,299	24,157	24,020	3.68	3.10
Ca-K	29,140.00	334,398	344,170	340,638	2.92	1.87
V-K	35.71	744	544	361	-26.88	-51.54
Cr-K	18.32	847	862	953	1.77	12.57
Mn-K	36.77	1,210	1,137	1,230	-6.03	1.62
Fe-K	92.51	6,440	6,541	6,679	1.57	3.71
Co-K	25.05	1,366	1,459	1,466	6.81	7.30
Ni-K	59.20	5,010	5,304	5,266	5.87	5.10
Cu-K	21.44	1,843	2,070	2,006	12.32	8.85
Zn-K	73.70	7,498	7,807	7,778	4.12	3.73
As-K	56.85	7,110	6,878	7,355	-3.26	3.45
Se-K	11.58	1,550	1,514	1,633	-2.32	5.38
Rb-K	12.51	2,261	2,338	2,394	3.41	5.89
Sr-K	311.00	53,986	54,644	54,749	1.22	1.41
Y-K	122.00	22,375	22,405	22,070	0.13	-1.36
Mo-K	114.20	22,119	21,174	20,483	-4.27	-7.40
Mo-L	114.20	5,117	5,832	5,517	13.97	7.82
Rh-L	n/a	50,984	52,629	52,236	3.23	2.46
Ba-L	513.10	6,638	7,114	7,064	7.17	6.42
Tl-L	6.82	1,032	760	1,246	-26.36	20.72
Pb-L	18.30	2,388	2,671	2,568	11.85	7.56
Bi-L	12.50	2,004	1,785	2,317	-10.93	15.61

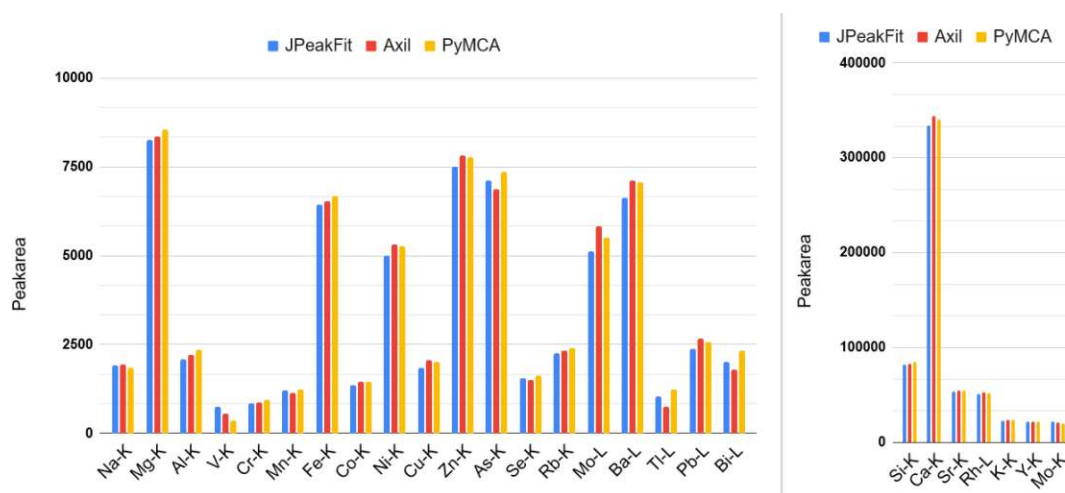


Figure 6.8.: Plot comparing calculated peak areas of NIST 1643F spectrum.

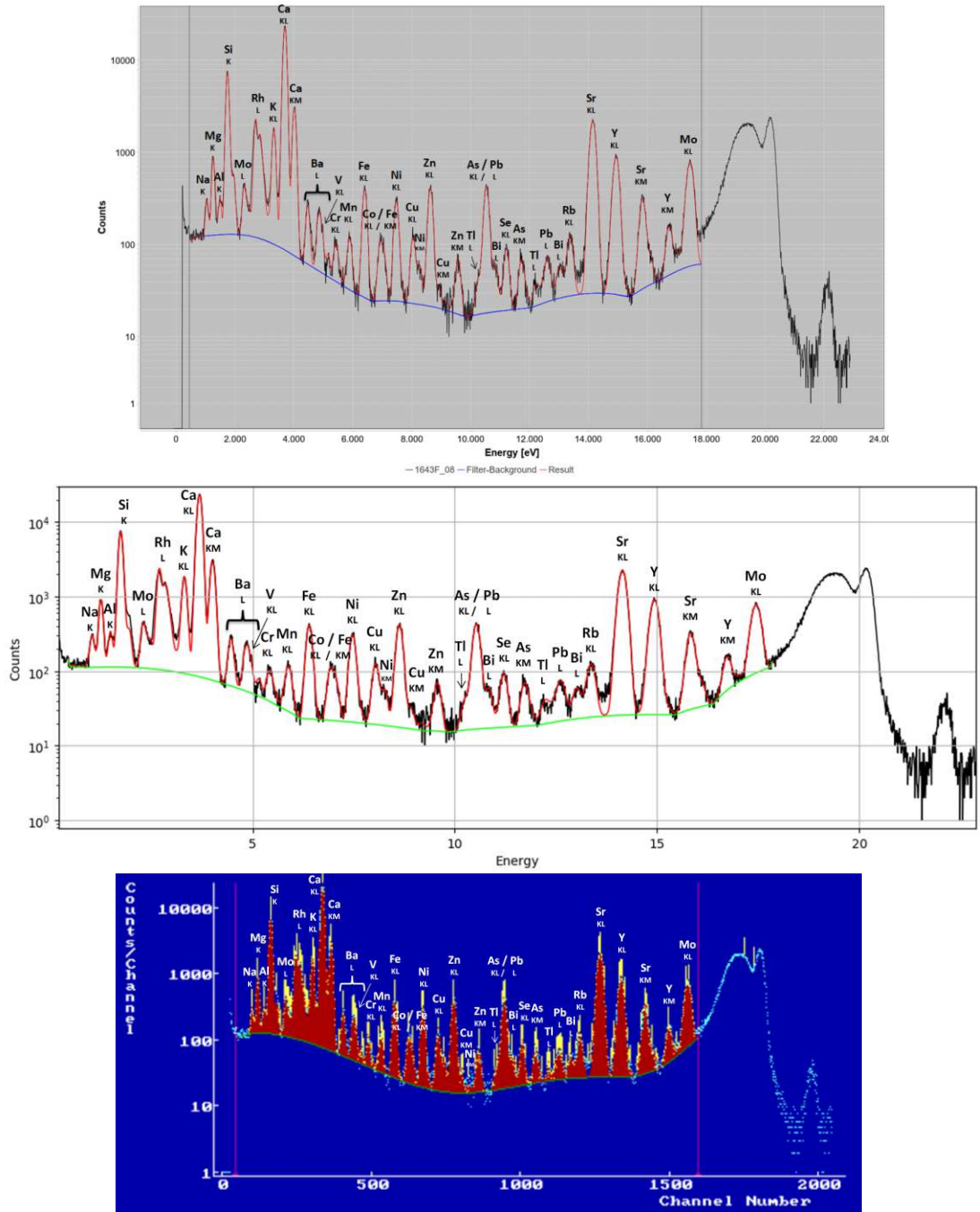
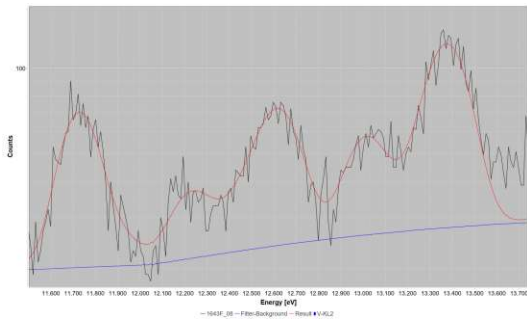
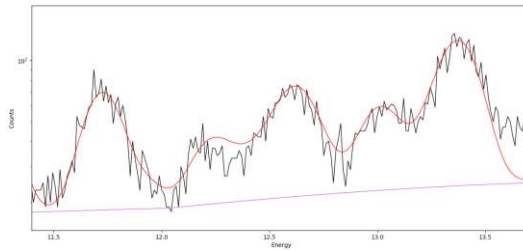


Figure 6.9.: Fitted spectra for NIST 1643F with labeled peaks. From top to bottom: JPeakFit, PyMCA, AXIL.



(a) JPeakFit



(b) PyMCA

Figure 6.10.: Comparison of the fitted region where Tl-L and Ba-L are located.

6.8. Discussion NIST 1643F

For the most part all three programs calculate similar peak areas for this spectrum.

The biggest percentage difference between PyMCA and JPeakFit is with V-K (-52%). This is a small peak that lies inside the Ba-L lines. JPeakFit gives a bigger area to V and PyMCA a bigger one to Ba. Another big percentage difference can be seen for Tl-L (+21%) and Bi-L (+16%). Those peaks are located in an area where a lot of lines overlap. It is hard to pinpoint exactly what causes the different counts. Both fits in the area look good (figure 6.10).

JPeakFit and AXIL are very close together on counts for this spectrum. The biggest percentage differences are V-K (-27%), which is also caused by the peak overlap of Ba-L lines, and Tl-L (-26%), where it is again hard to say exactly why this difference emerges.

6.9. Results NaMgAlCa25

Table 6.5.: Comparison of calculated peak areas of NaMgAlCa25 spectrum.

	Mass Fraction [mg/kg]	JPeakFit Peak Area	AXIL Peak Area	PyMCA Peak Area	AXIL Diff %	PyMCA Diff %
Na-K	25.00	9	12	10	33.33	11.11
Mg-K	25.00	152	156	155	2.63	1.82
Al-K	25.00	523	529	536	1.15	2.51
Si-K	n/a	3,870	3,856	3,882	-0.36	0.30
S-K	n/a	337	352	348	4.45	3.35
K-K	n/a	17	8	17	-52.94	0.00
Ca-K	25.00	245	228	252	-6.94	3.02
Rh-L	n/a	1,142	1,154	1,165	1.05	1.97

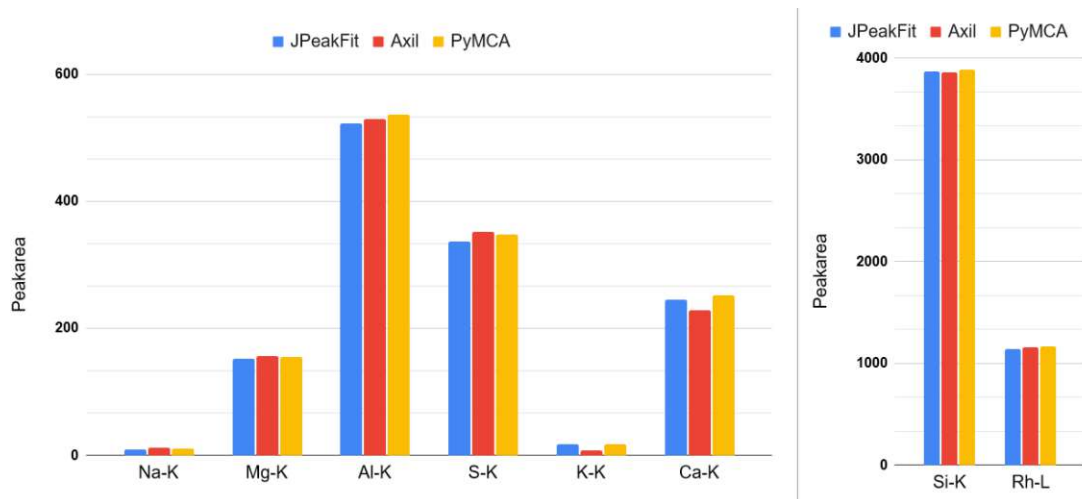


Figure 6.11.: Plot comparing calculated peak areas of NaMgAlCa25 spectrum.

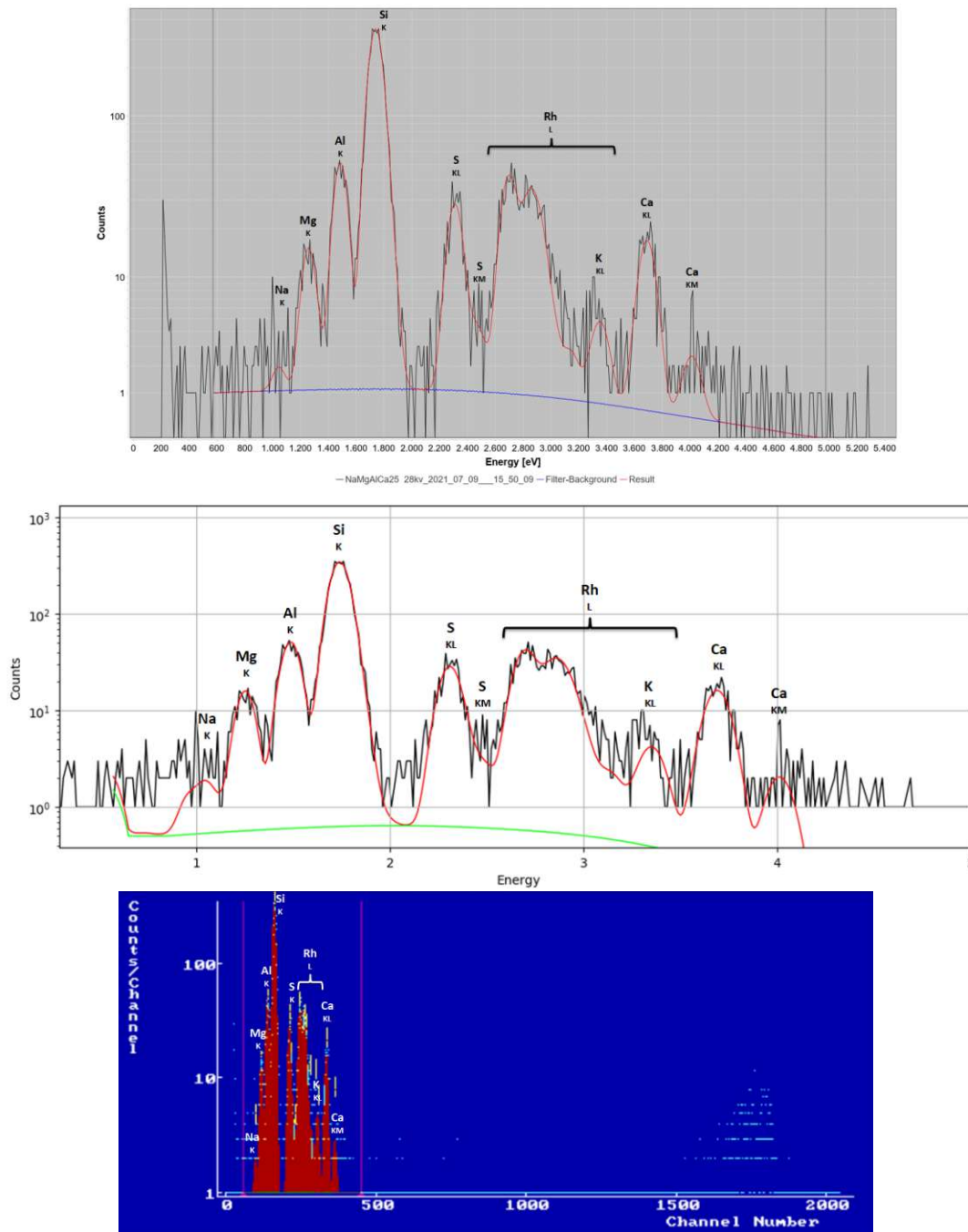


Figure 6.12.: Fitted spectra for NaMgAlCa₂₅ with labeled peaks. From top to bottom: JPeakFit, PyMCA, AXIL.

6.10. Discussion NaMgAlCa25

This spectrum has few elements and low count rates, which makes the percentage differences big.

In absolute numbers the 3 programs have very similar counts. All spectra in figure 6.12 pass the visual inspection. The low count rate however makes it difficult to see well defined peaks.

7. Conclusion and perspective

The goal of this thesis was to develop a deconvolution software for XRF-spectra with a GUI, that is both powerful and easy to use. As demonstrated with the example fit, the process of fitting a spectrum with JPeakFit is streamlined well. All the most important options for spectrum fitting are provided. Five different spectra have been analyzed and compared with results of the established programs AXIL and PyMCA, with all three programs obtaining similar counts for the peak areas.

As with any software there are still parts of the application that can be improved:

- The fit routine could be optimized to be faster, especially when doing a fit with energy calibration.
- It is also planned to include the option to use another fitting algorithm, as newton's method can get stuck in local minima. The way the software is built it is easy to add new functionality without having to change other parts of the software.
- An option to change the shape of the peaks could also be added, which is useful when the measured peaks can no longer be described as Gaussian.
- A model for how the intensity ratio of peaks changes when sample self absorption is relevant would also be a useful addition for the evaluation of some samples.

Bibliography

- [1] Demtröder W. *Experimentalphysik 3: Atome, Moleküle und Festkörper*. Springer, 2010. ISBN: 9783642039102.
- [2] Tipler P.A. *Physik*. Spektrum Akademischer Verlag, 2009. ISBN: 9783827419453.
- [3] Mini Physics. *Electromagnetic spectrum*. 2016. URL: https://www.miniphysics.com/electromagnetic-spectrum_25.html (visited on 11/07/2021).
- [4] Beckhoff B. et al. *Handbook of Practical X-Ray Fluorescence Analysis*. Springer, 2006. ISBN: 9783540367222.
- [5] Haschke M. *Laboratory Micro-X-Ray Fluorescence Spectroscopy*. Springer, 2014. ISBN: 9783319048635.
- [6] Van Grieken R. et al. *Handbook of X-Ray spectrometry, Second Edition, Revised and Expanded*. Marcel Dekker, 2001. ISBN: 0824706005.
- [7] University of Göttingen. *Abb. 6623 Übergänge von einem höheren auf ein freies, niedrigeres Energieniveau*. 2010. URL: <https://lp.uni-goettingen.de/get/bigimage/6623> (visited on 12/02/2021).
- [8] University of Göttingen. *Charakteristische Strahlung*. 2010. URL: <https://lp.uni-goettingen.de/get/text/6634> (visited on 12/02/2021).
- [9] Thermo Fischer. *Silicon Drift Detectors*. URL: https://tools.thermofisher.com/content/sfs/brochures/TN52342_E_0512M_SiliconDrift_H.pdf (visited on 06/17/2022).
- [10] Prost J. *Technische Verbesserungen an einem Spektrometer für Niederleistungs-Totalreflexions-Röntgenfluoreszenzanalyse und Anwendungen bei Umweltproben*. Technische Universität Wien, Atominstitut, 2012.
- [11] Wikipedia. *Plot of the centered Voigt profile for four cases*. 2017. URL: https://en.wikipedia.org/wiki/Voigt_profile#/media/File:VoigtPDF.svg (visited on 09/23/2022).
- [12] Liao Y. *Escape peak in EDS/X-ray profiles*. 2006. URL: <https://www.globalsino.com/EM/page3804.html> (visited on 09/23/2022).
- [13] Liao Y. *Sum peaks in x-ray/EDS profiles*. 2006. URL: <https://www.globalsino.com/EM/page3803.html> (visited on 09/23/2022).

- [14] Golay M.J. Savitzky A. “Smoothing and Differentiation of Data by Simplified Least Squares Procedures”. In: *Analytical Chemistry* 36.8 (July 1964), pp. 1627–1639.
- [15] Ryan C.G. et al. “SNIP, a statistics-sensitive background treatment for the quantitative analysis of PIXE spectra in geoscience applications”. In: *Nuclear Instruments and Methods in Physics Research Section B: Beam Interactions with Materials and Atoms* 34.3 (Sept. 1988), pp. 396–402.
- [16] O’Haver T.C. *Peak Finding and Measurement - Derivative-based peak measurement functions*. URL: <https://terpconnect.umd.edu/~toh/spectrum/PeakFindingandMeasurement.htm> (visited on 09/17/2022).
- [17] Clayton E. et al. “A discussion of PIXAN and PIXANPC: The AAEC PIXE analysis computer packages”. In: *Nuclear Instruments and Methods in Physics Research Section B: Beam Interactions with Materials and Atoms* 22.1-3 (Mar. 1987), pp. 64–67.
- [18] Grossmayer B. “Softwarepaket zur quantitativen röntgenfluoreszenzanalyse mittels fundamentaler parameter unter verwendung von röntgenoptiken”. MA thesis. Technische Universität Wien, Atominstitut, 2009.
- [19] Necker P. “Quantitative X-ray fluorescence analysis of samples with various matrices using a universal data evaluation software”. MA thesis. Technische Universität Wien, Atominstitut, 2017.
- [20] Holub E. “Spectral correction for a rhodium-anode transmission X-ray tube. Quantitative X-ray fluorescence analysis and comparison with a side-window rhodium-anode tube”. MA thesis. Technische Universität Wien, Atominstitut, 2020.
- [21] Fowler M. *GUI Architectures Model-View-Presenter (MVP)*. 2006. URL: <https://www.martinfowler.com/eaDev/uiArchs.html#Model-view-presentermvp> (visited on 07/01/2021).
- [22] Fowler M. *Passive View*. 2006. URL: <https://www.martinfowler.com/eaDev/PassiveScreen.html> (visited on 07/01/2021).
- [23] *JAXB*. URL: <https://javaee.github.io/jaxb-v2/> (visited on 05/21/2022).
- [24] Zlabinger J. *Implementation of a SNIP filter for continuum estimation of X-Ray spectra for spectrum deconvolution*. Project work. Technische Universität Wien, 2020.
- [25] *JFreeChart*. 2021. URL: <https://www.jfree.org/jfreechart/> (visited on 07/01/2021).

- [26] Hofstadler C. *Implementation of Peak Fitting Algorithms for Energy Dispersive X-ray Fluorescence Analysis*. Project work. Technische Universität Wien, 2013.
- [27] Polyan B.T. “Newton’s method and its use in optimization”. In: *European Journal of Operational Research* 181.3 (Sept. 2007), pp. 1086–1096.
- [28] Bearden J.A. “X-Ray Wavelengths”. In: *Reviews of Modern Physics* 39.1 (Jan. 1967), p. 78.
- [29] Scofield J.H. “Relativistic hartree-slater values for K and L X-ray emission rates”. In: *Atomic Data and Nuclear Data Tables* 14.2 (Aug. 1974), pp. 121–137.
- [30] National Institute of Standards and Technology. *SRM 1412 - Multicomponent Glass*. 2021. URL: https://www-s.nist.gov/srmors/view_detail.cfm?srm=1412 (visited on 03/17/2022).
- [31] Ingerle D. et al. “A monochromatic confocal micro-x-ray fluorescence (XRF) spectrometer for the lab”. In: *Review of Scientific Instruments* 91.12 (2020), p. 123107.
- [32] Streli C. et al. “A new total reflection X-ray fluorescence vacuum chamber with sample changer analysis using a silicon drift detector for chemical analysis”. In: *Spectrochimica Acta Part B: Atomic Spectroscopy* 59.8 (2004), pp. 1199–1203.

A. Data sheets

A.1. NIST 621 data sheet

National Bureau of Standards

Certificate

Standard Reference Material 621

Soda-Lime Container Glass

(In cooperation with the American Society for Testing and Materials)

This Standard Reference Material is for use in checking chemical methods of analysis and for calibrating optical emission and x-ray spectrometric methods of analysis.

<u>Constituent</u>	<u>Percent by weight</u>	<u>Uncertainty</u>
SiO ₂	71.13	0.03
Na ₂ O	12.74	0.05
CaO	10.71	0.05
Al ₂ O ₃	2.76	0.04
K ₂ O	2.01	0.03
MgO	0.27	0.03
SO ₃	0.13	0.02
BaO	0.12	0.05
Fe ₂ O ₃	0.040	0.003
As ₂ O ₃	0.030	0.001
TiO ₂	0.014	0.003
ZrO ₂	0.007	0.001

The certified values are the present best estimates of the "true" values based on the results of a cooperative analytical program. At NBS twelve statistically selected samples of the glass were tested for homogeneity by S.D. Rasberry and L. Zinger using x-ray fluorescence spectrometry. Based on their results the variations among samples are estimated to be less than the uncertainties given above.

The overall direction and coordination of the round-robin analysis leading to certification were performed by Paul Close, Chairman of ASTM Subcommittee C-14.02 on Chemical Analysis of Glass and Glass Products.

The technical and support aspects involved in the preparation, certification, and issuance of this Standard Reference Material were coordinated through the Office of Standard Reference Materials by G.W. Cleek, C.L. Stanley, and R.E. Michaelis.

Washington, D.C. 20234
January 21, 1982
(Revision of certificate
dated 3/13/75.)

George A. Uriano, Chief
Office of Standard Reference Materials

(over)

The material for this SRM was prepared for NBS by Owens-Illinois, Inc., Technical Center, Toledo, Ohio. The following laboratories cooperated in the chemical analysis of this container glass:

T.B. Bodkin, Pennsylvania State University, University Park, Pennsylvania.

G.D. Bowling, Owens-Corning Fiberglass Corp., Technical Center, Granville, Ohio.

W.P. Close, Owens-Illinois, Inc., Technical Center, Toledo, Ohio.

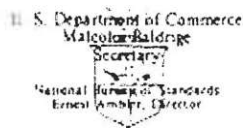
H.S. Moser, Owens-Illinois, Inc., Vineland, New Jersey.

Y.S. Su, Corning Glass Works, Corning, New York.

L.E. Stadler, Emhart Corp., Hartford Division, Hartford, Connecticut.

E.J. Maienthal, Analytical Chemistry Division, National Bureau of Standards.

A.2. NIST 1412 data sheet



National Bureau of Standards

Certificate

Standard Reference Material 1412

Multicomponent Glass

(In Cooperation with the American Society for Testing and Materials)

This Standard Reference Material (SRM) is intended for use in performance evaluation of chemical methods of analysis and in calibrating instrumental methods of analysis. The SRM consists of platelets having the composition shown below:

<u>Constituent</u>	<u>Percent by Weight¹</u>	<u>Uncertainty²</u>
SiO ₂	42.38	0.18
Al ₂ O ₃	7.52	0.24
CaO	4.53	0.10
MgO	(4.69)	----
SrO	4.55	0.09
Na ₂ O	4.69	0.07
K ₂ O	4.14	0.10
Li ₂ O	(4.50)	----
B ₂ O ₃	4.53	0.17
BaO	4.67	0.16
ZnO	4.48	0.12
PbO	4.40	0.17
CdO	4.38	0.08
Fe ₂ O ₃	(0.031)	----

¹The certified value listed for a constituent is the present best estimate of the "true" value based on the results of the cooperative program for certification. The values given in parenthesis are not certified and are given for information only.

²The estimated uncertainty listed for a constituent is based on judgment and represents an evaluation of the combined effects of method bias, between laboratory variability, and material variability.

The overall direction and coordination of the cooperative analysis leading to certification were performed by G.D. Bowling, Chairman of ASTM Subcommittee C-14.02 on Chemical Analysis of Glass and Glass Products.

The procurement and development of this material as an SRM was under the direction of the joint NBS-ASTM Glass Research Associate Program. This program was coordinated through ASTM by: M.J. Cellarosi, Chairman of ASTM Committee on Glass and Glass Products; H.E. Hagy, Chairman of Subcommittee 14.91 on Standard Reference Materials; and A.C. Seifert, NBS-ASTM Research Associate.

The technical and support aspects involved in the preparation, certification, and issuance of this SRM were coordinated through the Office of Standard Reference Materials by L.J. Kieffer.

Gaithersburg, MD 20899
August 2, 1985

Stanley D. Rasberry, Chief
Office of Standard Reference Materials

This material was tested for homogeneity at NBS by A. F. Marlow and P. A. Pella, Gas and Particulate Science Division, using x-ray fluorescence spectrometry. Four replicate measurements were made on eight elements in each of thirteen samples chosen at random from the lot of material. The results did not indicate any significant heterogeneity among the samples.

This material was batched, melted, ground and formed into plates at Corning Glass Works, Corning, N. Y.

The laboratories submitting data for certification of this SRM were:

Anchor Hocking, Lancaster, OH

Corning Glass Works, Corning, NY

Emhart Materials Testing Laboratory, Windsor, CT

Mobay Chemical Corporation, Baltimore, MD

National Bureau of Standards, Gaithersburg, MD

Owens-Corning Fiberglas, Granville, OH

Owens-Illinois, Toledo, OH

Owens-Illinois, Vineland, NJ

Page 2

SRM 1412

A.3. NIST 1640A data sheet



National Institute of Standards & Technology

Certificate of Analysis

Standard Reference Material[®] 1640a

Trace Elements in Natural Water

This Standard Reference Material (SRM) is intended for use in evaluating methods used in the determination of trace elements in fresh water. SRM 1640a consists of acidified spring water with mass fractions and mass concentrations assigned for 29 elements, 22 of which were gravimetrically added. The solution contains nitric acid at a volume fraction of approximately 2 %. A unit of SRM 1640a consists of 250 mL of solution in a high-density polyethylene (HDPE) bottle sealed inside an aluminized Mylar pouch.

Certified Values and Uncertainties: The certified values for 22 elements in SRM 1640a are given expressed in mass fraction units and mass concentration units in Tables 1 and 2, respectively. A NIST certified value is a value in which NIST has the highest confidence in its accuracy, in that all known or suspected sources of bias have been fully investigated or taken into account [1].

Each certified mass fraction value given in Table 1 is the average of the value calculated from the gravimetric preparation and the value determined using either inductively-coupled plasma optical emission spectroscopy (ICP-OES) or inductively-coupled plasma mass spectrometry (ICP-MS), adjusted upward for transpiration that may occur over the certification period while the SRM bottle remains sealed inside the aluminized Mylar pouch. (NOTE: *No correction has been applied for transpiration that will occur after the pouch seal has been broken.* See "Instructions for Use" for more information regarding transpiration.) The magnitude of the transpiration adjustment (0.11 %) is based upon the results of unpublished NIST studies of transpiration rates of similar HDPE bottles sealed inside similar aluminized Mylar pouches, and is such that the actual mass fraction is expected to be equal to the certified mass fraction value approximately halfway through the certification period. Each expanded uncertainty, U , in Table 1 is calculated as $U = ku_c$, where k is the coverage factor for the appropriate degrees of freedom (df) and a 95 % level of confidence (k and df are also given in Table 1) and u_c is the combined standard uncertainty calculated according to the ISO Guide [2]. The value of u_c is intended to represent, at the level of one standard deviation, the combined effect of uncertainty components associated with the gravimetric preparation, the ICP-OES or ICP-MS analysis, method bias [3], and the transpiration adjustment.

Each certified mass concentration value given in Table 2 is calculated from the corresponding certified mass fraction value in Table 1 through multiplication by the density of the SRM 1640a solution. Each expanded uncertainty, U , in Table 2 is calculated as $U = ku_c$, where k is the coverage factor for the appropriate degrees of freedom (df) and a 95 % level of confidence (k and df are also given in Table 2) and u_c is the combined standard uncertainty calculated according to the ISO Guide [2]. The value of u_c is intended to represent, at the level of one standard deviation, the combined effect of uncertainty components associated with the certified mass fraction value and the solution density.

Expiration of Certification: The certification of SRM 1640a is valid, within the measurement uncertainty specified, until **05 August 2020**, provided the SRM is handled and stored in accordance with instructions given in this certificate (see "Instructions for Use"). The certification is nullified if the SRM is damaged, contaminated, or otherwise modified.

Maintenance of SRM Certification: NIST will monitor this SRM over the period of its certification. If substantive technical changes occur that affect the certification before the expiration of this certificate, NIST will notify the purchaser. Registration (see attached sheet) will facilitate notification.

Coordination of the technical measurements leading to the certification of SRM 1640a was provided by M.R. Winchester of the NIST Analytical Chemistry Division.

Stephen A. Wise, Chief
Analytical Chemistry Division

Robert L. Watters, Jr., Chief
Measurement Services Division

Gaithersburg, MD 20899
Certificate Issue Date: 08 June 2010
See Certificate Revision History on Last Page

SRM 1640a

Page 1 of 6

This SRM was prepared by T.A. Butler, L.L. Yu, and M.R. Winchester of the NIST Analytical Chemistry Division. The ICP-OES analyses were performed by T.A. Butler, J.L. Molloy, and M.R. Winchester of the NIST Analytical Chemistry Division. The ICP-MS analyses were performed by J.L. Molloy, T.A. Butler, L.L. Yu, and M.R. Winchester of the NIST Analytical Chemistry Division.

Statistical consultation was provided by W.F. Guthrie of the NIST Statistical Engineering Division.

Support aspects involved in the issuance of this SRM were coordinated through the NIST Measurement Services Division.

Reference Values and Uncertainties: The reference values for seven elements in SRM 1640a are given expressed in mass fraction units and mass concentration units in Tables 3 and 4, respectively. Reference values are non-certified values that are best estimates of the true values. However, the values do not meet NIST criteria for certification and are provided with associated uncertainties that may not include all sources of uncertainty [1].

The reference mass fraction values and expanded uncertainties given in Table 3 are calculated using the same approach employed for the certified mass fraction values (see explanation above), including the use of the transpiration adjustment, except that each reference mass fraction value is based solely upon analysis using either ICP-OES or ICP-MS and uncertainty components are limited to those associated with the analysis and the transpiration adjustment. The reference mass concentration values and expanded uncertainties given in Table 4 are calculated using the same approach employed for the certified mass concentration values (see explanation above), except that they are calculated using the reference mass fraction values in place of the certified mass fraction values.

NOTICE AND WARNING TO USERS

CAUTION: This SRM is an acidic solution. All appropriate safety precautions, including use of gloves during handling, should be taken.

INSTRUCTIONS FOR USE

The SRM should be shaken before use to remix water that may have condensed on the inner surfaces of the bottle. To help prevent contamination, pipettes or other labware should **NOT** be inserted into the bottle. Instead, a portion of the solution should be decanted into another clean, dry container for use. Unused portions should not be returned to the SRM bottle.

The accuracy of trace element analysis is limited by contamination, especially at the microgram per kilogram (or microgram per liter) level. All apparatuses should be scrupulously clean, and only high-purity reagents should be employed. Sampling and manipulations, such as evaporations, should be done in a clean environment, such as a Class-100 clean hood.

The mass concentration values and uncertainties given in Tables 2 and 4 were calculated from the mass fraction values and uncertainties in Tables 1 and 3, respectively, taking into account the anticipated range of density values of the SRM solution in the temperature range 17 °C to 27 °C. Therefore, the mass concentration values and uncertainties given in the tables are valid when the SRM solution is used within a temperature range of 22 °C ± 5 °C. A more precise estimate of the mass concentration for a given temperature can be obtained by multiplying the mass fraction value by the accurately measured density of the solution at that temperature. The uncertainty associated with a mass concentration value calculated in this way can be estimated by combining the uncertainty components for the mass fraction value and the measured density following the ISO Guide [2].

Transpiration: The certified and reference values given in Tables 1 through 4 account for the effects of transpiration that may occur *prior to the first opening of the sealed pouch by the SRM user*. After the SRM bottle has been removed from the pouch, the rate of transpiration will rise, resulting in gradual increases in the mass fractions (and concentrations) of the elements. *It is the responsibility of the user of this SRM to account for this effect*. One approach is to weigh the SRM bottle both before and after each use. Mass loss observed during storage can be utilized to correct for transpiration. In order to minimize transpiration, the SRM bottle should be stored tightly closed and sealed inside an airtight container. The user should set a maximum shelf-life for a partially used SRM bottle commensurate with accuracy requirements.

PREPARATION OF MATERIAL

SRM 1640a was prepared at NIST using only high-purity reagents. An acid-cleaned HDPE tank of 2 kL capacity was filled with a known mass of commercially available spring water and enough concentrated nitric acid to adjust the acid volume fraction to approximately 2 %. After thorough mixing with a precleaned recirculating pump, a preliminary ICP-MS analysis was performed to determine the levels of the 29 elements of interest. The levels of the 22 elements to be certified were gravimetrically adjusted to target values by additions of aliquots of known masses of the SRMs in the SRM 3100 series of single-element standard solutions. For each of these elements, the target value was approximately 80 % of the Maximum Contaminant Level (MCL) listed in either the National Primary Drinking Water Regulations or the National Secondary Drinking Water Regulations maintained by the United States Environmental Protection Agency (EPA) [4], or approximately the mass fraction that was present in SRM 1640 Trace Elements in Natural Water, whichever was less. After addition of the aliquots and thorough mixing, the SRM solution was packaged in acid-cleaned HDPE bottles of 250 mL capacity and sealed inside aluminized Mylar pouches.

Table 1. Certified Values for Elements in SRM 1640a Expressed in Mass Fraction Units^(a)

Element	Mass Fraction ($\mu\text{g}/\text{kg}$)		k	df
Aluminum	52.6	± 1.8	2.069	23
Antimony	5.064	± 0.045	2.365	7
Arsenic	8.010	± 0.067	1.980	120
Barium	150.60	± 0.74	1.984	98
Beryllium	3.002	± 0.027	2.060	25
Boron	300.7	± 3.1	2.365	7
Cadmium	3.961	± 0.072	2.365	7
Chromium	40.22	± 0.28	2.021	40
Cobalt	20.08	± 0.24	2.447	6
Copper	85.07	± 0.48	2.228	10
Iron	36.5	± 1.7	2.447	6
Lead	12.005	± 0.040	1.970	227
Manganese	40.07	± 0.35	2.201	11
Molybdenum	45.24	± 0.59	2.017	43
Nickel	25.12	± 0.12	2.026	37
Selenium	19.97	± 0.16	2.228	10
Silver	8.017	± 0.042	2.086	20
Strontium	125.03	± 0.86	2.179	12
Thallium	1.606	± 0.015	2.365	7
Uranium	25.15	± 0.26	2.145	14
Vanadium	14.93	± 0.21	2.447	6
Zinc	55.20	± 0.32	2.010	49

- ^(a) Certified mass fraction values are the equally weighted means of results from gravimetry and ICP-OES or ICP-MS, adjusted upward for transpiration that may occur over the certification period while the SRM bottle remains sealed inside the aluminized Mylar pouch. (NOTE: *No correction has been applied for transpiration that will occur after the pouch seal has been broken.* See "Instructions for Use" for more information.) The magnitude of the transpiration adjustment (0.11 %) was selected so that the actual mass fractions are expected to be equal to the corresponding certified values approximately halfway through the certification period. The uncertainty listed with each value is an expanded uncertainty about the mean. The expanded uncertainty is calculated following the ISO Guide [2] as $U = ku_c$, where u_c is intended to represent, at the level of one standard deviation, the combined effect of uncertainty components associated with the gravimetric preparation, the ICP-OES or ICP-MS analysis, method bias [3], and the transpiration adjustment. The coverage factor (k) for each analyte is determined from the Student's t -distribution corresponding to the degrees of freedom (df) and a 95 % level of confidence.

Table 2. Certified Values for Elements in SRM 1640a Expressed in Mass Concentration Units^(a)

Element	Mass Concentration ^(b) ($\mu\text{g/L}$)	<i>k</i>	<i>df</i>
Aluminum	53.0 ± 1.8	2.064	24
Antimony	5.105 ± 0.046	2.262	9
Arsenic	8.075 ± 0.070	1.977	142
Barium	151.80 ± 0.83	1.976	151
Beryllium	3.026 ± 0.028	2.045	29
Boron	303.1 ± 3.1	2.306	8
Cadmium	3.992 ± 0.074	2.365	7
Chromium	40.54 ± 0.30	2.008	51
Cobalt	20.24 ± 0.24	2.365	7
Copper	85.75 ± 0.51	2.120	16
Iron	36.8 ± 1.8	2.447	6
Lead	12.101 ± 0.050	1.965	517
Manganese	40.39 ± 0.36	2.160	13
Molybdenum	45.60 ± 0.61	2.013	46
Nickel	25.32 ± 0.14	2.001	59
Selenium	20.13 ± 0.17	2.160	13
Silver	8.081 ± 0.046	2.040	31
Strontium	126.03 ± 0.91	2.120	16
Thallium	1.619 ± 0.016	2.306	8
Uranium	25.35 ± 0.27	2.120	16
Vanadium	15.05 ± 0.25	2.365	7
Zinc	55.64 ± 0.35	1.995	68

- (a) Certified mass concentration values are calculated from the certified mass fraction values in Table 1 through multiplication by the density of the SRM 1640a solution. The uncertainty listed with each value is an expanded uncertainty about the mean. The expanded uncertainty is calculated following the ISO Guide [2] as $U = ku_c$, where u_c is intended to represent, at the level of one standard deviation, the combined effect of uncertainty components associated with the certified mass fraction value and the solution density. The coverage factor (*k*) for each analyte is determined from the Student's *t*-distribution corresponding to the degrees of freedom (*df*) and a 95 % level of confidence.
- (b) The certified mass concentration values and expanded uncertainties are valid when the SRM solution is used within the temperature range ($22\text{ }^\circ\text{C} \pm 5\text{ }^\circ\text{C}$).

Table 3. Reference Values for Elements in SRM 1640a Expressed in Mass Fraction Units^(a)

Element	Mass Fraction (mg/kg)		<i>k</i>	<i>df</i>
Calcium	5.570	± 0.016	2.120	16
Magnesium	1.0502	± 0.0034	2.262	9
Potassium	0.5753	± 0.0020	2.179	12
Silicon	5.169	± 0.017	2.074	22
Sodium	3.112	± 0.031	2.776	4
	(µg/kg)			
Lithium	0.4034	± 0.0092	2.776	4
Rubidium	1.188	± 0.011	1.961	3204

^(a) Reference mass fraction values are the ICP-OES or ICP-MS values, adjusted upward for transpiration that may occur over the certification period while the SRM bottle remains sealed inside the aluminized Mylar pouch. (NOTE: *No correction has been applied for transpiration that will occur after the pouch seal has been broken.* See "Instructions for Use" for more information.) The magnitude of the transpiration adjustment (0.11 %) was selected so that the actual mass fractions are expected to be equal to the corresponding reference values approximately halfway through the certification period. The uncertainty listed with each value is an expanded uncertainty about the mean. The expanded uncertainty is calculated following the ISO Guide [2] as $U = ku_c$, where u_c is intended to represent, at the level of one standard deviation, the combined effect of uncertainty components associated with the ICP-OES or ICP-MS analysis and the transpiration adjustment. The coverage factor (*k*) for each analyte is determined from the Student's *t*-distribution corresponding to the degrees of freedom (*df*) and a 95 % level of confidence.

Table 4. Reference Values for Elements in SRM 1640a Expressed in Mass Concentration Units^(a)

Element	Mass Concentration ^(b) (mg/L)		<i>k</i>	<i>df</i>
Calcium	5.615	± 0.021	2.005	54
Magnesium	1.0586	± 0.0041	2.045	29
Potassium	0.5799	± 0.0023	2.040	31
Silicon	5.210	± 0.021	2.005	54
Sodium	3.137	± 0.031	2.571	5
	(µg/L)			
Lithium	0.4066	± 0.0094	2.776	4
Rubidium	1.198	± 0.011	1.961	3657

^(a) Reference mass concentration values are calculated from the reference mass fraction values in Table 3 through multiplication by the density of the SRM 1640a solution. The uncertainty listed with each value is an expanded uncertainty about the mean. The expanded uncertainty is calculated following the ISO Guide [2] as $U = ku_c$, where u_c is intended to represent, at the level of one standard deviation, the combined effect of uncertainty components associated with the reference mass fraction value and the solution density. The coverage factor (*k*) for each analyte is determined from the Student's *t*-distribution corresponding to the degrees of freedom (*df*) and a 95 % level of confidence.

^(b) The reference mass concentration values and expanded uncertainties are valid when the SRM solution is used within the temperature range (22 °C ± 5 °C).

REFERENCES

- [1] May, W.; Parris, R.; Beck II, C.; Fassett, J.; Greenberg, R.; Guenther, F.; Kramer, G.; Wise, S.; Gills, T.; Colbert, J.; Gettings, R.; MacDonald, B.; *Definition of Terms and Modes Used at NIST for Value-Assignment of Reference Materials for Chemical Measurements*; NIST Special Publication 260-136 (2000); available at <http://ts.nist.gov/MeasurementServices/ReferenceMaterials/PUBLICATIONS.cfm> (accessed Jun 2010).
- [2] JCGM 100:2008; *Evaluation of Measurement Data — Guide to the Expression of Uncertainty in Measurement* (ISO GUM 1995 with Minor Corrections); Joint Committee for Guides in Metrology (2008); available at http://www.bipm.org/utis/common/documents/jcgm/JCGM_100_2008_E.pdf (accessed Jun 2010); see also Taylor, B.N.; Kuyatt, C.E.; *Guidelines for Evaluating and Expressing the Uncertainty of NIST Measurement Results*; NIST Technical Note 1297; U.S. Government Printing Office: Washington, DC (1994); available at <http://www.nist.gov/physlab/pubs/index.cfm> (accessed Jun 2010).
- [3] Levenson, M.S.; Banks, D.L.; Eberhardt, K.R.; Gill, L.M.; Guthrie, W.F.; Liu, H.K.; Vangel, M.G.; Yen, J.H.; Zhang, N.F.; *An Approach to Combining Results From Multiple Methods Motivated by the ISO GUM*; J. Res. Natl. Inst. Stand. Technol., Vol, 105; p. 571 (2000).
- [4] *Drinking Water Contaminants*, United States Environmental Protection Agency, available at <http://www.epa.gov/safewater/contaminants/index.html#listsec> (accessed Jun 2010).

Certificate Revision History: 08 June 2010 (This revision includes corrected lithium values in Tables 3 and 4 and minor editorial changes.); 03 December 2009 (Original certificate date).

Users of this SRM should ensure that the Certificate of Analysis in their possession is current. This can be accomplished by contacting the SRM Program: telephone (301) 975-2200; fax (301) 926-4751; e-mail srminfo@nist.gov; or via the Internet at <http://www.nist.gov/srm>.

A.4. NIST 1643F data sheet



National Institute of Standards & Technology

Certificate of Analysis

Standard Reference Material® 1643f

Trace Elements in Water

This Standard Reference Material (SRM) is intended primarily for use in evaluating methods used in the determination of trace elements in fresh water. A unit of SRM 1643f consists of approximately 250 mL of acidified water in a polyethylene bottle, which is sealed in an aluminized plastic bag to maintain stability. SRM 1643f simulates the elemental composition of fresh water. The solution contains nitric acid at a volume fraction of approximately 2 %, equivalent to an amount of substance concentration (molarity) of approximately 0.32 mol/L.

Certified Values: The certified values for elements in SRM 1643f are listed in Table 1. All values are reported both as mass fractions ($\mu\text{g}/\text{kg}$) and as mass concentrations ($\mu\text{g}/\text{L}$). A NIST certified value is a value for which NIST has the highest confidence in its accuracy in that all known or suspected sources of bias have been investigated or taken into account [1]. The certified mass fraction values are consensus estimates that blend the results of the gravimetric preparation value and a value determined by either inductively coupled plasma mass spectrometry (ICP-MS) or inductively coupled plasma optical emission spectrometry (ICP-OES) [2]. The certified mass concentration values are derived from the certified mass fraction values using the measured density of SRM 1643f. Additional information about the certification of SRM 1643f is given under “Certification of Material”.

The expanded uncertainty for each certified value is calculated as

$$U = ku_c$$

where k is the coverage factor for a 95 % confidence interval and u_c is the combined standard uncertainty calculated through the application of the Monte Carlo method described in the ISO/JCGM Supplement 1 [3]. The value of u_c for the certified mass fraction values is intended to represent, at the level of one standard deviation, the combined effect of uncertainty components associated with the gravimetric preparation, the ICP-MS or ICP-OES determination, method bias, and stability. Additionally, the uncertainty evaluations associated with the certified mass concentration values assume that the temperature at which the material will be measured is between 15 °C and 25 °C.

Expiration of Certification: This certification of **SRM 1643f** is valid, within the measurement uncertainty specified, until **31 October 2023**, provided the SRM is handled and stored in accordance with instructions given in this certificate (see “Instructions for Use”). This certification is nullified if the SRM is damaged, contaminated, or modified.

Maintenance of SRM Certification: NIST will monitor this SRM over the period of its certification. If substantive technical changes occur that affect the certification before the expiration of this certificate, NIST will notify the purchaser. Registration (see attached sheet or register online) will facilitate notification.

Coordination of the NIST technical measurements was under the direction of T.A. Butler, J.L. Molloy and M.R. Winchester of the NIST Chemical Sciences Division. The density, ICP-MS and ICP-OES analyses were performed by T.A. Butler and J.L. Molloy.

Statistical analysis of the experimental data was performed by A.M. Possolo of the NIST Statistical Engineering Division.

Support aspects involved in the issuance of this SRM were coordinated through the NIST Office of Reference Materials.

Carlos A. Gonzalez, Chief
Chemical Sciences Division

Robert L. Watters, Jr., Director
Office of Reference Materials

Gaithersburg, MD 20899
Certificate Issue Date: 18 August 2015

SRM 1643f

Page 1 of 3

Table 1. Certified Values, Expanded Uncertainties, and Coverage Factors (*k*) for Elements in SRM 1643f

Element	Mass Fraction ($\mu\text{g}/\text{kg}$)			<i>k</i>	Mass Concentration ($\mu\text{g}/\text{L}$)			<i>k</i>
	Value	±	<i>k</i>		Value	±	<i>k</i>	
Aluminum (Al)	132.5	±	1.2	1.9	133.8	±	1.2	1.9
Antimony (Sb)	54.90	±	0.39	1.9	55.45	±	0.40	2.0
Arsenic (As)	56.85	±	0.37	2.0	57.42	±	0.38	2.0
Barium (Ba)	513.1	±	7.3	2.1	518.2	±	7.3	2.1
Beryllium (Be)	13.53	±	0.11	2.1	13.67	±	0.12	2.1
Bismuth (Bi)	12.50	±	0.10	1.9	12.62	±	0.11	1.9
Boron (B)	150.8	±	6.6	2.2	152.3	±	6.6	2.2
Cadmium (Cd)	5.83	±	0.13	2.2	5.89	±	0.13	2.2
Calcium (Ca)	29 140	±	320	2.1	29 430	±	330	2.1
Chromium (Cr)	18.32	±	0.10	2.0	18.50	±	0.10	2.1
Cobalt (Co)	25.05	±	0.17	2.0	25.30	±	0.17	2.0
Copper (Cu)	21.44	±	0.70	2.1	21.66	±	0.71	2.2
Iron (Fe)	92.51	±	0.77	2.1	93.44	±	0.78	2.1
Lead (Pb)	18.303	±	0.081	2.0	18.488	±	0.084	2.1
Lithium (Li)	16.42	±	0.35	2.2	16.59	±	0.35	2.2
Magnesium (Mg)	7 380	±	58	1.9	7 454	±	60	2.0
Manganese (Mn)	36.77	±	0.58	2.1	37.14	±	0.60	2.2
Molybdenum (Mo)	114.2	±	1.7	2.1	115.3	±	1.7	2.1
Nickel (Ni)	59.2	±	1.4	2.2	59.8	±	1.4	2.2
Potassium (K)	1 913.3	±	9.0	2.0	1 932.6	±	9.4	2.1
Rubidium (Rb)	12.51	±	0.12	2.0	12.64	±	0.13	2.0
Selenium (Se)	11.583	±	0.078	2.0	11.700	±	0.081	2.0
Silver (Ag)	0.9606	±	0.0053	2.0	0.9703	±	0.0055	2.0
Sodium (Na)	18 640	±	240	2.1	18 830	±	250	2.1
Strontium (Sr)	311	±	18	2.1	314	±	19	2.2
Tellurium (Te)	0.9672	±	0.0082	2.0	0.9770	±	0.0084	2.0
Thallium (Tl)	6.823	±	0.034	1.9	6.892	±	0.035	2.0
Vanadium (V)	35.71	±	0.27	2.0	36.07	±	0.28	2.0
Zinc (Zn)	73.7	±	1.7	2.1	74.4	±	1.7	2.1

(a) The measurand is the total mass fraction for each element. Metrological traceability is to the SI unit for mass, expressed as micrograms per kilogram and micrograms per liter.

Preparation of Material: SRM 1643f was prepared at NIST using only high purity reagents. A polyethylene cylindrical tank was filled with deionized water and sufficient nitric acid to bring the nitric acid amount of substance concentration (molarity) to approximately 0.32 mol/L. Known masses of the matrix elements (sodium, potassium, calcium, and magnesium) were added to the tank as solutions prepared from the same materials used to prepare the SRM 3100 series of single element solutions. Known masses of the other elements were then added to the tank solution using weighed aliquots of the SRM 3100 series. After mixing thoroughly, the tank solution was transferred into the acid-cleaned, 250 mL, polyethylene, SRM bottles and immediately sealed in individual aluminized plastic bags.

Certification of Material: Each of the certified elements was determined using either ICP-MS or ICP-OES. The final total mass of the tank solution prior to bottling was determined from the sum of the mass fraction values of the elements in Table 1 and the sum of the known masses of those elements added to prepare the solution, therefore allowing calculation of the gravimetric preparation mass fraction for each element. Certified mass fraction values were calculated by combining the gravimetric preparation values with the ICP-MS or ICP-OES values, as described under Certified Values. Certified mass concentration values were calculated using the measured density of 1.0101 g/mL ± 0.0012 g/mL, where the uncertainty is expressed at a confidence level of approximately 95 %, within the temperature range of 15 °C to 25 °C.

INSTRUCTIONS FOR USE

Precautions: The SRM should be shaken before use because of possible water condensation on the inner surfaces of the bottle. To prevent possible contamination of the SRM, **DO NOT** insert pipettes into the bottle. Samples should be decanted at a room temperature of 15 °C to 25 °C. After use, the bottle should be recapped tightly and returned to the aluminized plastic bag, which should be folded and sealed with sealing tape. This safeguard will protect the SRM from possible environmental contamination and long-term evaporation.

The accuracy of trace element determinations, especially at the micrograms per liter level, is limited by contamination. Apparatus should be scrupulously cleaned and only high purity reagents employed. Sampling and manipulations, such as evaporations, should be done in a clean environment, such as a Class-100 clean hood.

REFERENCES

- [1] May, W.; Parris, R.; Beck, C.; Fassett, J.; Greenberg, R.; Guenther, F.; Kramer, G.; Wise, S.; Gills, T.; Colbert, J.; Gettings, R.; MacDonald, B.; *Definition of Terms and Modes Used at NIST for Value-Assessment of Reference Materials for Chemical Measurements*; NIST Special Publication 260-136, U.S. Government Printing Office: Washington, DC (2000); available at <http://www.nist.gov/srm/publications.cfm> (accessed Aug 2015).
- [2] DerSimonian, R.; Laird, N.; *Meta-Analysis in Clinical Trials*; Control. Clin. Trials, Vol. 7, pp. 177–188 (1986).
- [3] JCGM 101:2008; *Evaluation of Measurement Data — Supplement 1 to the “Guide to the Expression of Uncertainty in Measurement” — Propagation of Distributions using a Monte Carlo Method*; Joint Committee for Guides in Metrology (JCGM) (2008); available at http://www.bipm.org/utis/common/documents/jcgm/JCGM_101_2008_E.pdf (accessed Aug 2015).

Users of this SRM should ensure that the Certificate of Analysis in their possession is current. This can be accomplished by contacting the SRM Program: telephone (301) 975-2200; fax (301) 948-3730; e-mail srminfo@nist.gov; or via the Internet at <http://www.nist.gov/srm>.